Materials Sciences Corporation

THERMO-MECHANICAL ANALYSIS OF OXIDATION RESISTANT CARBON-CARBON COMPOSITES

Technical Final Report

MSC TFR 3511/1507

July, 1995

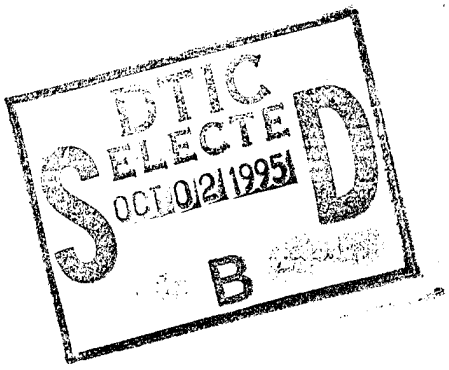

Prepared For:

USAF, AFSC
Air Force Office of Scientific Research
Building 410
Bolling AFB, DC 20332-6448

REPORT DOCUMENTATION PAGE

Form Approved
OMB No. 0704-0188

1. AGENCY USE ONLY (*Leave blank*)	2. REPORT DATE	3. REPORT TYPE AND DATES COVERED
	July, 1995	Technical Final Report - 2/92 thru 4/95

4. TITLE AND SUBTITLE
Thermo-Mechanical Analysis of Oxidation Resistant Carbon-Carbon Composites

5. FUNDING NUMBERS
F49620-92-C-0024

AFOSR-TR-95
0555

6. AUTHORS(S)
Mark Jones, Zvi Hashin, Jerry Rubinsky, Guido Teti, Steve Yurgartis

7. PERFORMING ORGANIZATION NAME(S) AND ADDRESS(ES)
Materials Sciences Corporation
500 Office Center Drive, Suite 250
Fort Washington, PA 19034

MSC TFR 3511/1507

9. SPONSORING/MONITORING AGENCY NAME(S) AND ADDRESS(ES)
~~USAF, AFSC~~
Air Force Office of Scientific Research
Building 410
Bolling AFB, DC 20332-6448

N A

10. SPONSORING/MONITORING AGENCY REPORT NUMBER
F49620-92-C-0024

11. SUPPLEMENTARY NOTES

12a. DISTRIBUTION/AVAILABILITY STATEMENT
Approved for public release, distribution unlimited

12B. DISTRIBUTION CODE

13. ABSTRACT (*Maximum 200 words*)

The objective of this program was to develop a methodology for investigating the thermo-mechanical interactions between coatings and substrates in advanced oxidation resistant carbon-carbon composites.

During the course of the program, two model sets were developed: the Micro-Mechanics of Oxidation Protection (MMOP) model and the Crack Management (CM) model. The MMOP model used closed-form classical micromechanics solutions to study the impact of various oxidation concepts on substrate thermo-mechanical properties. MMOP concepts evaluated included matrix fillers, crack fillers, and fiber coatings. Model predictions were correlated against experimental data from current generation carbon-carbon materials.

The (CM) model is based on conservation of energy principles, and was developed to study the impact of substrate and coating material parameters on the initiation and development of the coating crack network during the processing cycle. Results from the model were validated against crack pattern measurements acquired during the parallel experimental program.

The MMOP and CM models provide a set of powerful tools for use in the development of oxidation resistant carbon-carbon composites and coatings.

14. SUBJECT TERMS	15. NUMBER OF PAGES
Composite micro-mechanics, oxidation resistant carbon-carbon, ceramic coatings, fracture mechanics, thermo-mechanical analyses	93
	16. PRICE CODE

17. SECURITY CLASSIFICATION OF REPORT	18. SECURITY CLASSIFICATION OF THIS PAGE	19. SECURITY CLASSIFICATION OF ABSTRACT	20. LIMITATION OF ABSTRACT
Unclassified	Unclassified	Unclassified	None

NSN 7540-01-280-5500

Standard From 298 (rev. 2-89)
Prescribed by ANSI Std. Z39-18
298-102

ABSTRACT

The objective of this program was to develop a methodology for investigating the thermo-mechanical interactions between coatings and substrates in advanced oxidation resistant carbon-carbon composites. This methodology was to be utilized to suggest thermo-mechanically compatible material solutions for reducing the susceptibility of these materials to oxidation attack, or for controlling the rate of oxygen influx to the substrate by controlling the development of microcracks in the primary oxygen barrier - the external CVD coating.

At any temperature, the oxidation rate of carbon-carbon composites is controlled by the oxidation rate of the base substrate and by the rate at which oxygen reaches the substrate via defects (cracks) in the external coating. Current, and proposed, advanced carbon-carbon oxygen protection systems seek to extend oxidation life by modifying both controlling mechanisms, i.e., by active and passive substrate oxidation inhibition concepts, and by active and passive crack management concepts. Substrate inhibition concepts which have been utilized, or proposed, include: particulate matrix inhibitors, matrix modifiers, matrix crack fillers, and fiber coatings. Coating crack management concepts have included: crack sealers, multi-layer coatings, modified interface layers, and thermal cycling.

Thermo-mechanical interactions are very important in the carbon-carbon oxidation process. A major reason for the difficulty in finding an effective long-life oxidation resistant carbon-carbon coating lies in the large mismatch in thermal expansion between the substrate, and the coatings. Given this interaction, it is important that the thermo-mechanical effects of proposed oxidation concepts be considered during the material selection process. Materials which either increase the mismatch in thermal expansion or induce large stresses in the substrate or coating should be avoided, e.g., crack fillers, or fiber coatings will be ineffective if they debond or generate new cracks.

During the course of the program, two model sets were developed: The Micro-Mechanics of Oxidation Protection (MMOP) model and the Crack Management (CM) model. The MMOP model used closed-form classical micromechanics solutions to study the impact of various oxidation concepts on substrate thermo-mechanical properties. MMOP concepts evaluated included matrix fillers, crack fillers, and fiber coatings. The predominant effect of these material modifications was to significantly increase the matrix dominated properties of the substrate and increase the thermal expansion coefficient. SiC was the most effective

material in this regard. Model predictions were correlated against experimental data from current generation carbon-carbon materials.

The (CM) model was based on conservation of energy principles, and was developed to study the impact of substrate and coating material parameters on the initiation and development of the coating crack network during the processing cycle. It was confirmed that the coating:substrate thermal expansion ratio was the single most important factor driving crack initiation, and that coating material toughness determined the number of cracks. Both of these effects were quantified. This would indicate a preferred CM strategy of high expansion substrates and low expansion, low toughness, coatings. Results from the model were validated against crack pattern measurements acquired during the parallel experimental program.

The MMOP and CM models provide a powerful set of tools for use in the development of oxidation resistant carbon-carbon composites and coatings. In addition, the constitutive nature of these codes renders them applicable to other composite types where there is an interest in fiber coatings, matrix cracks, and matrix modifiers, particularly ceramic matrix and metal matrix composites.

PREFACE

This report represents the results of a study performed under Air Force Office of Scientific Research (AFOSR) Contract Number F49620-92-C-0024. The Contract Monitor at AFOSR was Dr. Walter Jones. Dr. B.W. Rosen was the Program Manager at Materials Sciences Corporation (MSC), with Dr. Mark L. Jones as Principal Investigator. Prof. Zvi Hashin acted as an internal consultant and technical advisor. Mr. Jerry Rubinsky performed the MicroMechanics of Oxidation Protection (MMOP) studies and encoded the models developed under this activity. Mr. Guido Teti encoded the Crack Management model and performed the parametric material sensitivity studies supported by Dr. Sailen Chatterjee. Messrs. Michael Bidinger and Thomas Cassin provided technical support with regard to finite element modeling. The experimental microstructural characterization work was performed by Prof. Steve Yurgartis at Clarkson University, Potsdam, NY.

TABLE OF CONTENTS

1.0 INTRODUCTION AND BACKGROUND

1.1 PROGRAM DEFINITION

The objectives of this program were two fold: 1). To develop a methodology for evaluating the impact of various oxidation protection schemes on the thermo-mechanical properties of carbon-carbon substrate materials; and 2). To determine the interactions between substrate thermo-mechanical properties and coating material parameters which drive the initiation and development of the microcrack pattern in the external oxidation resistant ceramic coatings.

Analytical work was conducted in two areas: The development of a Micro-Mechanics of Oxidation Protection (MMOP) model to study substrate properties, and the development of a Crack Management (CM) model to investigate coating microcracking. A schematic representation of these models and how they may be used in an integrated analysis of substrate/coating interactions is given in Figure 1.

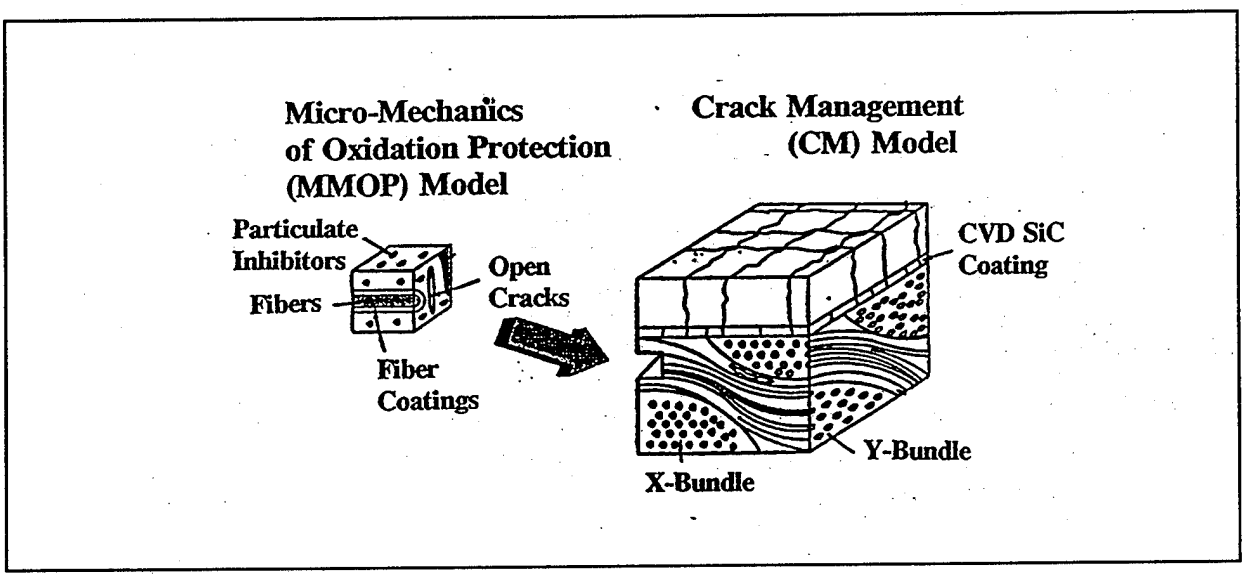

Figure 1. The program objectives were accomplished by a two level modeling approach for thermo-mechanical analysis of oxidation resistant carbon-carbon (ORCC) composites.

In support of the analytical activities at MSC, a parallel experimental program was conducted by Prof. Steve Yurgartis of Clarkson University, Potsdam, NY, under a subcontract agreement with MSC. The objective of the Clarkson program was to perform quantitative microstructural characterization of the crack networks within the substrate and external coatings. This data was necessary for validation of the MSC MMOP and CM models. In order to accomplish this objective, third generation (state-of-the-art as of 2/92) coated oxidation resistant carbon-carbon (ORCC) materials were procured from Rohr Inc. (Chula Vista, CA) for coating at BFGoodrich (Brecksville, OH). A series of preliminary studies were performed on Chromalloy (Orangeburg, NY) coated Hitco (Gardena, CA) substrate material.

1.2 CARBON-CARBON OXIDATION PROTECTION

Over the last 10 years, carbon-carbon composites have received much attention as candidate materials for use in a number of high temperature turbine engine and airframe applications. The reason for this interest lies in carbon-carbon's unique combination of high specific strength, good specific stiffness, and low creep rate and retention of these characteristics up to 4000°F. However, excellent as these properties may be, carbon-carbon suffers from one major disadvantage: in the unprotected state, in an oxidizing environment, carbon-carbon materials begin to oxidize at temperatures as low as 800°F [1]. The carbon oxidation reaction gives rise to gaseous products (CO and CO2) and an associated mass loss. Onset of oxidation is accompanied by a very severe loss in mechanical properties with as little as 2% mass loss causing a 20% loss in axial strength, and a 50% loss in matrix dominated strength properties [2]. Thus, the application of carbon-carbon in high temperature oxidizing environments requires the application of various oxidation protection schemes. These oxidation schemes include some form of external oxidation resistant coating as the primary oxygen barrier, and some form of oxidation "inhibitors" distributed within the matrix.

Typical mechanical properties for a structural carbon-carbon material and candidate coating material (SiC) are given in Table 1. It may be seen that in comparison to SiC, the carbon-carbon substrate has a relatively low elastic modulus, and very low coefficient of thermal expansion (CTE).

Table 1. Typical properties for Carbon-Carbon and Silicon Carbide Coating Material.

PROPERTY	CARBON-CARBON SUBSTRATE	SiC COATING MATERIAL
Modulus, Msi	12 - 18	60
Thermal Expansion, 10-6/°F	-0.5 @ 70°F 1.4 @ 2000°F	2.2

As a result of this property mismatch, it is very difficult to fabricate and maintain adherent/coherent silicon carbide based coatings on carbon-carbon materials exposed to repeated elevated temperature thermal cycling. During cooldown from typical coating conditions (≈ 2000°F) the differential thermal expansions of coating and substrate tend to produce high tensile stresses in the brittle ceramic coating, and compressive stresses in the substrate. Under the action of these tensile stresses, the coating exhibits multiple failures which manifest in the form of a network of fine microcracks along the coating surface. These microcracks then act as defect sites for oxygen penetration and oxidation of the carbonaceous substrate. As carbon oxidation occurs with no solid products of reaction, there is no passivation mechanism which might seal, or close, these cracks, and the oxidation reaction continues unimpeded until all the substrate material is consumed leaving a hollow shell of coating as observed in [3].

As a result of such experiences, it was very quickly realized in the development of oxidation resistant carbon-carbon materials, that external coatings, alone, could not provide reliable oxidation protection for long-life applications. These coatings were very effective as first-level oxygen barriers, but strategies were required to protect the substrate from oxidation via penetration through the coating microcrack network. These strategies include:

Matrix Fillers - Substrate Inhibition

The concept of adding chemical species that reduce or inhibit the susceptibility of carbon oxidation has been practiced for many years [4, 5, 6]. It has been shown that within the

carbon-carbon substrate the amorphous carbon matrix is more susceptible to oxidation than the highly graphitic reinforcement phase [7]. In consequence, most of the approaches for improving the oxidation resistance of the substrate have relied on adding fillers and chemical species to the matrix phase [8].

Matrix Crack Fillers

Carbon-carbon substrates are generally highly cracked. The type and orientation of these cracks is shown in Figure 2. These cracks are a result of both volumetric shrinkages of the matrix precursor material during carbon-carbon processing, and of the multiple high temperature cycles involved in the process. Within the matrix these cracks have an adverse affect on the substrate oxidation rate; not only do they provide a penetration path for oxygen ingress, but they also increase the surface area of exposed carbon for oxidation. Thus, one of the strategies proposed for improving the oxidation resistance of the substrate is to fill these cracks with oxidation resistant materials such as silicon carbide, silicon nitride, or boron carbide.

Fiber Coatings

While it has been noted that the graphite fibers are less susceptible to oxidation than the amorphous carbon matrix material, the strength properties of the fibers are very sensitive to even small amounts of oxidation attack. As the value of the composite lies primarily in its fiber-dominated strength properties, the application of oxidation resistant coatings to the fibers represents a strategy for reducing the effects of oxidation on mechanical properties and perhaps increasing survivability under given oxidation conditions [9].

Substrate/Coating Interactions

As previously mentioned, oxidation of the substrate material is controlled by ingress of oxygen through the microcrack network in the external ceramic coating. The development of this crack network is a function of the difference in thermo-mechanical properties of the carbon-carbon substrate and the ceramic coating. The strategies proposed for improving the

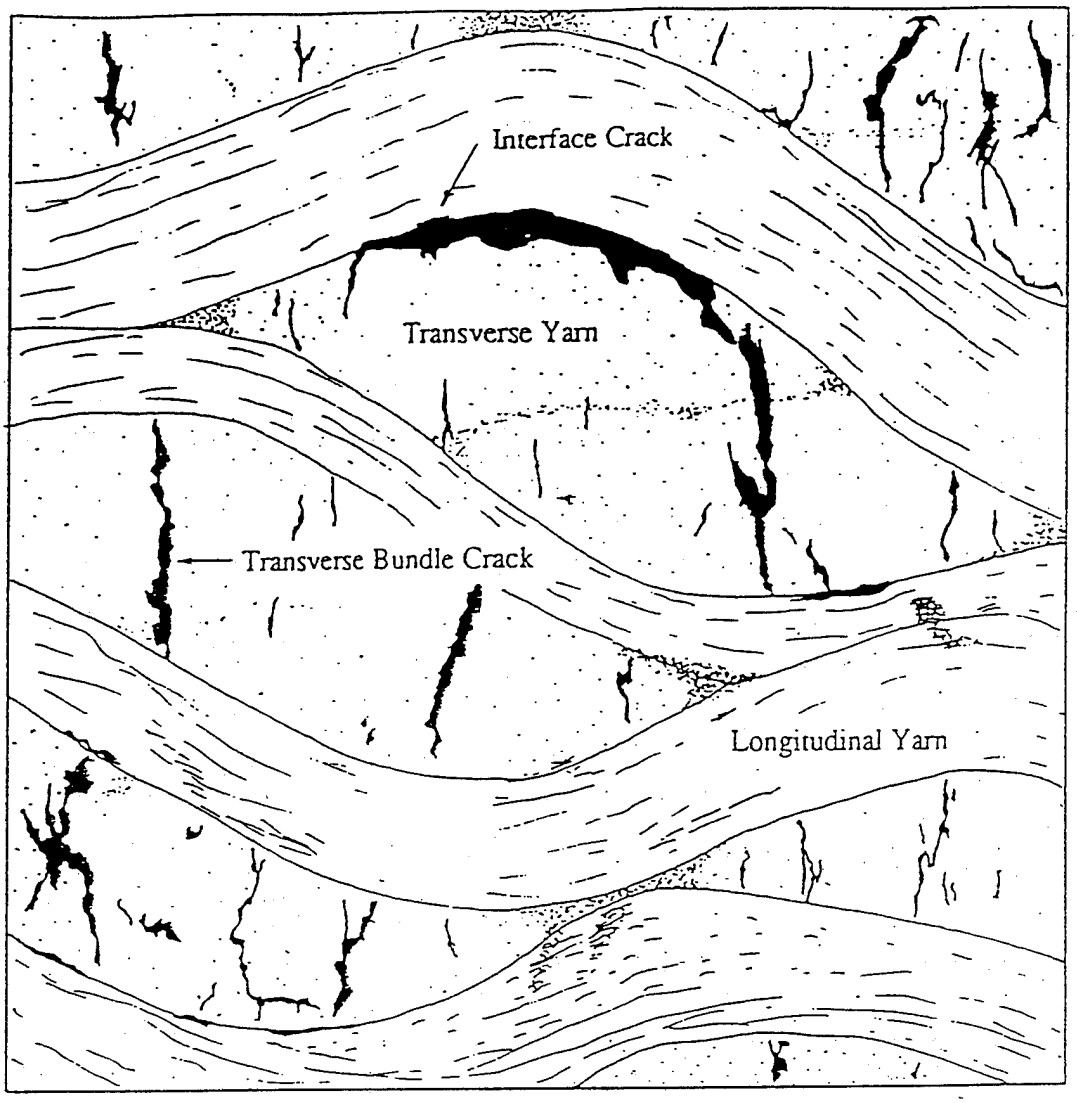

Figure 2. A schematic illustration of the typical damages found in an as-processed ORCC substrate material.

oxidation resistance of C-C materials are based primarily on thermo-chemical considerations. However, the addition of ceramic materials to the C-C substrate in the form of fillers, crack sealers, or fiber coating will tend to change the thermo-mechanical properties of the substrate which will, in turn, have an affect on the coating crack formation, which will affect the substrate oxidation rate.

The root-cause of the ORCC oxidation problem is a mismatch in thermo-mechanical properties between the substrate and the viable oxidation protection coatings. Thus, it

behooves the Materials Scientist recommending changes to the basic coating substrate or coating components, based on thermo-chemical considerations alone, to be aware of the impact of these changes in terms of the thermo-mechanical interactions as well. Materials solutions which appear attractive based on thermo-chemical considerations, may have a deleterious effect on oxidation based on an undesirable change in the thermo-mechanical factors.

Thus, the objective of this program was to develop the tools whereby the impact of these various ORCC material strategies may be determined with respect to changes in the substrate properties, and how these changes in substrate properties may be interpreted in changes to the development of cracks in the coating.

The results and findings from the experimental program conducted at Clarkson University will be discussed first. The Clarkson results will be drawn upon heavily during discussion of the MMOP and CM models.

2.0 MICROSTRUCTURAL CHARACTERIZATION

The purpose of this experimental activity, performed at Clarkson University (under the direction of Prof. Steve Yurgartis), was to provide quantitative microstructural information on the carbon-carbon substrates and coatings to support the analytical model development.

During the course of this activity, a total of seven carbon-carbon coupons were evaluated in the coated and uncoated condition. These coupons represented the general state-of-the-art in ORCC materials systems as of 1992. They included two different substrate materials and process types (Hitco -CVI, and Rohr LOPIC); and two different coating systems (a multi-layer B4C/SiC coating from Chromalloy, and a single layer SiC from BFGoodrich). A summary of the materials evaluated is given in Table 2. Low magnification metallographic cross-sections of the seven material types, including the coating, are given in Figures 3 through 9.

2.1 SUBSTRATE MICROSTRUCTURE

A generalized schematic of the substrate microstructure with typical features indicated was given in Figure 2. Each of the substrate materials examined had a distinct and well defined crack pattern with and between the fiber bundles. These cracks were in the form of transverse yarn bundle cracks within the bundles, and interface cracks between the bundles. Typical transverse bundle crack length distributions and crack orientations for specimen 1652-16 (for two section orientations parallel to the fiber axes) are given in Figures 10 and 11. It may be seen that the average transverse bundle crack length was 0.004 ins. with a 90° orientation, i.e., the bundle cracks were approximately half the bundle height and were perpendicular to the plane of the plate.

Bundle cracking was not observed in the longitudinal bundle direction indicating that all matrix shrinkage during processing takes place in the transverse bundle direction. Shrinkage in the longitudinal direction is constrained by the presence of the fiber bundles oriented in that direction. The presence of the woven fiber reinforcement constrains the free volumetric shrinkage of the resin during pyrolysis to a 2D plane perpendicular to the fiber bundles. This plane is coincident with the orientation of the transverse bundles which are able to crack in an unconstrained manner.

Table 2. A Summary of the Specimens Examined and the Measurements Made.

SPECIMEN IDENTIFICATION	DESCRIPTION	MICROSTRUCTURAL DATA
1515-10	Coating: Chromalloy RT42 (Multi-Layer B4C and SiC)	Coating: Thickness, Crack Type, Crack Spacing, Crack Area
	Substrate: Hitco CC139, Uninhibited	Substrate: None
1652-16	Coating: Chromalloy RT42	Coating: Thickness, Crack Type, Crack Spacing, Crack Area
	Substrate: Hitco CC139 EH - Inhibited, 5HS Weave	Substrate: Bundle crack Lengths and Orientations, and Densities
Panel 1-WA-21	Coating: BFGoodrich SiC	Coating: Thickness, Crack Type, Crack Spacing, Crack Area
	Substrate: Rohr Uninhibited, 8HS Weave, 2650°C Heat Treat	Substrate: Porosity, Bundle Porosity, Bundle crack Lengths and Orientations, and Densities
Panel 20-WA-11	Coating: BFGoodrich SiC	Coating: Thickness, Crack Type, Crack Spacing, Crack Area
	Substrate: Rohr Uninhibited, 8HS Weave, 2150°C Heat Treat	Substrate: Porosity, Bundle Porosity, Bundle crack Lengths and Orientations, and Densities, Fiber Fract.
Panel 31-WA-11	Coating: BFGoodrich SiC	Coating: Thickness, Crack Type, Crack Spacing, Crack Area
	Substrate: Rohr, 62% Inhibitor, 8HS Weave, 2650°C Heat Treat	Substrate: Porosity, Bundle Porosity, Bundle crack Lengths and Orientations, and Densities, Fiber Fract.
Panel 62-WA-11	Coating: BFGoodrich SiC	Coating: Thickness, Crack Type, Crack Spacing, Crack Area
	Substrate: Rohr, 15% SiC Whiskers, 8HS Weave, 2150°C Heat Treat	Substrate: Porosity, Bundle Porosity, Bundle crack Lengths and Orientations, and Densities, Fiber Fract.
Panel 137-WA-11	Coating: BFGoodrich SiC	Coating: Thickness, Crack Type, Crack Spacing, Crack Area
	Substrate: Rohr 40% Inhibitor, Plain Weave, 2150°C Heat Treat	Substrate: Porosity, Bundle Porosity, Bundle crack Lengths and Orientations, and Densities, Fiber Fract.

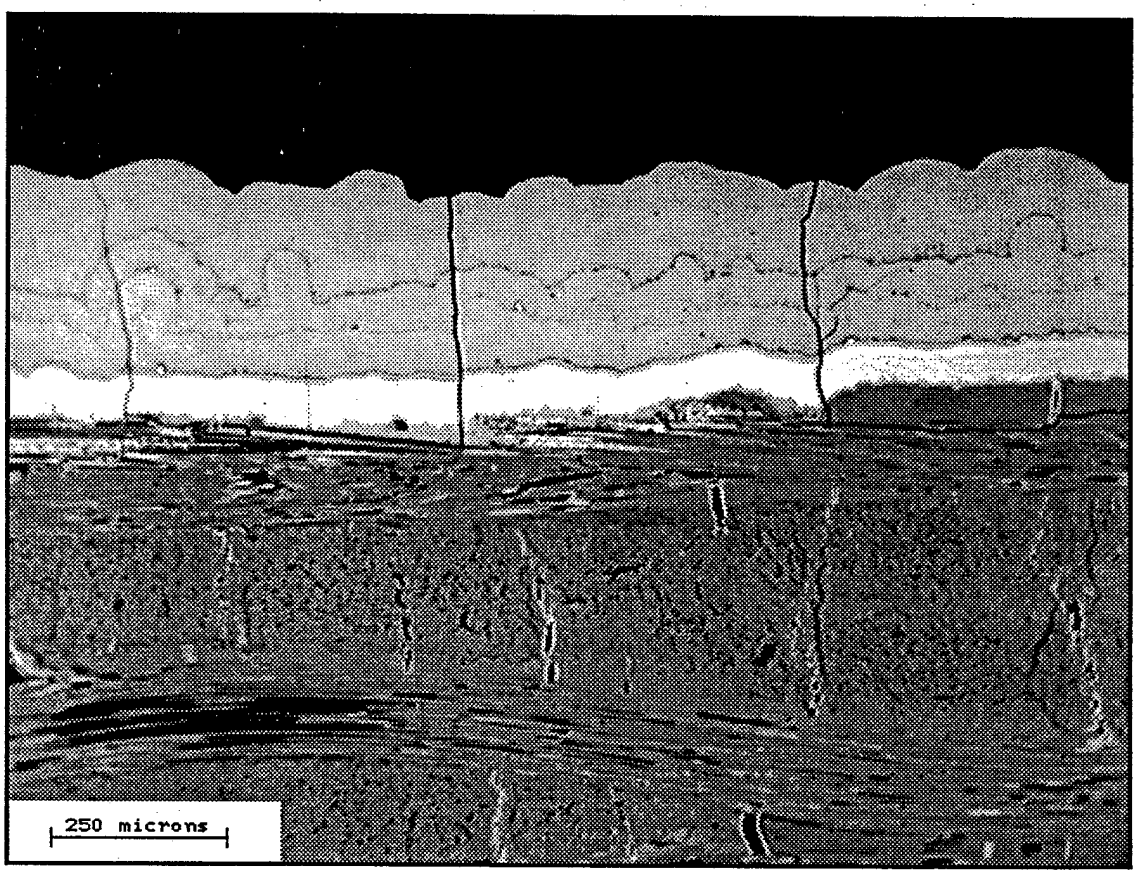

Figure 3. A polished metallographic cross-section of Hitco Specimen 1515 showing the cracked substrate, and the layered ceramic overcoat with cracks.

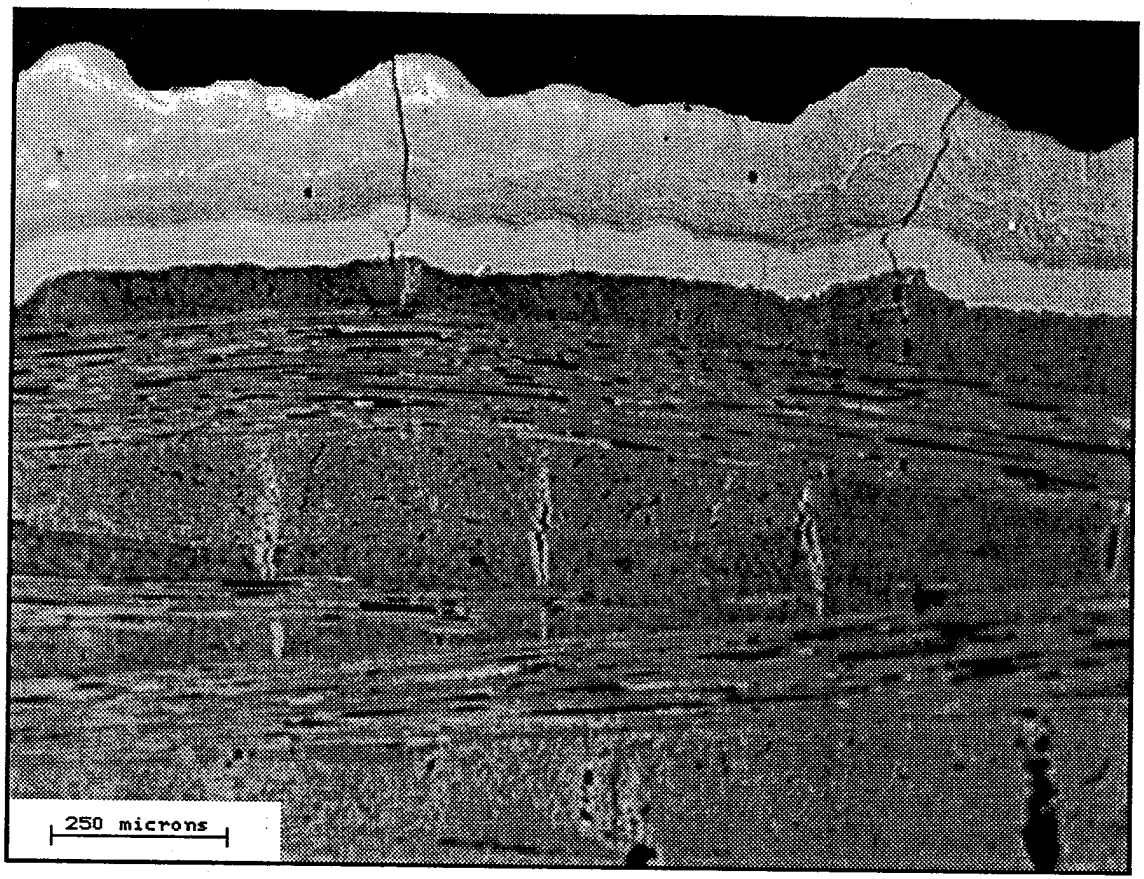

Figure 4. A polished metallographic cross-section of Hitco Specimen 1652 showing the cracked substrate, and the layered ceramic overcoat with cracks.

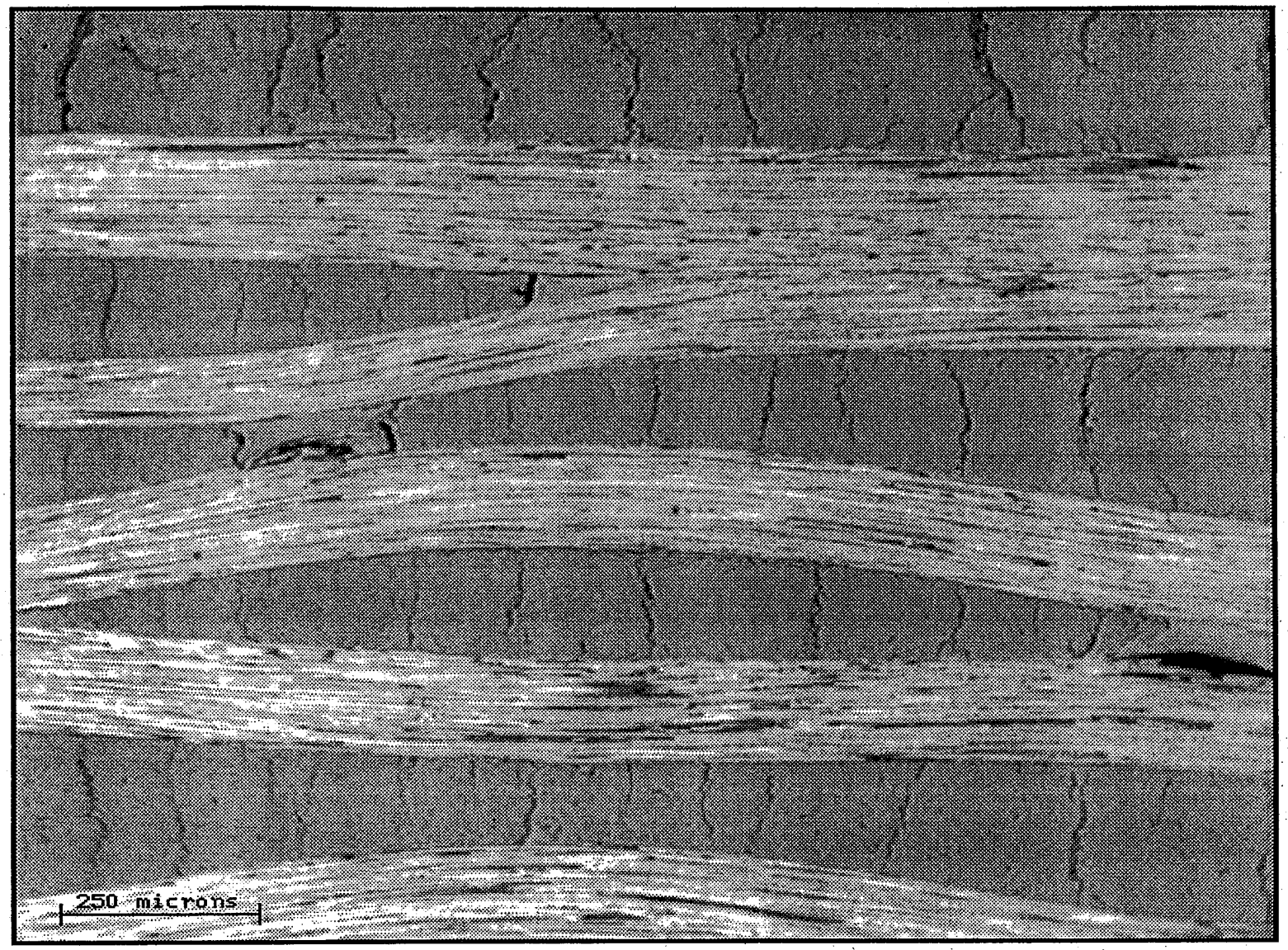

Figure 5. A polished metallographic cross-section of a coated coupon from Rohr panel No. 1.

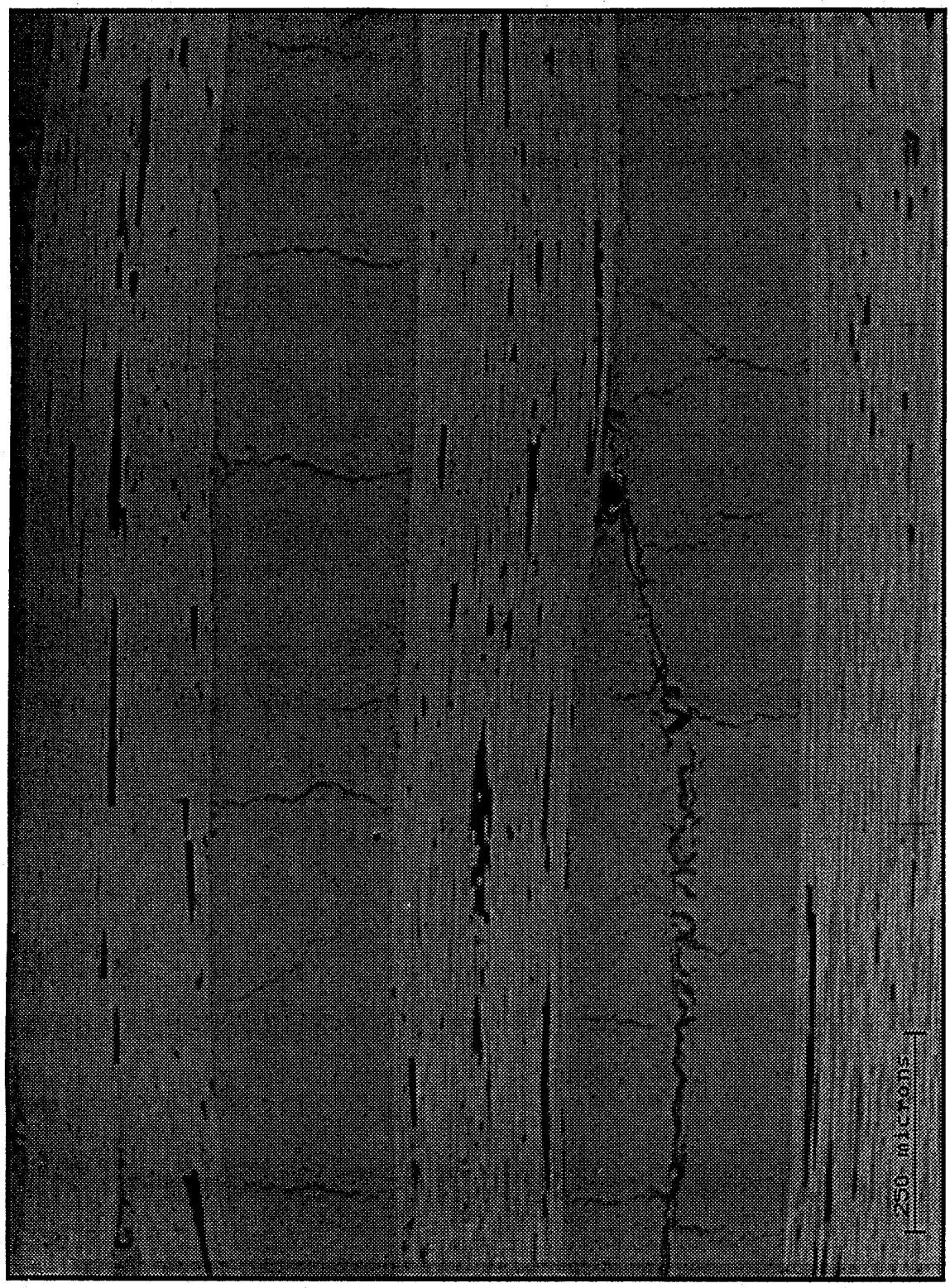

Figure 6. A polished metallographic cross-section of a coated coupon from Rohr panel No. 20.

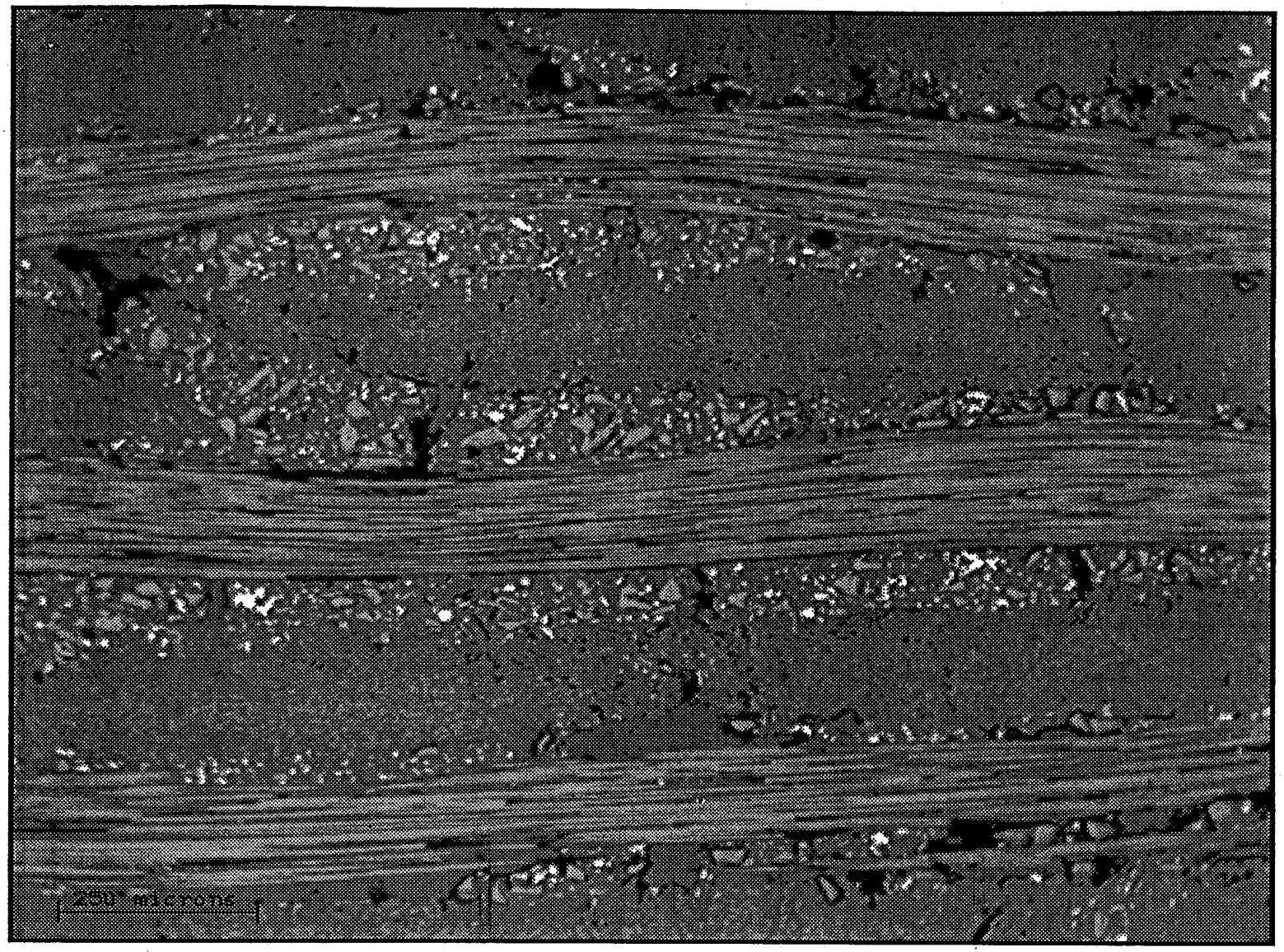

Figure 7. A polished metallographic cross-section of a coated coupon from Rohr panel No. 31.

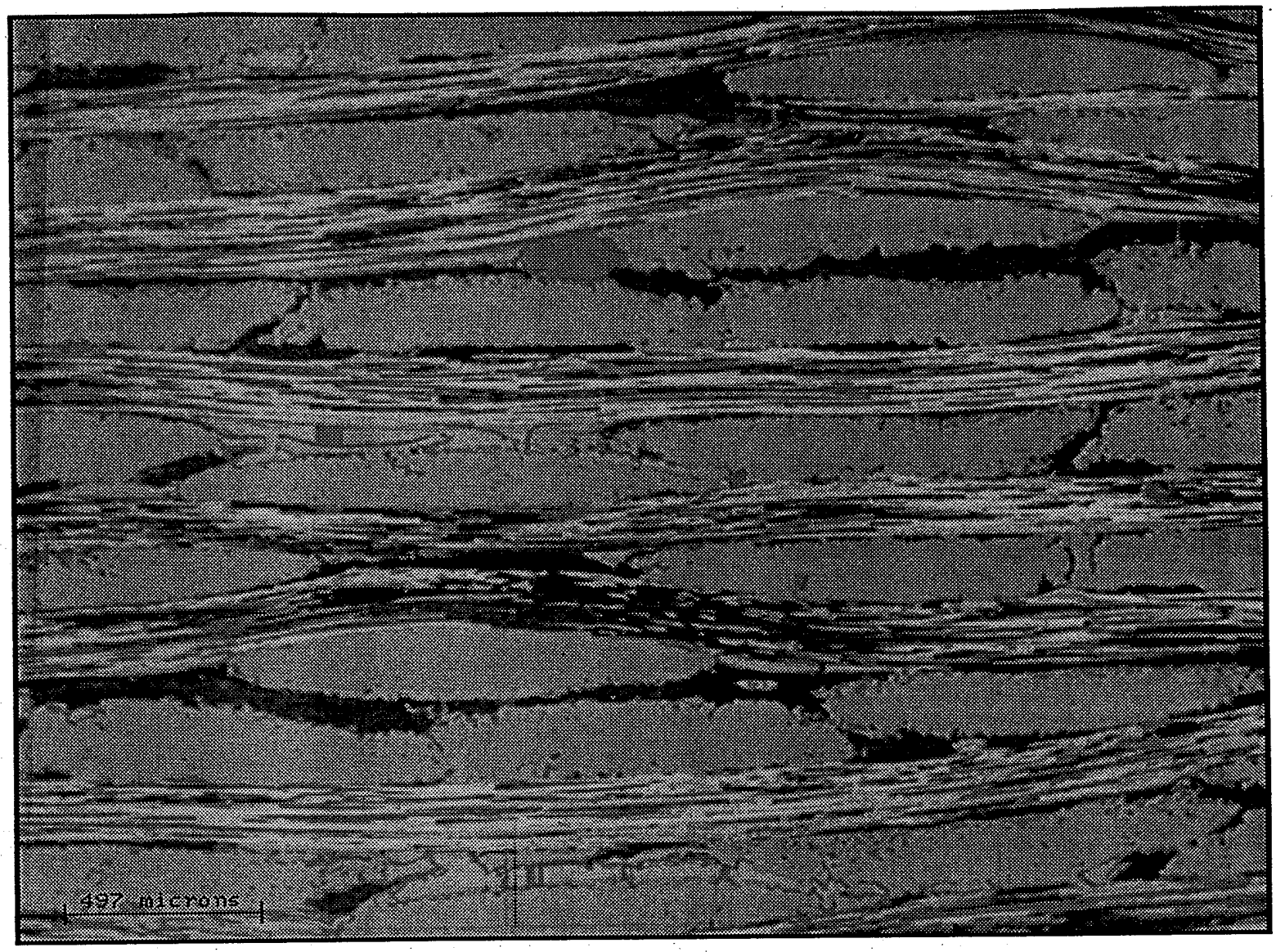

Figure 8. A polished metallographic cross-section of a coated coupon from Rohr panel No. 62.

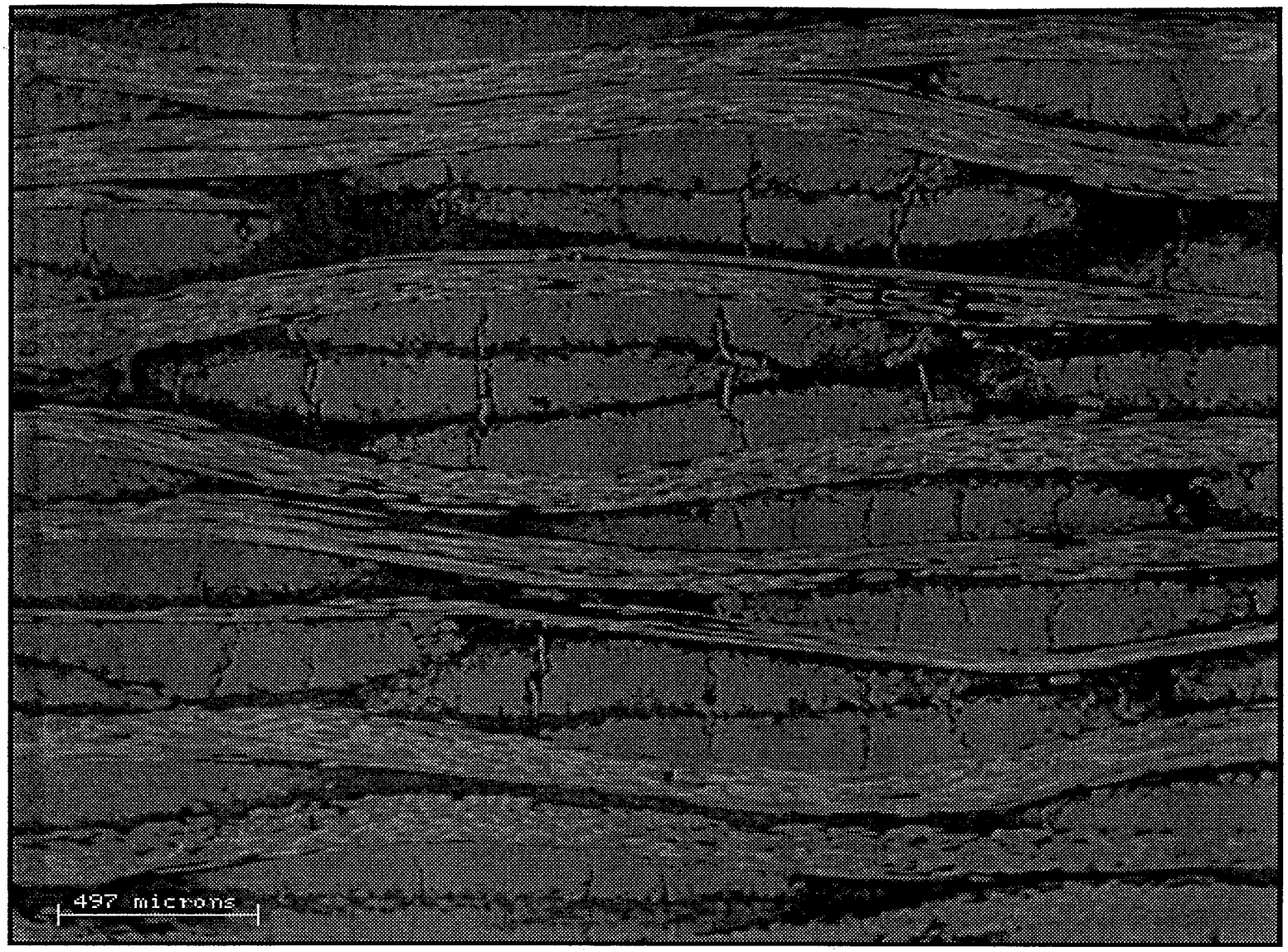

Figure 9. A polished metallographic cross-section of a coated coupon from Rohr panel No. 137.

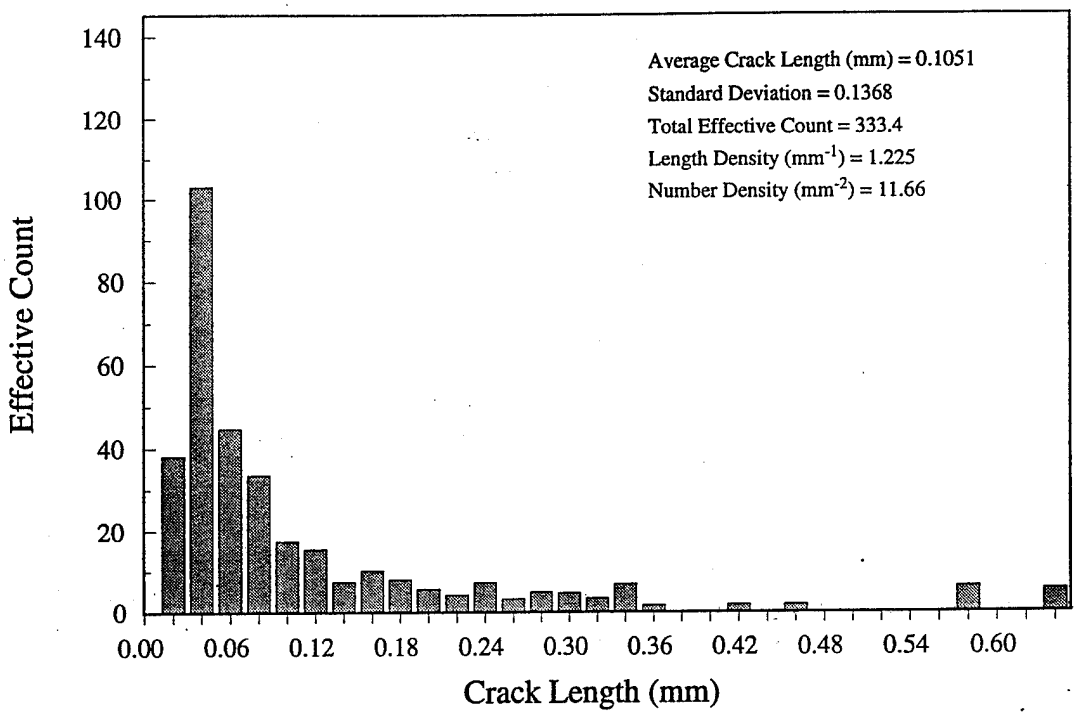

Figure 10. The measured substrate transverse crack length distribution found in Hitco coupon 1652-16.

The Rohr materials (Panels 1, 20, 31, 62, and 137) were subject to a closer examination than the Hitco coupons, including a quantification of the degree of substrate porosity, and a qualitative description of the substrate condition.

The data in Table 3 confirms the tendency for transverse bundle cracking rather than interface bundle cracks. It also would indicate that transverse bundle cracking is much more prevalent in the pitch-resin densified Rohr materials (panel 1) than in the chemical vapor infiltration (CVI) densified Hitco materials (coupon 1652).

In addition to the measurements made as shown in Tables 3 and 4, the following observations were made on the materials from Rohr Inc.

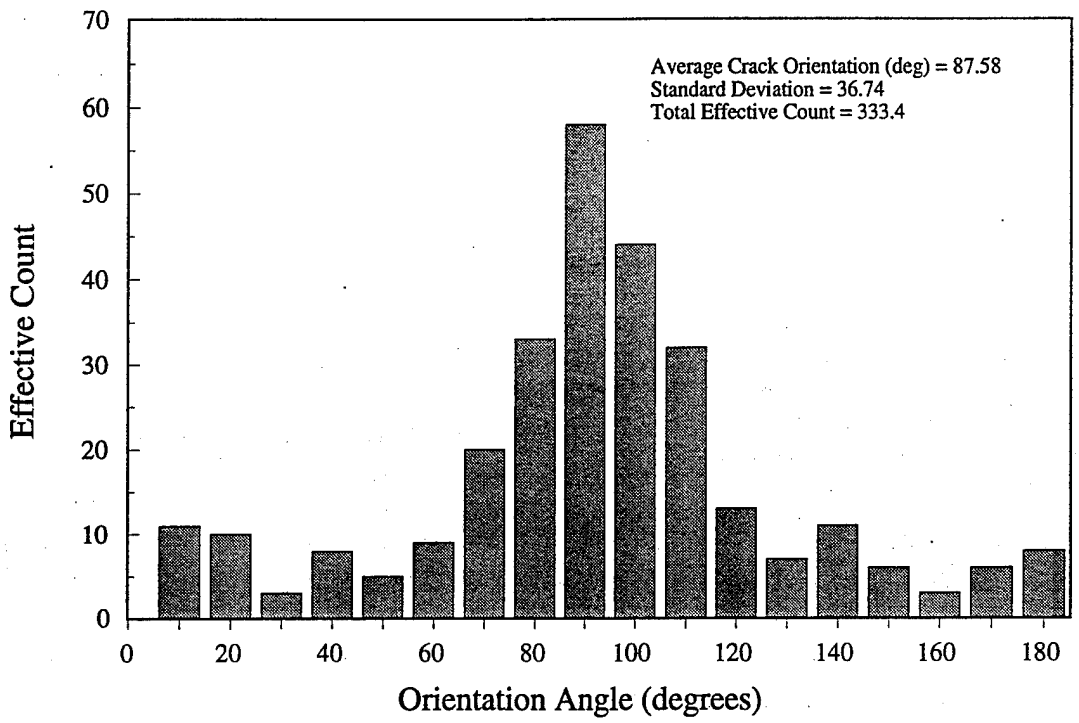

Figure 11. The measured substrate transverse crack orientation found in Hitco coupon 1652-16.

Table 3. Substrate Crack Measurements form Three Coupons

SPECIMEN ID	CRACK TYPE	AVG. LENGTH (mm).	AVG. SPACING (mm).	AVG. ORIENTATION (mm).	CRACK DENSITY (cracks/mm^2)
1652-16 Warp	Transverse	0.208	0..257	90.8	3.74
	Interface	0.057	NA	NA	0.02
1652-16 Fill	Transverse	0.269	0.223	87.3	4.21
	Interface	.084	NA	99.7	0.21
Panel 1	Transverse	0.117	NA	95.6	27.23
	Interface	0.068	NA	38.3	9.13

Table 4. Measured Values of Porosity and Fiber Fraction for the Rohr Materials

SPECIMEN ID	TOTAL POROSITY (%)	INTRABUNDLE POROSITY (%)	FIBER FRACTION (%)
1	3.8	3.5	76
20	NA	NA	80
31	21.6	19.1	47
62	3.9	0.2	71
137	3.0	2.3	73

Panel 1 (Figure 5)

This is an uninhibited matrix material, i.e., no particulates were added to the matrix during manufacture to improve oxidation resistance. Very few yarn interface cracks were observed, and there was very little fiber pullout during polishing, indicating a well-wetted fiber/matrix interface. The material appeared to have moderate density with a general low level of porosity apart from the transverse bundle cracks. These cracks were well developed, uniformly spaced, and traversed the full bundle width. Material had a high fiber volume fraction with few matrix-rich regions.

Panel 20 (Figure 6)

This was also an uninhibited matrix material, and as with Panel 1, there were very few yarn interface cracks observed. The cracking observed was comprised of very regular, fully developed, but narrow transverse bundle cracks. Overall material density appeared lower than Panel 1, but still only moderate porosity was observed with the exception of a number of large voids at the yarn bundle interfaces. Fiber volume fraction was high, but high levels of fiber pullout during specimen preparation suggested inadequate wet-out of the fiber/matrix interface.

Panel 31 (Figure 7)

Inhibited matrix material appeared dark and granular, due to the presence of the filler particulates. Two phase inhibitor mixture was visible as irregular flakes and granules within the matrix. There was poor penetration of the inhibited matrix into the fiber bundles, and the fiber volume fraction was lower than previous materials. Incomplete penetration of matrix material into the fiber bundles resulted in a high level of non-crack porosity. This material was noted as being "unusual".

Panel 62 (Figure 8)

Although the data sheet does not specify an inhibited matrix, the dark granular nature of the matrix-rich regions suggest that there is an inhibitor added. The SiC whiskers that have been added to the matrix are not visible in the micrographs, but are visible under the microscope as a dark second phase in the matrix. Whiskers appear to be only in the matrix external to the fiber bundles, they were not observed to be within the fiber bundles. There are large matrix rich regions, leading to a relatively low overall fiber volume fraction. The extensive fiber pullout during specimen preparation, even in the specimen with fluorescent epoxy impregnation, suggests that fiber/matrix bonding is poor. The porosity is quite high, as evidenced by the fluorescence micrographs. Most of the porosity is external to the fiber bundles, i.e., bundle porosity is low (Table 4). Many of the larger voids have been partially filled with additional matrix; this matrix is not inhibited, and has been through a carbonization cycle as evidenced by the volumetric shrinkage that has caused the matrix to shrink away from the original void walls. There is a moderate density of narrow transverse bundle cracks.

Material 137 (Figure 9)

Inhibited matrix, which appears also within the fiber bundles. Large matrix-rich regions, and consequent moderate fiber volume fraction. Moderate porosity; on par with typical carbon-carbons. Very few yarn interface cracks. A well developed set of transverse bundle cracks that are quite wide. These cracks have been partially filled with what appears to be uninhibited matrix material; subsequent carbonization has caused this matrix material to shrink

away from the crack walls, leaving partially filled cracks. Spacing of transverse bundle cracks larger than typical. There is moderate cracking at the fiber/matrix interface, and appears to be good fiber-matrix integrity. The yarns in this specimen are considerably more wavy than in the other specimens as indicative of the plain weave graphite fabric used for panel 137, rather than the 8 harness satin material used for all other panels.

General note: All these materials were reinforced with Heat Treated T-300 graphite fibers. Heat treatments were either 2150°C or 2650°C as noted in Table 2.

2.2 COATING MICROSTRUCTURE

General Coating Microstructure

Figures 12 and 13 illustrate section views of the coating cracks. Figure 14 shows a view of a polished planar section of the coating, with a fluorescent epoxy resin infiltrated into the coating cracks to highlight them. The details on specimen preparation are given in [10].

Of particular interest, and as observed in all the coatings sectioned, was the presence of partial cracks in the external coatings, as may be seen Figures 12 and 13. Almost all these partial cracks were found to start at the coating-substrate interface and were arrested before reaching the coating surface. This observation suggests that coating cracks nucleate at the

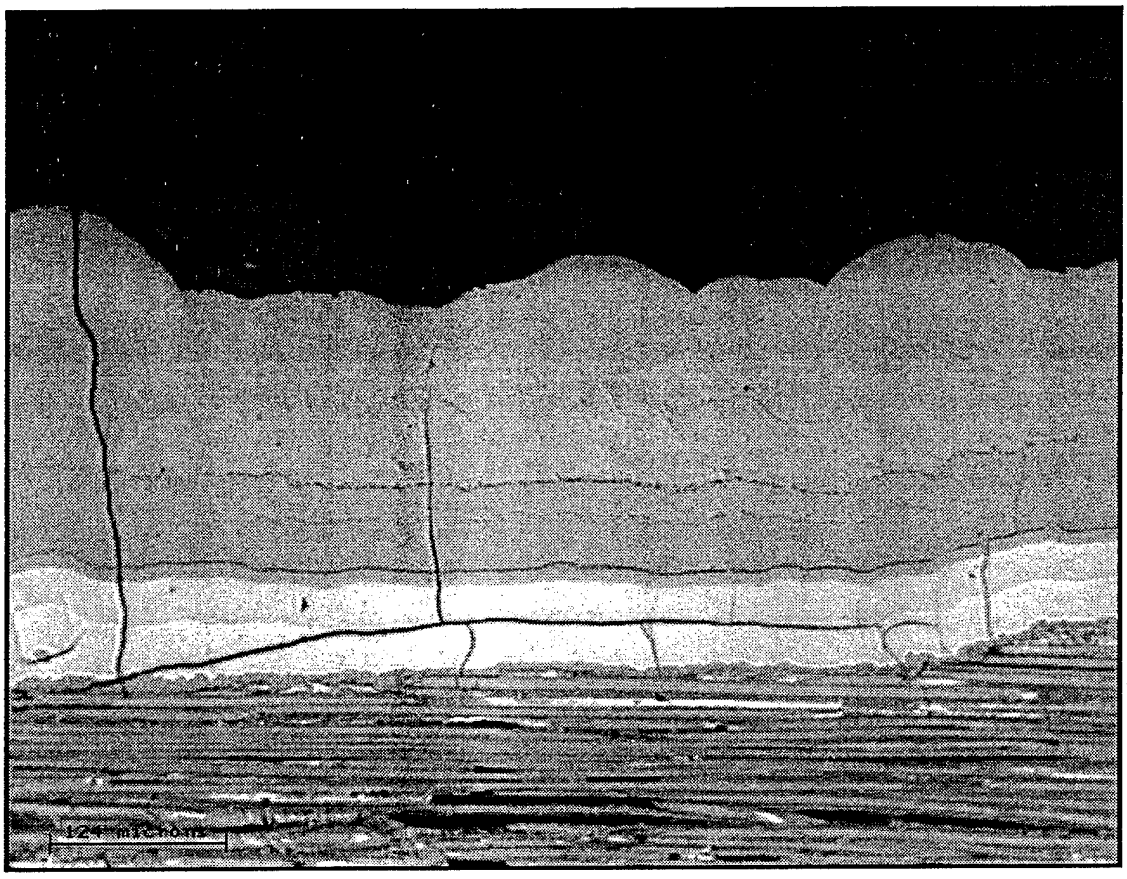

Figure 12. One of the cracking features observed in the dense ceramic overcoats was separation parallel to the substrate interface.

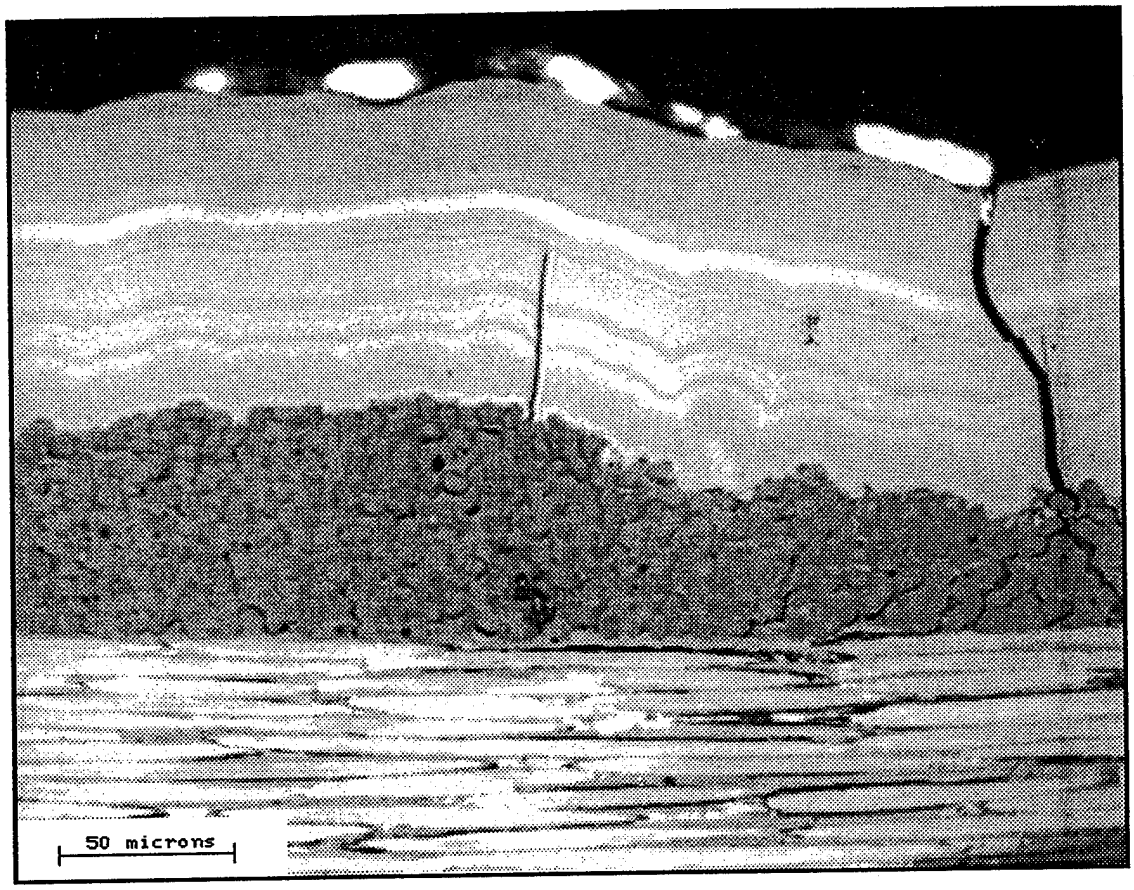

Figure 13. Another interesting feature of the overcoat cracking was the predominance of partial cracks which may have initiated at the substrate interface.

coating substrate interface. The arrest of sharp cracks part way through the brittle coating is surprising, and not yet understood. It is apparent that there must be some mechanism acting for stress relief other than continued propagation of these cracks.

Another interesting observation is the many sub-layers within the coating. In the case of Specimen 1652 , one of the sublayers is clearly due to an intentional change in the reaction gas chemistry (Figure 12). However, the sublayers are also found in specimens 1, 20, 31, 62, and 137 (Figure 13) which were reported to have been coated in a single CVD SiC run. The origin of the sublayers has been attributed to re-nucleation of crystallographic orientation of the SiC due to small fluctuations in the CVD process [11].

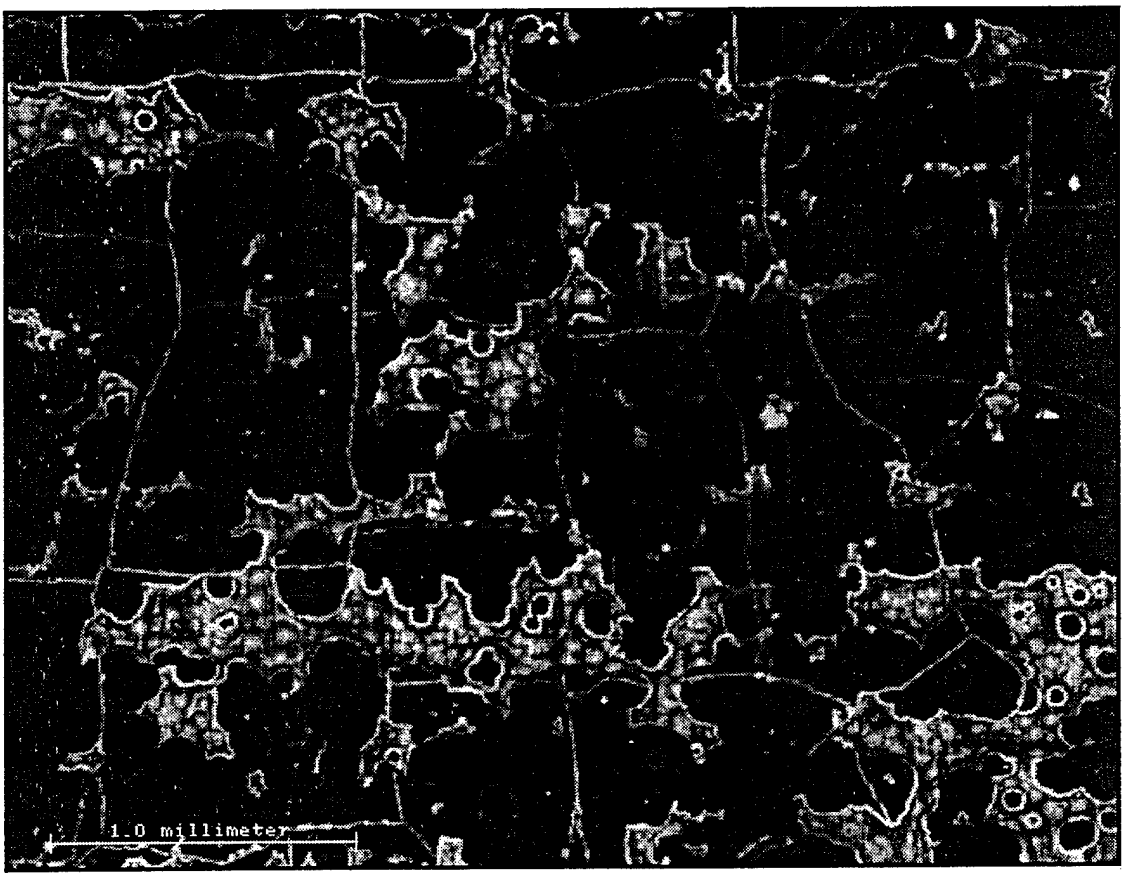

Figure 14. Fluorescent penetrant inspection of the coating crack pattern revealed a generally rectangular crack pattern oriented parallel to the specimen major axes.

Also of interest in the micrographs is the observation that cracks in the coating often extend into the substrate (Figure 13). This occurs for transverse cracks which can extend by relatively weak transverse tensile failure of the adjacent reinforcement yarn.

Coating Thickness

Coating thickness measurements are given in Table 5. Coating thicknesses ranged from 302 microns to 59 microns. The 1, 20, 31, 62. 137 specimens had significantly different coating thicknesses on the top and bottom of the coupons indicative of the one step coating

process. In the CVD process, the specimen surface directly exposed to the reactant gas path (the top surface) usually receives a thicker coating deposit than the surface in the shadow of the gas path.

Table 5. Measured Coating Thicknesses - All Coupons

SPECIMEN ID	SIDE OR LAYER	AVG. THICKNESS (microns)[1]	STD. DEV. (microns)
1515	First Layer	64	12
	All Layers	302	39
1652	First Layer	66	6
	All Layers	279	28
1	A	72	7
	B	147	27
20	A	142	21
	B	82	20
31	A	120	17
	B	59	8
62	A	194	36
	B	93	9
137	A	66	7
	B	112	13

1. Average of at least 20 measurements

Crack Spacing and Lineal Density

Figure 15 gives the distribution of through-crack spacing for specimens 1515 and 1652. A related measure of crack spacing is the lineal density; these measurements are reported in Table 6. In some cases a distinction is made between longitudinal and transverse cracks.

Crack Orientation

Figure 16 shows the orientation distribution of the maximum feret dimension, i.e., the diagonal length of a crack cell. Of particular interest in this figure is the bimodal distribution with peaks at 45° and 135°; this quantifies the rectangular nature of the cells and their preferred orientation with respect to the weave geometry and/or the major specimen axes.

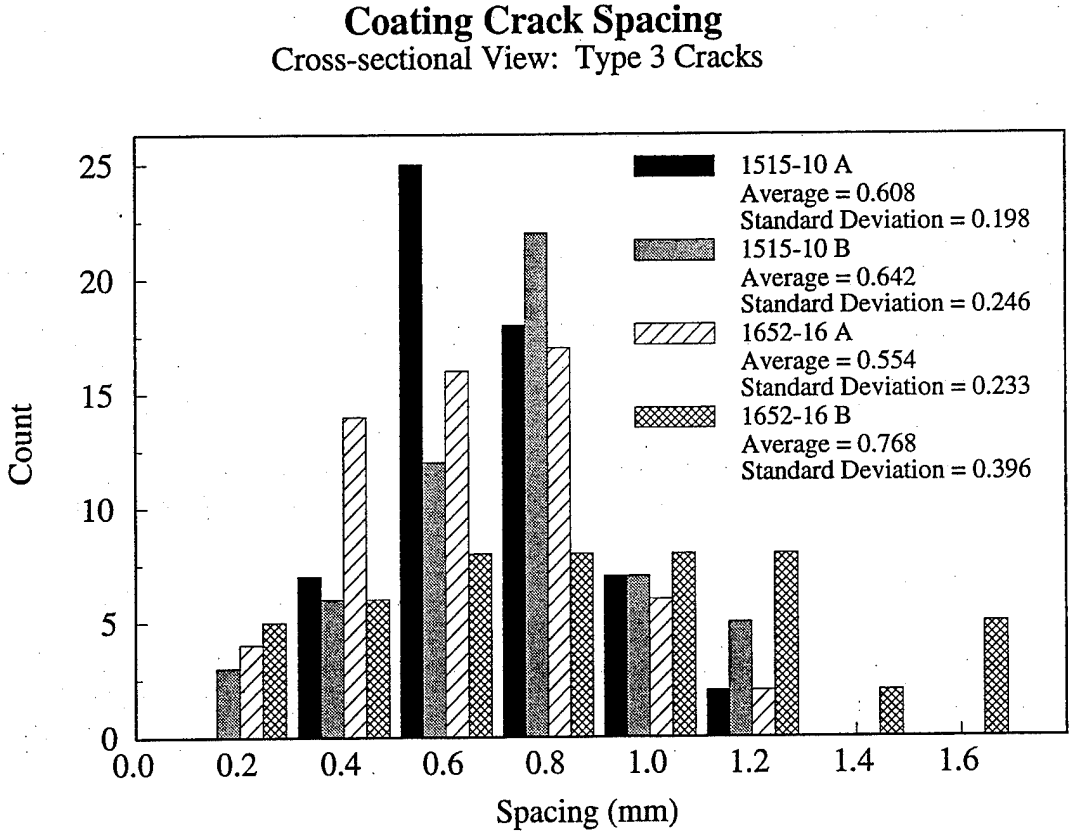

Figure 15. The average through crack (Type 3) spacing for the two Hitco coupons examined was between 0.55 and 0.77 mm (20 - 30 mils).

Table 6. Average Lineal Crack Densities - All Coupons.

COUPON ID	CRACK TYPE	SIDE	TRANSVERSE AVG. LINEAL DENSITY (mm^{-1})	LONGITUDINAL CRACK AVG. LINEAL DENSITY (mm^{-1})	ALL CRACKS AVG. LINEAL DENSITY (mm^{-1})
1515	All	NA	3.78	4.61	4.41
	Full Through	NA	1.36	1.66	1.58
1652	All	NA	4.19	5.82	4.71
	Full Through	NA	1.34	1.86	1.52
1	All	A	1.56	4.54	1.77
	All	B	2.22	3.36	2.41
20	All	A	1.56	2.68	2.48
	All	B	2.38	3.47	3.20
31	All	A	1.78	3.20	2.99
	All	B	2.15	3.46	2.28
62	All	A	1.73	2.21	2.14
	All	B	1.58	2.24	1.64
137	All	A	2.02	3.95	2.88
	All	B	1.71	3.06	2.57

Crack Width

Table 7 gives the average crack widths for all of the specimens. As seen in the micrographs, it was found that the crack width was uniform across the whole coating thickness, so no distinction was made in terms of where the crack width was measured, i.e., at the top or bottom of the crack. A distinction was made between transverse and longitudinal cracks, since there appeared to be an effect from the adjacent substrate reinforcement bundles. The implications of these results are discussed in a later section.

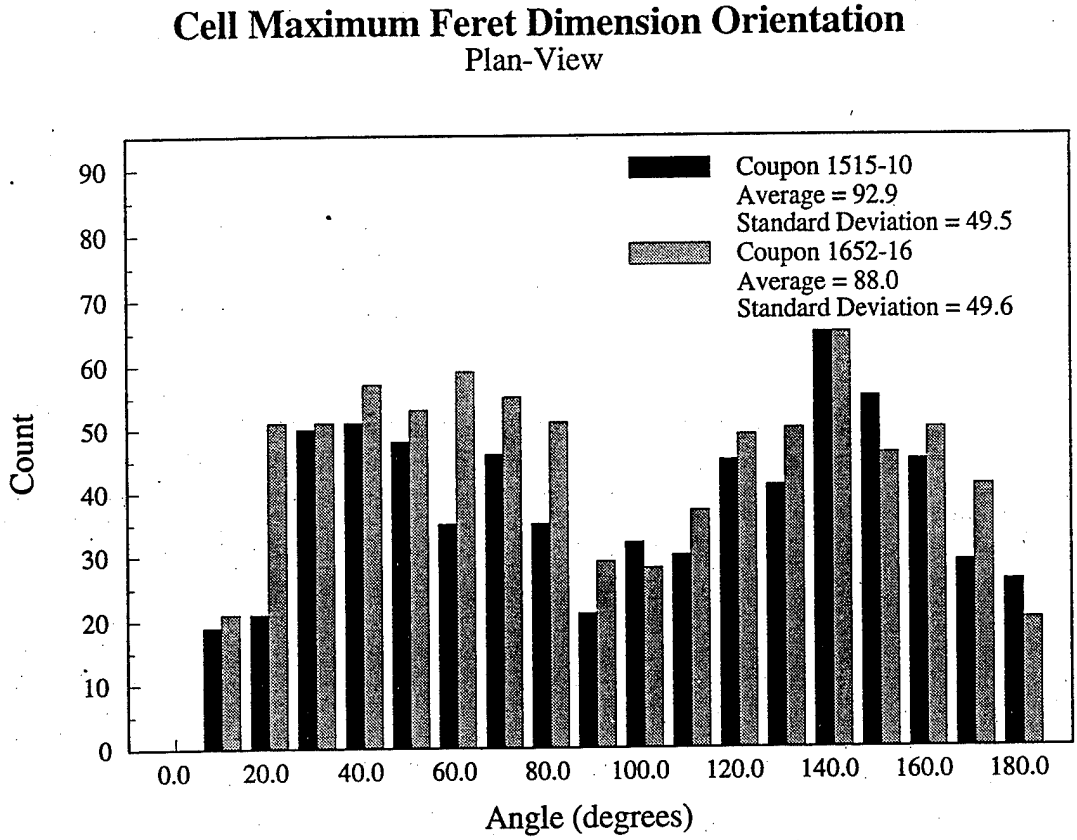

Figure 16. The rectangular orientation of the crack pattern was confirmed by the bimodal distribution of the maximum feret orientation at 45° and 135°.

Figure 17 shows the distribution of crack widths in specimens 1515 and 1652. The distribution of crack widths is quite broad, with narrower cracks being more frequent than wider cracks. The latter observation suggests that there are even finer cracks present, below our observation resolution.

Table 7. The Average Crack Width Data - All Coupons

SPECIMEN ID	SIDE	AVG. CRACK WIDTH, LONGITUDINAL (microns)	AVG. CRACK WIDTH, TRANSVERSE (microns)	AVG. CRACK WIDTH, ALL CRACKS (microns)
1515	NA	0.95	1.96	1.72
1652	NA	0.98	2.55	2.05
1	A	1.34 (std 0.69)	3.27 (std 1.72)	3.13
	B	1.85 (std 0.89)	2.96 (std 1.84)	2.78
20	A	1.74 (std 0.77)	2.30 (std 1.11)	1.84
	B	1.42 (std 1.14)	2.66 (std 1.23)	1.73
31	A	1.56 (std 0.79)	4.12 (std 2.41)	1.94
	B	0.72 (std 0.56)	2.96 (std 1.57)	2.74
62	A	2.51 (std 1.66)	4.20 (std 1.05)	2.77
	B	2.34 (std 1.09)	3.84 (std 3.27)	3.71
137	A	1.45 (std 0.95)	3.43 (std 1.64)	2.55
	B	1.55 (std 0.90)	2.32 (std 1.08)	1.83

Crack Area Density

Crack area/unit substrate area is a measure of the exposed substrate area due to cracks in the coating. This quantity was measured in two ways. For specimens 1515 and 1652, the availability of plan view data made possible the estimate of crack area density by multiplying the measured crack length (in a unit substage area) by the average crack width. The unavailability of plan view data for the remaining specimens required that crack area density be estimated by multiplying the crack lineal density by the average crack width. If the crack orientation distribution is isotropic, this result provides a good estimate of crack area density. From qualitative observations of the coating crack plan view, the assumption of isotropy appears reasonable for these specimens.

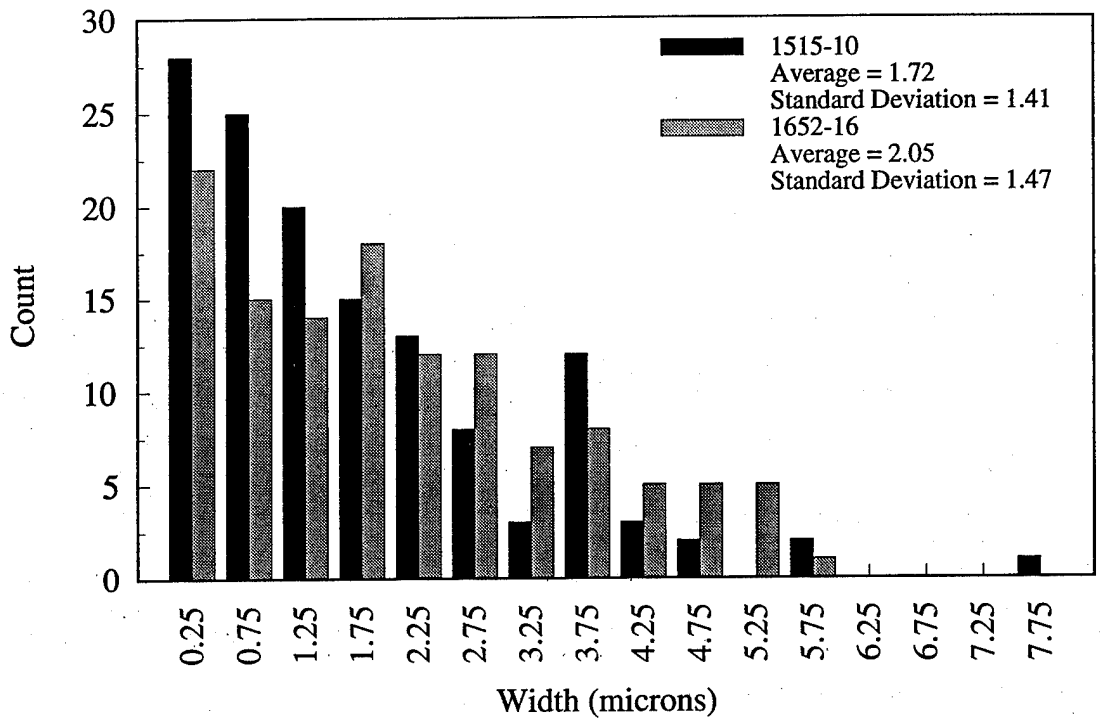

Figure 17. Scanning electron microscopy measurement of the crack widths in the Hitco coupons showed average widths of the order of 1.7 to 2.0 microns (0.065 to 0.08 mils).

The results of this analysis showed a crack areal density of between 0.005 and 0.013 mm^2/mm^2 of open crack area. If the crack area density is predicted simply by assuming that all of the thermal strain mismatch between coating and substrate is relieved by cracks in the coating, the predicted crack area density is .0084 mm^2/mm^2. This calculation was made assuming the CTE is 1.0e-6 for the substrate, the CTE is 4.6e-6 for the SiC coating, and that the deposition temperature was 1100°C. However, even with these assumptions, it is apparent that there is general agreement between the measured crack area densities and the predicted open crack areas based the thermal strain considerations only.

Correlation of Crack Data

Several previous analyses have suggested that the coating crack pattern (orientation, number, and width of cracks) will depend on the coating thickness [10,11]. To test these analyses, the measured crack data from the seven coupons examined in this work was correlated against coating thickness measurements. Figures 18 and 19 show lineal crack density against coating thickness, for cracks adjacent to transverse reinforcement and longitudinal reinforcement. From the data presented in these figures, it would appear that there was no strong correlation between crack spacing and coating thickness, for either crack

Correlation of coating crack lineal density against coating thickness

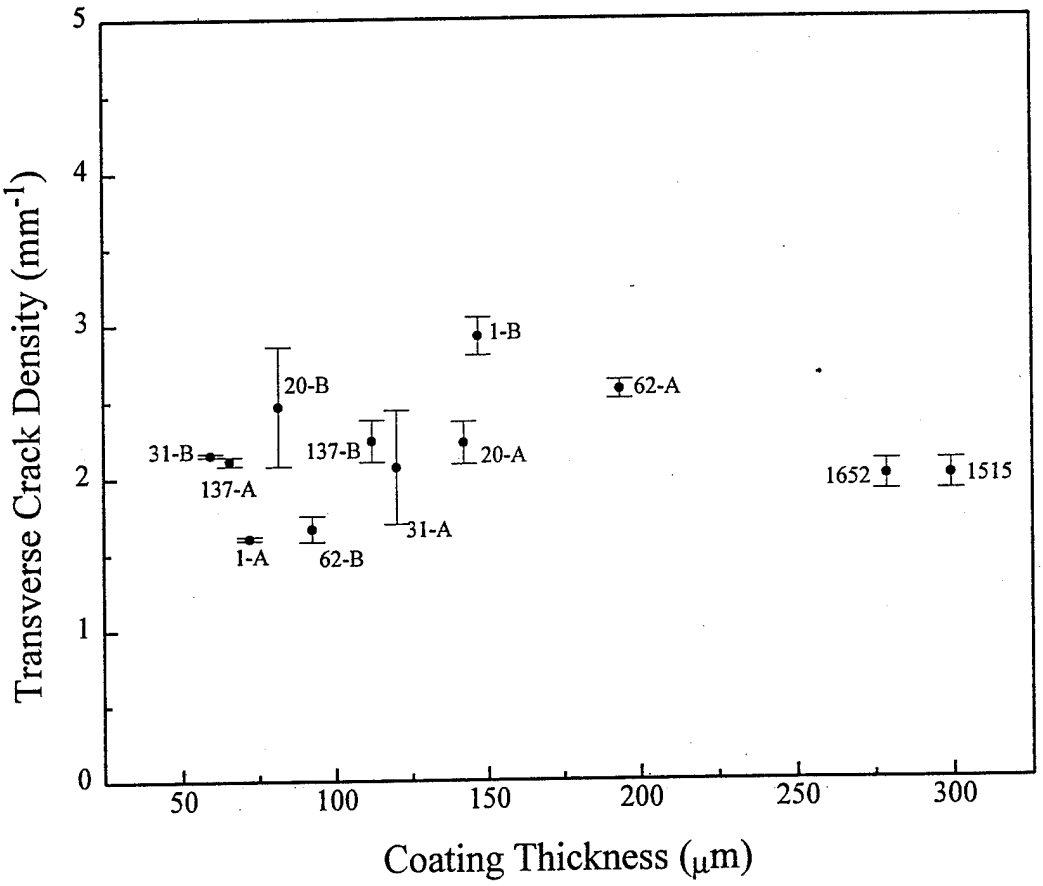

Figure 18. There was little correlation between transverse coating crack density and coating thickness for all the seven coupons examined.

Correlation of coating crack lineal density against coating thickness

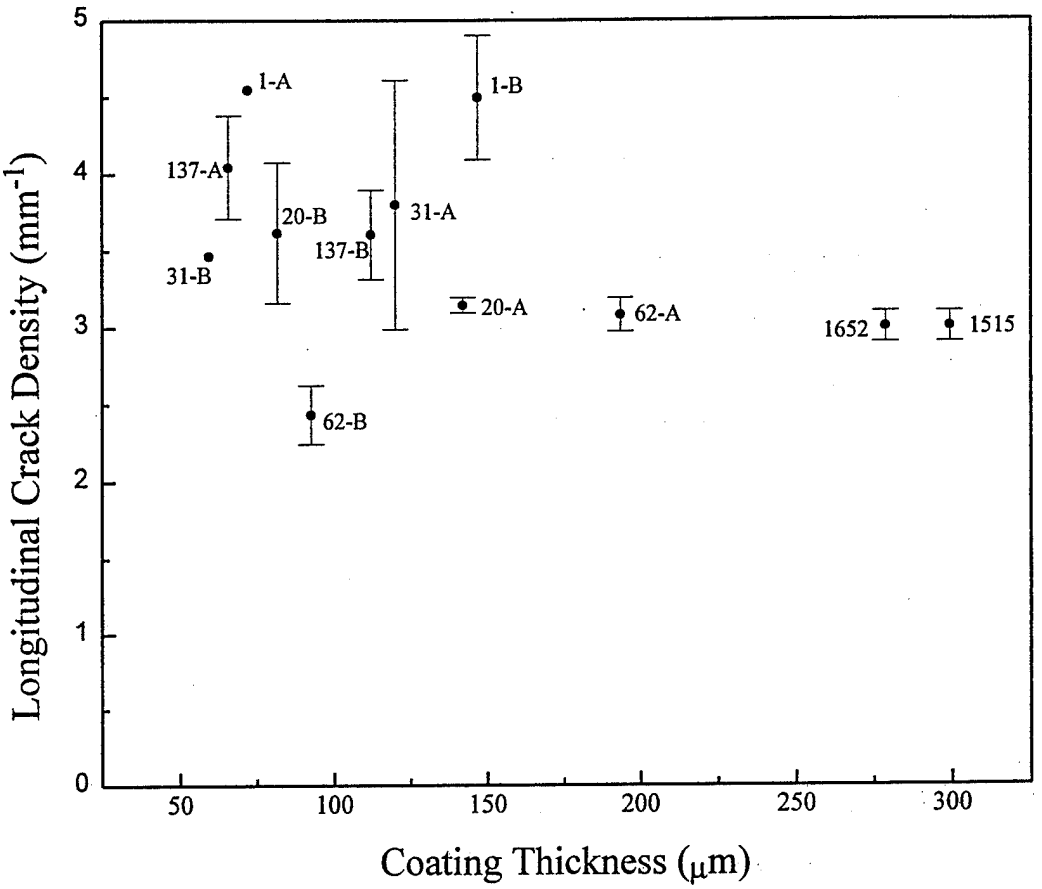

Figure 19. There was little correlation between longitudinal coating crack density and coating thickness for all the seven coupons examined.

type. However, it should be noted that the longitudinal crack density is approximately twice as large as the transverse crack density.

A plot of the percentage of through-cracks as a function of coating thickness is given in Figure 20. Unlike the previous correlations, the results presented in this figure do show a strong inverse dependence on coating thickness. As coating thickness increases, the likelihood of a crack penetrating through the coating decreases, i.e., the number of partial cracks increases. The mechanism of partial crack formation is not understood, but it may be related to multi-layer coatings whereby cracking in the first layers and propagation into the substrate provide sufficient strain relief to limit crack propagation through the coating as subsequent layers are deposited.

Correlation of partial cracks coating cracks to coating thickness

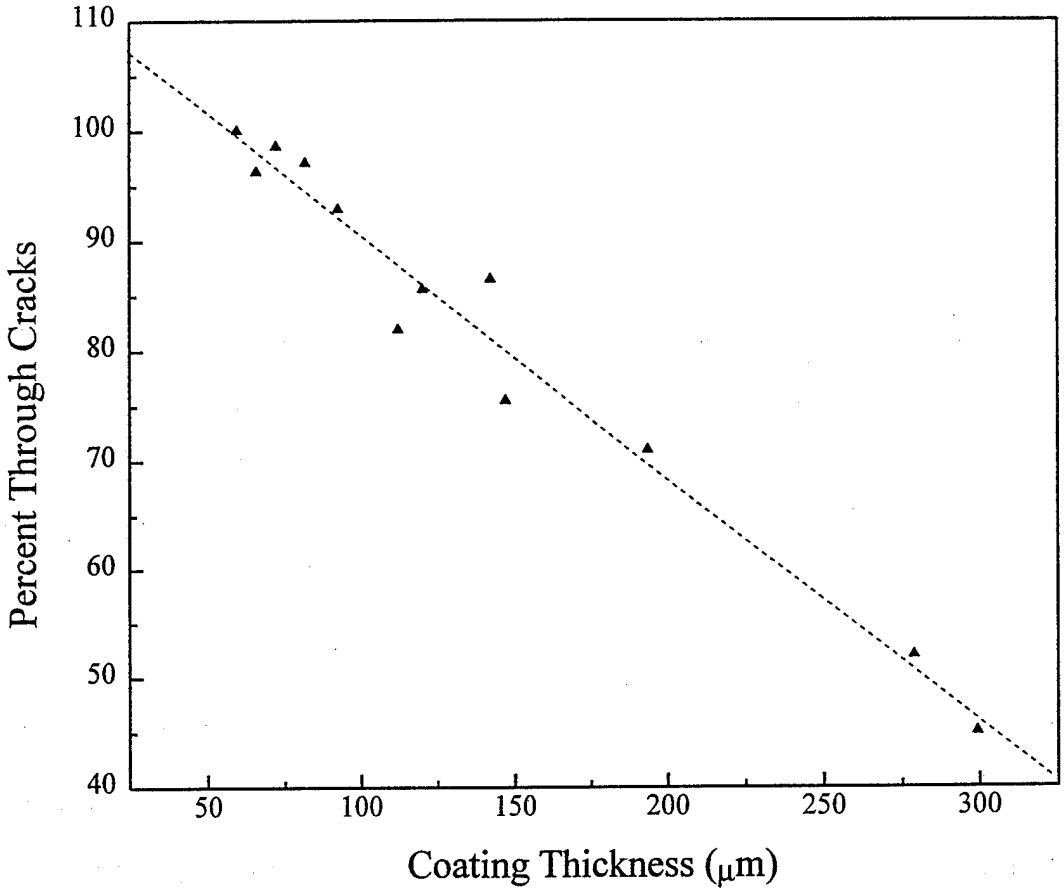

Figure 20. There did appear to be an inverse correlation between coating thickness and crack penetration.

Figures 21 and 22 show the relationship between crack width and coating thickness. As with the crack spacing data there is no strong dependence between crack width and coating thickness. However, it should be noted that the crack width of longitudinal cracks is less than the width of transverse cracks. Recalling that the lineal density of longitudinal cracks was higher than the transverse crack density, then this would indicate that increased density is compensated for by the reduced crack width, and that the total open crack area remains constant. This difference in crack width may be related to the modulus of the underlying material. Longitudinal cracks are constrained from opening freely by the high stiffness longitudinal bundles, while the transverse cracks are less constrained by the low modulus in the transverse bundle direction, and are able to open more fully.

Correlation of coating crack width to coating thickness

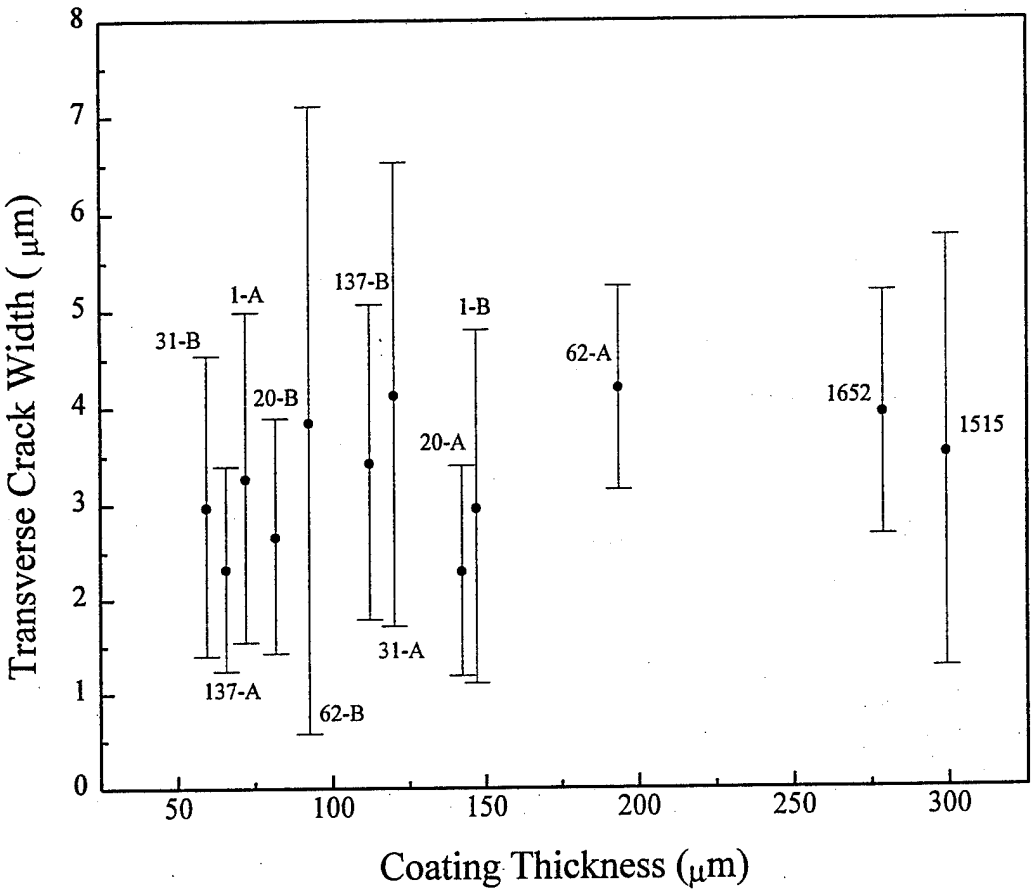

Figure 21. There was little correlation between transverse coating crack width and coating thickness for all the seven coupons examined.

This speculation is supported by Figure 23, which shows the coating crack areal density plotted against coating thickness. This figure would indicate that crack area density is independent of coating thickness. Also shown on the Figure 23, by the horizontal dashed line, is a predicted open crack area based on a very simple assumption that the total thermal strain mismatch is relieved by cracking.

Correlation of coating crack width to coating thickness

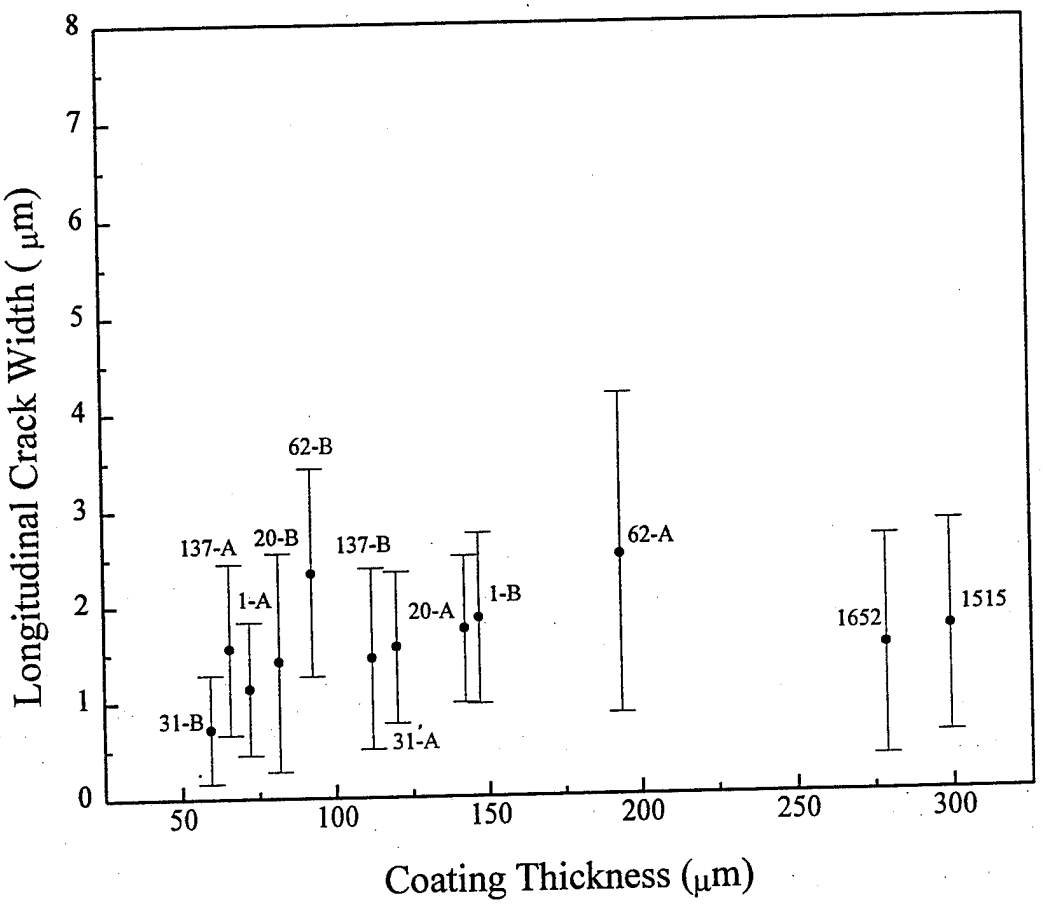

Figure 22. There was little correlation between longitudinal coating crack width and coating thickness for all the seven coupons examined.

2.3 SUMMARY

Within the range of the seven coated ORCC coupons evaluated, two general conclusions may be reached with regard to the substrate crack pattern and the crack network in the coatings:

1. The crack area density results provide strong evidence that there is a one-to-one correspondence between the open crack width, and the thermal mismatch strain between the coating and substrate. Within

Correlation of crack area density to coating thickness

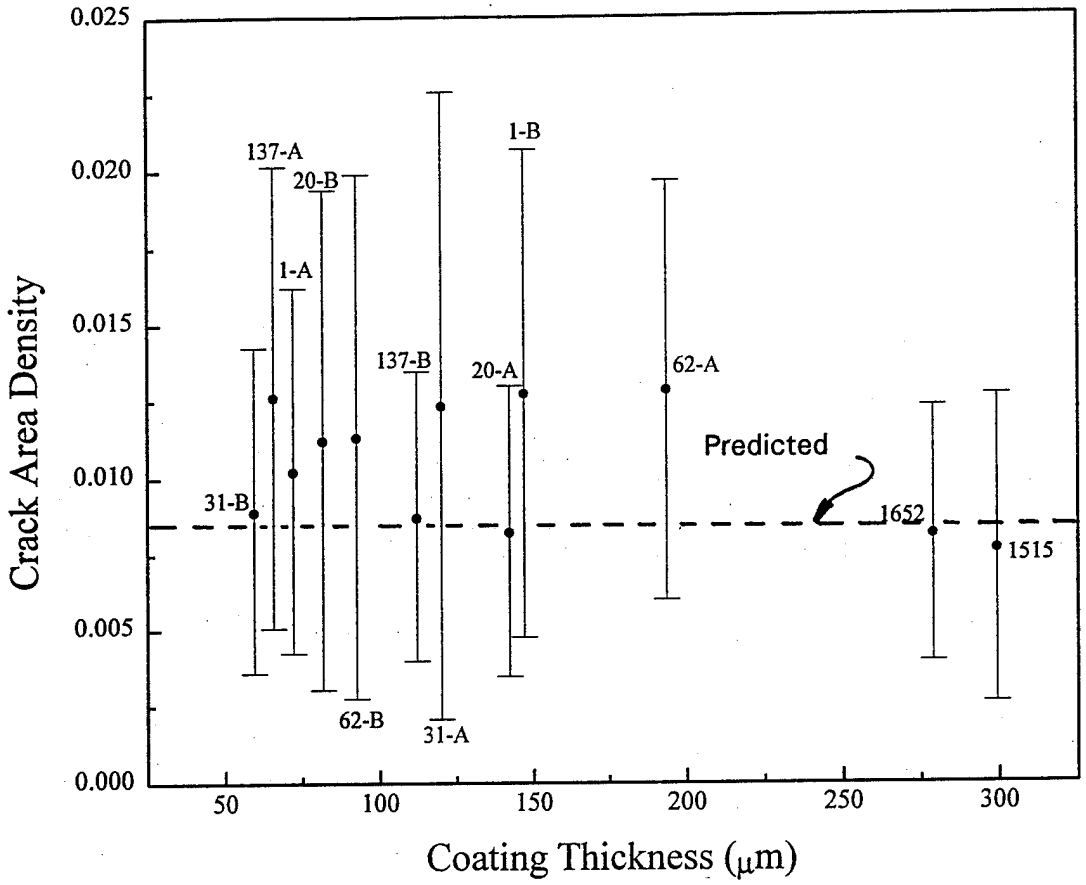

Figure 23. The measured open crack areas generally fell within the range of expected values based on consideration of the thermal strain mismatch between coating and substrate on cooldown from processing.

the range of specimens examined there was no evidence that this cracking could have been avoided. However, there were differences in the details of the coating crack morphology about which crack management strategies may be developed.

2. Coating thickness did not appear to influence the coating crack morphology in any way, except for the likelihood of thicker cracks to form partial cracks. The presence of these cracks illustrate an interesting phenomenon, i.e., crack arrest in a brittle ceramic materials.

3.0 MICRO-MECHANICS OF OXIDATION PROTECTION (MMOP) MODEL

The objective of the MMOP modeling task was to develop a set of tools whereby the impact of various oxidation protection concepts on the thermo-mechanical response of carbon-carbon substrates could be determined. Changes in the substrate thermo-mechanical properties are of interest for optimization of structural performance, and also for optimization of external coatings.

The development of a modular analysis scheme is essential to the utility and efficiency of a uniform design method. The development of analytical models for the design and analysis of basic (non-ORCC) carbon-carbon substrates has been at the core of Materials Sciences Corporation's activities over the last 20 years, and the modular framework and basic modules are already in existence, as described in [12, 13]. However, there is the need to address changes in substrate properties caused by ORCC material modifications which this program addresses. The individual features of the ORCC concepts were developed as add-on modules to the existing analysis capability which may be turned on and off as required. Incorporation into the existing framework provides a vehicle for integration of the MMOP results into a macro-mechanics analysis as required for investigation of substrate/coating interactions.

During the course of this program, three separate, but compatible MMOP modules were developed:

1. A thermal stress analysis module for determining the state of stress in and around matrix inclusions (crack fillers);
2. An oriented crack module for predicting the effects of oriented cracks (filled and unfilled) on the fiber bundle and the composite thermo-mechanical properties; and
3. A coated fiber module for determining the effects of fiber coating materials and thicknesses on the ORCC bundle and composite thermo-mechanical properties.

The details of these modules are given in the following sections.

3.1 THERMAL STRESS OF INCLUSIONS

The severe temperature cycles and very large volumetric changes associated with pyrolysis of the matrix during the carbon-carbon manufacturing process give rise to a multiplicity of cracks within and between the fiber bundles in the finished composite, as shown in Figure 2. The preferential size, shape, and orientations of these cracks was fully documented during Prof. Yurgartis' activities at Clarkson, as described in the previous section.

An important aspect of oxidation protection of C-C composites is the filling out of internal cracks and voids with SiC. The purpose of this procedure is the prevention of oxidation of the free surfaces of the cracks and voids. It is well known that cracks and voids in homogeneous materials which are subjected to uniform temperature changes do not give rise to thermal stresses. The cracks and pores in the interstitial matrix are sufficiently large with respect to microstructure dimensions to regard them as being situated in a homogeneous material. This is also true, though to a lesser extent, for the cracks in the fiber bundle. Thus, uniform temperature changes would not produce thermal stresses of any significance near these cracks and voids.

The situation becomes entirely different when these voids are filled in with SiC, or Si3N4 (two proposed oxidation protection concepts) for now they become high expansion inclusions in a low expansion matrix. In this case, temperature changes will produce internal stresses. Tensile thermal stresses at the inclusion/matrix interface may produce separation of inclusions from the matrix, which would result in a re-exposure of the "sealed" carbon crack surface to oxidative attack. This motivates the analysis of the thermal stresses near and inside the various matrix inclusions in order to investigate the effectiveness of such an oxidation protection concept.

Analytical Approach

There exists a large amount of literature on the stress analysis of inclusions embedded in large bodies with remote uniform strain or stress prescribed. As described, for example, in [14]. By contrast, there is only scant literature on thermal stress analysis of inclusions. In the course of the present research, a novel method was devised for the thermal stress

analysis of inclusions which converts the thermoelastic problem into an isothermal elasticity problem.

The general result is as follows: Consider an elastic body of material 1 in which there are embedded elastic inclusions of material 2. The composite body is subjected to a uniform temperature change ϕ and the surface displacements are prescribed as $u(S) = u^o$.

Let the thermoelastic solution in the phases 1, 2 be denoted $u^1(x)$, $u^2(x)$. Then the thermoelastic solution can be expressed as

$$u^1 = \tilde{u}^1 + \beta x \qquad (1)$$
$$u^2 = \tilde{u}^2 + \beta x$$

where $\tilde{u}^1$, $\tilde{u}^2$ are phase displacements for the isothermal elasticity problem with displacement boundary condition

$$\tilde{u}(S) = u^0(S) - \beta x (S) \qquad (2)$$

The second rank tensor β is defined as

$$\beta = -(C^2 - C^1)^{-1} (\Gamma^2 - \Gamma^1) \phi \qquad (3)$$

where C is elastic moduli tensor and Γ is thermal stiffness tensor which define the thermoelastic stress strain relations.

Thus

$$\sigma = C\epsilon + \Gamma\phi \qquad (4)$$
$$\Gamma = -C\alpha$$

Filled Matrix Crack

This refers to cracks (a) above which are filled out with SiC. The cracks will be modeled as very flat oblate spheroids of radius a and small diameter 2c, Figure 24. The problem then is to find the thermal stresses in and near such a spheroidal inclusion when the temperature is uniformly changed by an amount ϕ.

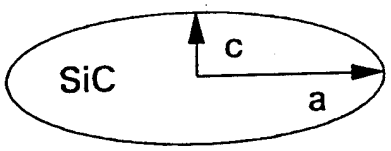

Graphitic Matrix

Figure 24. The inclusions were represented as spheroidal particles within a graphitic matrix.

On the basis of the previously summarized general solution, the problem can be solved in terms of the well known solution for a spheroidal inclusion with remote uniform strain. Thus, the strain $\epsilon^{(2)}$ in the inclusion for the present problem is given by

$$(SS^1C^2 - S + I)\,\epsilon^2 = S(S^1C^2 - I)\,\beta + \alpha^1\varphi \tag{5}$$

where

- S - Eshelby Tensor
- S^1 - Matrix Compliance
- C^2 - Inclusion Stiffness
- ϵ^2 - Inclusion Strain
- I - 4th Rank Unit Tensor
- α^1 - Matrix Thermal Expansion Tensor

For an **isotropic** matrix and inclusion, these equations assume the form

$$\left[\frac{1}{3}\left(\frac{k_2}{k_1} - \frac{G_2}{G_1}\right)S_{ijmm}\,d_{kl} + \left(\frac{G_2}{G_1} - 1\right)S_{ijkl} + I_{ijkl}\right]\epsilon_1^2 = \left[\frac{k_2\alpha_2 - k_1\alpha_1}{k_1}\,S_{ijmm} + \alpha_1 d_{ij}\right]\varphi \tag{6}$$

where k and G are bulk and shear modulus, respectively.

A sample calculation has been performed for the case of a SiC inclusion of aspect ratio c/a = 0.1 which is embedded in ATJ graphite isotropic matrix. Note that the tensile ultimate stress of such a matrix is only 500 psi. It was found that for a temperature cooldown of 2000°F, the stress normal to the surface of the inclusion varies within the limits 880, 8300 psi. It follows that the inclusion will separate from the matrix on its entire surface and thus the oxidation protection fails.

Filled Bundle Crack

Bundle cracks (b) observed are long cracks parallel to the fibers which are assumed to be cylindrical with generator in fiber direction and flat elliptical in the transverse plane of the bundle, Figure 25. It is further assumed that the crack length is large enough compared to fiber diameters so that it may be assumed that the material surrounding the crack is transversely isotropic with the effective properties of the unidirectional bundle material. The crack is now filled out with isotropic SiC inhibitor material. Thus the problem activity is modeled as the thermoelastic analysis of an isotropic elliptic cylinder which is embedded in a transversely isotropic matrix.

Note that the general solution for the thermal inclusion problem as given by (5) is applicable to the present problem with the following interpretation.

S^1 - Transversely isotropic compliance tensor of "matrix" (unidirectional bundle)

C^2 - Isotropic stiffness tensor of SiC

α^1 - Transversely isotropic TEC of "matrix"

S - Eshelby tensor for elliptical cylindrical region in transversely isotropic matrix

The major difficulty is evaluation of the components of S and this has been carried out on the basis of a method described in Mura [14].

Once $\epsilon^{(2)}$ has been determined for (S), the inclusion stresses are given by

We have performed a sample calculation of a SiC filled crack in a bundle consisting of T300 fibers embedded in ATJ graphite isotropic matrix for fiber volume concentration $V_f = 0.60$.

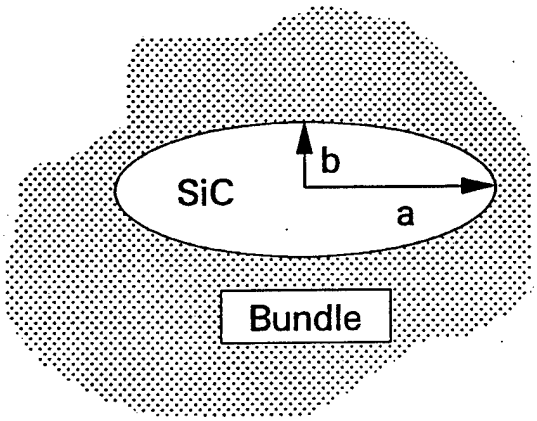

Figure 25. The filled bundle cracks were also represented as spheroidal inclusions.

$$\sigma^2 = C^2\epsilon^2 + \Gamma^2\varphi \tag{7}$$

For a cooldown of 2000°F, we obtained compressive transverse stresses in the SiC and an axial tensile stress which varies between 350 - 380 ksi for various aspect ratios of the ellipse. Since the ultimate tensile stress of SiC is about 45 ksi, this implies that the SiC will fail by transverse cracking in many places. The filled SiC crack will literally shatter into small pieces and thus the inhibitor is ineffective.

Interphase Failure

Graphite fibers are frequently coated for reasons of surface protection. The integrity of this protection depends on the ability of the fiber coating, from now on referred to as the interphase to withstand the internal stresses in the interphase. We have considered the case of very thin interphase and have been able to derive novel results for the interphase stresses on the basis of the Composite Cylinder Assemblage (CCA) model and the Generalized Self Consistent Scheme (GSCS) model, as described in [15]. It has been proven possible to evaluate the interphase stresses solely in terms of effective thermoelastic properties of the composite.

We are primarily interested in the interphase stresses due to temperature change. A sample calculation for the case of T300 fibers, embedded in ATJ graphite matrix at 0.60

volume fraction and a temperature cooldown of -2000°F, assuming reasonable interphase properties, has given the following results for interphase stresses.

$$G_{rr} = 1.37 \text{ ksi}$$

$$\sigma_{\theta\theta} = 7.27 \text{ ksi}$$

$$\sigma_{zz} = 13.1 \text{ ksi}$$

It is believed that the axial stress σ_{zz} will fail the interphase.

Summary - Filled Crack Analysis

It appears that a temperature cooldown of the order of -2000°F will produce severe thermal stress which will lead to separation of inhibitor (SiC) from the internal surface (crack) which it is suppose to protect. Similarly, such temperature drops will probably fail the interphase between fibers and matrix. Thought must be given as to the effectiveness of the crack fillers and fiber coatings under such circumstances.

3.2 MICRO-MECHANICAL MODELING ENHANCEMENTS

The objective this task was to provide improvements in the analytical procedures utilized in the modeling of oxidation inhibited carbon-carbon composites. The general approach was to identify analysis modules based on previously published theories and to incorporate these modules into the MSC's existing micro-mechanical analysis code - NDP 9.2 [16,]. Modules would be integrated into NDP 9.2 to enhance the capability of the code with respect to the several features of oxidation resistant C-C composites not previously addressed, specifically: multi-directionally reinforced composites containing oriented cracks, filled inclusions, and/or coated fibers. The analysis modules considered are based upon previous efforts and the details of these methodologies are given in [17, 18].

NDP 9.2 was selected as the vehicle for incorporation of these modules as it is a code with a proven capability in the modeling of uninhibited ORCC materials and it has the capability of modeling fully multi-directionally reinforced materials. NDP 9.2 is a MSC developed composite analysis software package and allows the calculation of elastic constants, thermal expansions, thermal conductivities, and strengths of composite materials.

NDP 9.2 is based on a "building-block" approach and this structure facilitates the introduction of alternate analysis modules which may be called into the analysis as the user requires.

The modules which were implemented into the NDP 9.2 code included the Differential Scheme and Multi-Phase Composite Cylinder Assemblage Models. The Differential Scheme Model enables the modeling of materials with oriented inclusions and unfilled cracks. The inclusions can be defined based on their cross sectional shape, effective length, volume fraction, and orientation. The modeling procedure utilizes the differential scheme approach in determining effective orthotropic properties of the inclusions in an orthotropic media. Cracks are defined as unfilled inclusions which are imbedded in an orthotropic matrix. The resulting material properties represent those of an "effective" matrix and are currently limited to the orthotropic case. Multiple cracks at different orientations may be introduced via a stepped procedure which utilizes the effective matrix and a new crack orientation. By selection of appropriate properties, the inclusions may be taken to represent simple cracks or as filled inclusions.

The Multi-Phase Composite Cylinder Assemblage (MPCCA) Model was incorporated into NDP 9.2 to provide a method for modeling coated fibers in multi-directionally reinforced materials. Since both the coating and the fiber are represented as cylindrically orthotropic materials, this model is particularly well suited for modeling fibers with coatings deposited in a layer-wise fashion around the circumference. The coated fiber properties which are determined from the MPCCA model are transversely isotropic, and are treated as effective fiber properties which can be utilized in bundle property predictions.

The integration of both the inclusion model and the coated fiber model into NDP 9.2, enables efficient modeling of 2D and multidirectionally reinforced ORCC materials with these characteristics.

Fiber bundles with cracks and/or filled inclusions may be represented by reinforcing the effective matrix with the appropriate fiber. The method utilized for the determination of the bundle properties is dependent upon the isotropy of the effective matrix material. When the properties are such that the effective matrix is transversely isotropic, the Composite Cylinder Assemblage (CCA) model may be utilized. However, for those cases where the effective matrix is orthotropic, the Differential Scheme is required in order to predict the resulting bundle properties. The current capability allows the prediction of the bundle full [6x6]

stiffness matrix, and the effective bundle properties may, therefore, be fully anisotropic. The resulting fiber bundles may then be oriented and assembled to form the N-D composite.

The enhancements which have been incorporated into the NDP 9.2 software provide a means by which data correlation studies may be utilized to quantify a substrate crack morphology (orientation and volume fraction) resulting from the various ORCC elevated temperature processing steps. Following definition of the substrate crack geometry and orientation, analyses may then be performed to determine the effects of post filling the cracks with inhibitors.

Data Correlation Studies

Following implementation of the model enhancements, the modified NDP 9.2 software was utilized along with experimental data to correlate crack volume fractions in various carbon-carbon substrate materials. The materials, descriptions of which are presented in Table 2, were all of 2D construction and contained various inhibitors. The reinforcing fiber in all cases was T300. Data sheets on each of the materials provided fiber volume, filler type, and limited mechanical properties.

As previously discussed, the materials shown in Table 2 were provided to Clarkson University for metallographic evaluation. The results of those evaluations provided insight into crack orientation, crack density, and general composite integrity. This information along with thermal expansion measurements [19] obtained from the Energy Materials Laboratory of Fiber Materials Inc., Biddeford, ME, enabled correlation studies to be performed to determine crack distributions and provide verifications of the material models.

The constituent properties utilized to represent the reinforcing fiber and the resulting graphite matrix are presented in Tables 8 and 9, respectively. The T300 fiber properties shown in Table 8 are based on correlation studies performed on early nozzle and nosetip materials. The ATJ matrix properties given in Table 9 are based on data from early Aerospace measurements and are representative of uncracked material. Where required, particulate or whisker reinforcement was added to represent any filler material which was present in the panel material.

Table 8. T300 Fiber Properties Utilized in Analysis

Obtained from Data Correlations on Billet F-11

Temp °F	E_A Msi	E_T Msi	G_A Msi	ν_A	ν_T	$\Delta L/L_A$ $x10^{-3}$	$\Delta L/L_T$ $x10^{-3}$
75	57.6	1.44	2.89	0.41	0.45	0.00	0.00
600	57.6	1.44	2.89	0.41	0.45	-0.30	3.64
1000	57.8	1.45	2.90	0.41	0.45	-0.25	6.23
2000	61.0	1.53	3.06	0.41	0.45	0.39	11.8
3000	62.2	1.56	3.12	0.42	0.46	1.40	17.2
4000	53.4	1.34	2.68	0.44	0.47	2.67	26.7
5000	33.2	0.83	1.67	0.47	0.49	4.16	40.3

Table 9. ATJ Matrix Properties Utilized in Analysis

Expansion Measurements on 15V Pitch - From Aerospace

Temp °F	E Msi	ν -	Δ L/L $x10^{-3}$
75	1.32	0.110	0.00
600	1.34	0.110	1.20
1000	1.36	0.120	2.10
2000	1.46	0.130	4.40
3000	1.66	0.140	7.05
4000	1.50	0.150	10.0
5000	0.87	0.175	14.5

Data Correlation - Panel 001

Panel 001 was manufactured by Rohr Inc., and was comprised of layers of T300 8HS fabric which was heat treated to 4800°F, prior to densification. The total fiber content was reported to be 63%. The maximum graphitization temperature was 3000°F. There was no inhibitor present within this material.

The results from the Clarkson observations showed very few yarn interface cracks along with little fiber pullout. The low degree of fiber pullout indicated relatively good fiber/matrix interface integrity. The density of the fiber/matrix interface cracks was reported to be moderate. The transverse bundle cracks were well developed, narrow, uniformly spaced, and ran the full width of the bundle. The transverse bundle crack density was typical, however, on the low side. The fiber volume was reported to be high, with very few matrix rich regions. The specimen appeared to be fully densified. In addition, Clarkson indicated an unusual "residue" of matrix material which lined or was within, many of the transverse bundle cracks. A photomicrograph of panel 001 is presented in Figure 5.

Thermal expansion measurements obtained from reference 18 were utilized to correlate the degree of cracking present within the composite. Cylindrical cracks were oriented through

the thickness of the composite with a length to diameter ratio of 25, and effective composite properties were determined. The resulting composite thermal expansions which were determined from NDP 9.2 are presented in Figure 26 for various amounts of unfilled inclusions. As the results indicate, a figure of 60% for the fraction of oriented cracks within the ATJ matrix provide the required agreement.

Data Correlation - Panel 020

Panel 020 was manufactured by Rohr Inc., and was comprised of layers of T300 8HS fabric which was heat treated to 3900°F, prior to densification. The total fiber content was reported to be 71%. The maximum graphitization temperature was 3000°F. There was no inhibitor present within this material.

The results from the Clarkson observations showed very few yarn interface cracks. The transverse bundle cracks were reported to be narrow, very regular, and fully developed. The density of panel 020 appeared to be less than that of panel 001, but with moderate porosity. A number of large voids were observed at the yarn bundle interfaces. The composite exhibited a high fiber content. The density of fiber/matrix interface cracks was observed to be low. During the preparation of the specimen, a good deal of fiber pullout was present, which suggests the fiber/matrix integrity was poor to moderate. A photo micrograph of panel 020 is presented in Figure 6.

Thermal expansion measurements obtained from [19] were utilized to correlate the degree of cracking present within the composite. The results from these correlations indicated that minimal microcracking was present. The resulting composite thermal expansions which were determined from NDP 9.2 are presented in Figure 27 and are based on an assumption of no cracking within the composite.

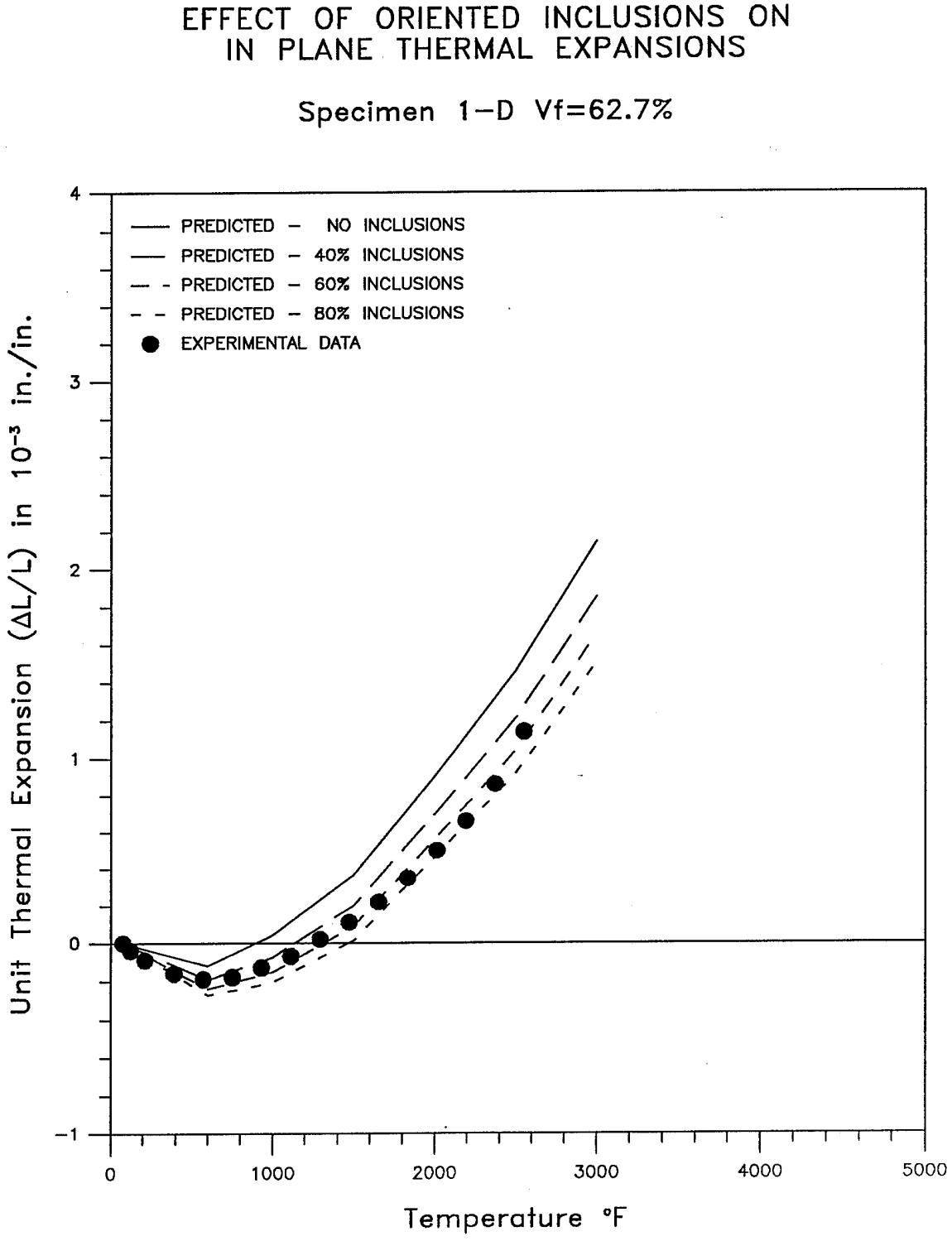

Figure 26. The results of the data correlation on the thermal expansion data for Rohr panel 1.

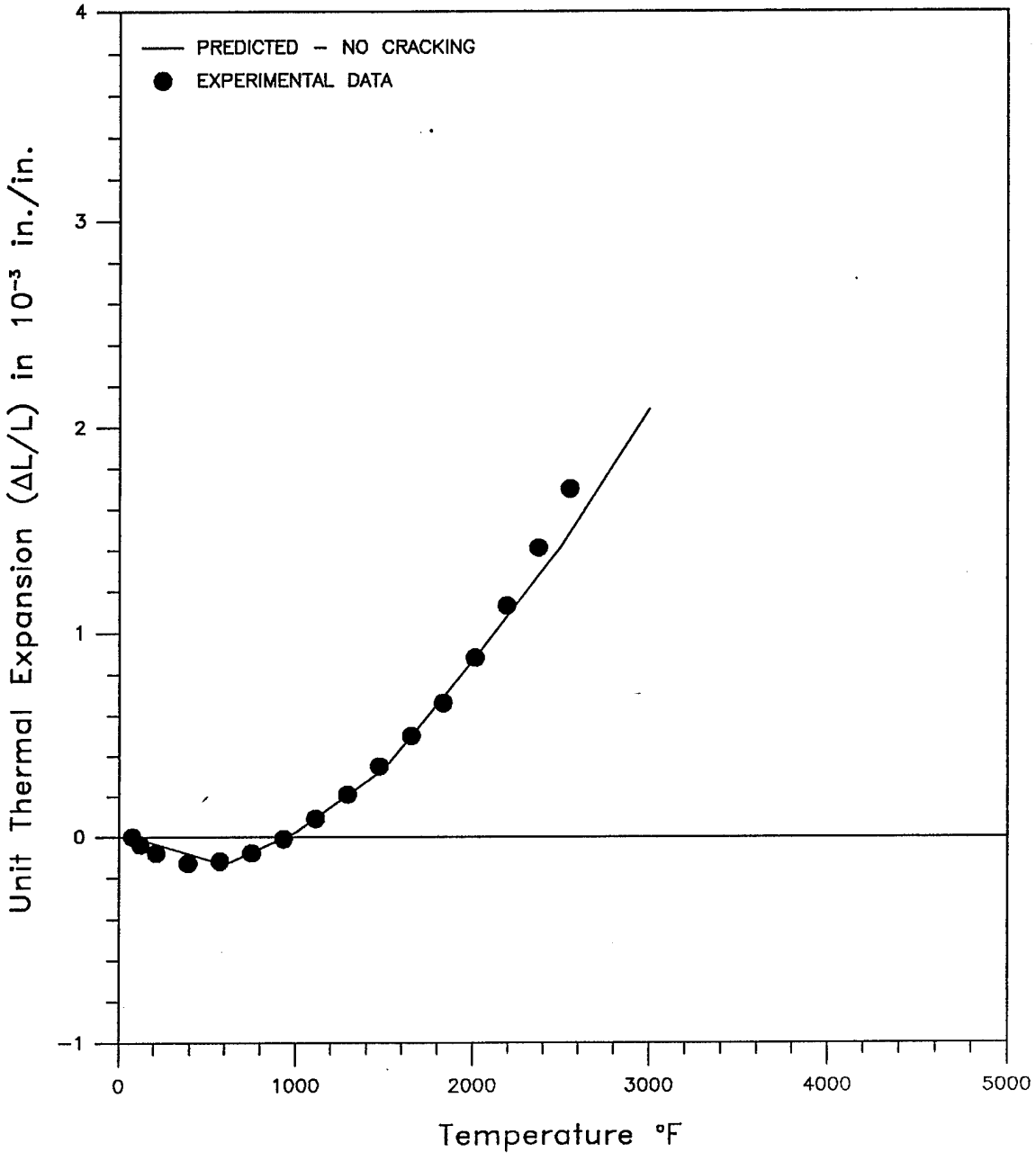

Figure 27. The results of the data correlation on the thermal expansion data for Rohr panel 20.

Data Correlation - Panel 031

Panel 031 was comprised of layers of T300 8HS fabric which was heat treated to 3900°F, prior to densification. The total fiber content was reported to be 42%. The maximum graphitization temperature was 3000°F. An RICC X6A particulate inhibitor introduced as a matrix filler was reported to be present at a 62% volume within the carbon matrix. Since the properties of the RICC X6A filler were not known, SiC properties were utilized for an initial estimate. Correlations were then performed to define effective particulate moduli which provided the required agreement with the thermal expansion data assuming a reasonable degree of cracking. The resulting RICC X6A properties are presented in Table 10.

Table 10. RICC-X6A Filler Properties Utilized in Analysis of Panel 31

Temp °F	E Msi	ν -	Δ L/L $x10^{-3}$
75	14.8	0.14	0.00
500	14.1	0.13	0.94
1000	13.7	0.12	2.04
1500	13.4	0.13	3.69
2000	13.0	0.13	5.49
2500	9.30	0.13	7.42

The results from the Clarkson observations indicated a dark and granular matrix, which indicated that an inhibitor had been added. There was a definite appearance of two types of large flakes or granules which had been added to the matrix. There was poor penetration of the inhibited matrix into the fiber bundles. The material was extremely porous, such that the identification of any microcracks becomes ambiguous. A photo micrograph of panel 031 is presented in Figure 7.

Thermal expansion measurements obtained from [18] were utilized to correlate the degree of cracking present within the composite. Based upon the Clarkson observations, the

assumption was taken that spherical voids be utilized to represent the porous nature of the material, and correlations with the expansion data were made to determine the amount present. The results from these correlations indicated that 50% voids were present within the filled carbon matrix. The resulting composite thermal expansions which were determined from NDP 9.2 are presented in Figure 28, along with the measured data.

Data Correlation - Panel 062

Panel 062 was comprised of layers of T300 8HS fabric which was heat treated to 3900°F, prior to densification. The total fiber content was reported to be 51%. The maximum graphitization temperature was 3000°F. The composite contained a SiC whisker inhibitor with a 17% volume in the carbon matrix.

The results from the Clarkson observations indicated a dark granular nature to the matrix rich regions of the material, which indicated that an inhibitor had been added. The SiC whiskers appeared only to be present in the matrix material external to the fiber bundles. Extensive fiber pullout during the specimen preparation indicated a poor fiber/matrix integrity. A high level of porosity appeared external to the fiber bundles with a low interbundle porosity. Many of the larger voids have been partially filled with the uninhibited matrix. There was a moderate density of narrow transverse bundle cracks. A photo micrograph of panel 062 is presented in Figure 8.

Thermal expansion measurements obtained from [19] were utilized to correlate the degree of cracking present within the composite. Based upon the Clarkson observations, the assumption was taken that spherical voids be utilized to represent the porous nature of the material, and correlations with the expansion data were made to determine the amount present. The results from these correlations indicated that 20% voids were present within the inhibited carbon matrix. The resulting composite thermal expansions which were determined from NDP 9.2 are presented in Figure 29, along with the measured data.

Data Correlation - Panel 137

Panel 137 was comprised of layers of T300 PW fabric which was heat treated to 3900°F, prior to densification. The total fiber content was reported to be 43%. The

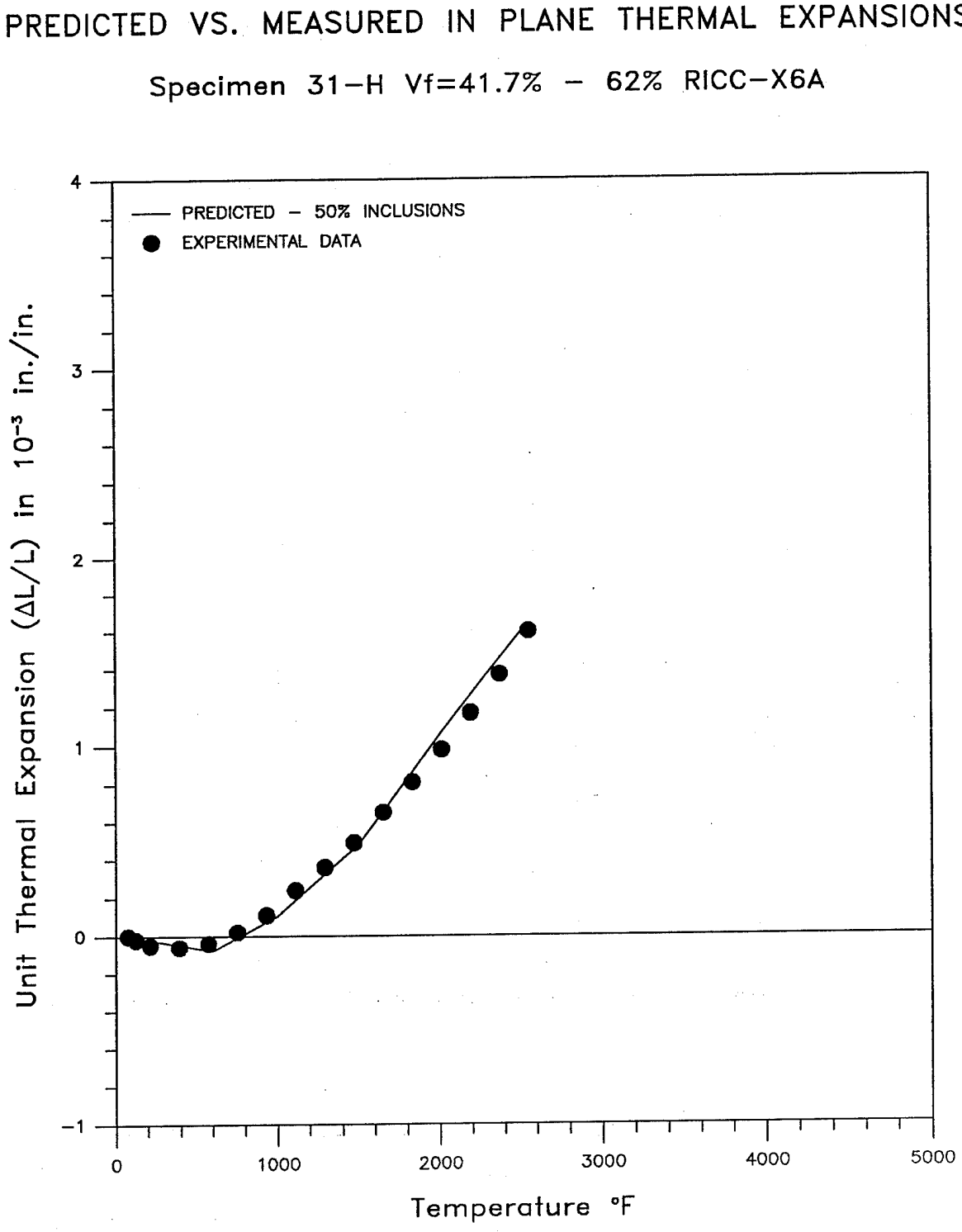

Figure 28. The results of the data correlation on the thermal expansion data for Rohr panel 31.

PREDICTED VS. MEASURED IN PLANE THERMAL EXPANSIONS

Specimen 62-H Vf=50.6% - 17% Sic Whiskers in ATJ Matrix

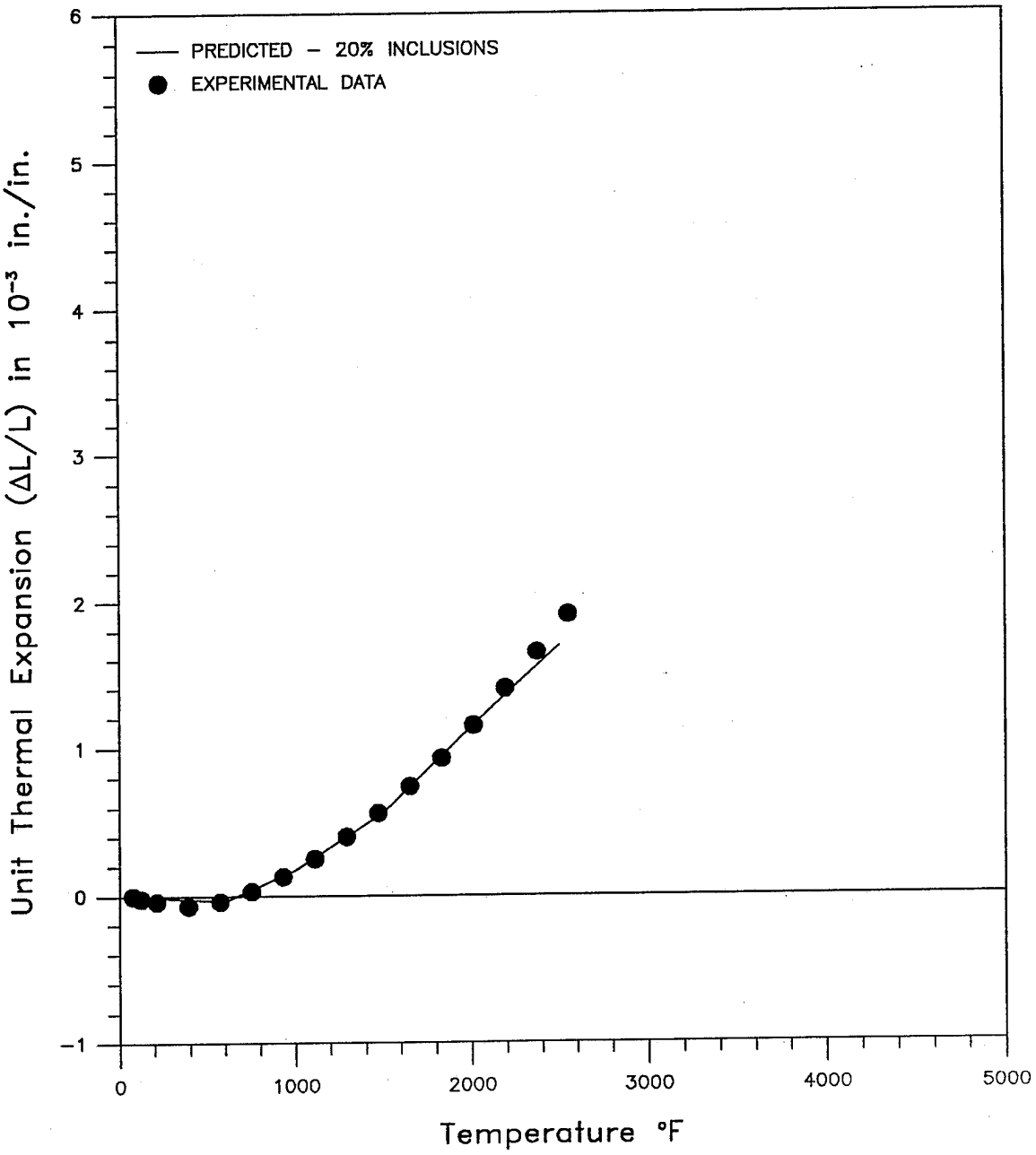

Figure 29. The results of the data correlation on the thermal expansion data for Rohr panel 62.

maximum graphitization temperature was 3000°F. The composite contained an RICC X7A particulate filler with a 40% volume in the carbon matrix. SiC properties were utilized to represent the filler material.

The results from the Clarkson observations indicated that the inhibited matrix was present within the fiber bundles. Large matrix rich regions were observed along with a moderate porosity. There were very few yarn interface cracks present; however, there the transverse bundle cracks were well developed and quite wide. The transverse bundle cracks were partially filled with what appeared to be uninhibited matrix material and exhibited a crack spacing larger than typical. The fiber matrix interface exhibited moderate cracking which indicated good integrity. The yarns within the specimen appeared to be more wavy than others. A photo micrograph of panel 137 is presented in Figure 9.

As with previous panels, thermal expansion measurements obtained from [19] were utilized to correlate the degree of cracking present within the composite. Based upon the Clarkson observations, the assumption was taken that spherical voids be utilized to represent the porous nature of the material, and correlations with the expansion data be made to determine the amount present. The results from these correlations indicated that 30% voids were present within the filled carbon matrix. The resulting composite thermal expansions which were determined from NDP 9.2 are presented in Figure 30, along with the measured data.

EVALUATION OF FILLED INCLUSIONS

The results from the data correlation studies were utilized to study the influence of filling open cracks on ORCC material properties. The data correlations identified volume, shape, and orientation of the cracks which were present within each material. The material models were utilized to specify filler material to create filled inclusions of the same size, shape, and volume as the identified cracks. Three specific filler materials were considered: boron carbide (BN), silicon nitride (Si_3N_4), and silicon carbide (SiC). Properties used to represent each of these fillers are presented Tables 11 through 13, respectively.

The results obtained for panel 001 are presented in Figure 31. This figure shows in plane Young's modulus, shear modulus, and free thermal strain, all as a function of temperature. Results are given for each of the three filler types considered. It may be seen

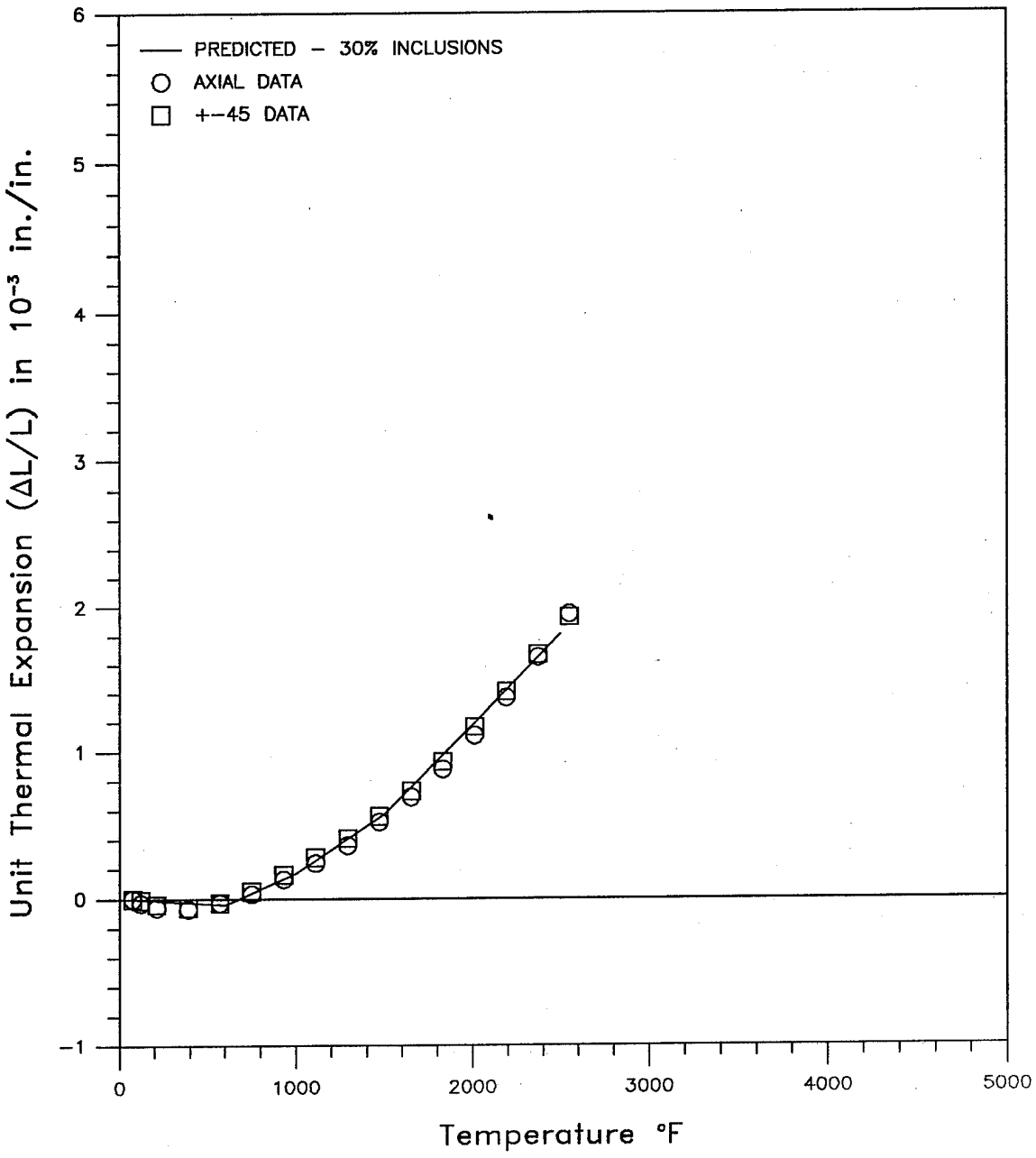

Figure 30. The results of the data correlation on the thermal expansion data for Rohr panel 137.

that filler material has a negligible effect on fiber dominated elastic modulus. A small increase in Young's modulus was predicted when the cracks were filled. However, as may be expected the effect of crack fillers on matrix dominated properties such as shear modulus was much more significant, with a large increase in shear modulus predicted when the cracks are filled. However, one interesting effect was the ability of the crack fillers to eliminate the fiber dominated negative expansion behavior of the composite as shown in Figure 31. Thus, crack fillers may have utility as thermal expansion modifiers in terms of an overall crack management strategy.

Table 11. Boron Carbide Material Properties Utilized in Analysis

Temp °F	E Msi	ν -	$\Delta L/L$ $x10^{-3}$
75	55.4	0.19	0.0
500	52.8	0.19	1.0
1000	49.5	0.19	2.3
1500	45.6	0.19	4.0
2000	38.6	0.19	6.0
2500	31.6	0.19	8.0

Table 12. Silicon Nitride Material Properties Utilized in Analysis

Temp °F	E Msi	ν -	$\Delta L/L$ $x10^{-3}$
75	43.0	0.270	0.00
500	41.0	0.241	0.63
1000	40.0	0.231	1.79
1500	39.0	0.252	3.25
2000	38.0	0.258	4.85
2500	27.0	0.258	6.50

Table 13. Silicon Carbide Material Properties Utilized in Analysis

Temp °F	E Msi	ν -	Δ L/L $x10^{-3}$
75	59.0	0.14	0.00
500	56.3	0.13	0.94
1000	54.9	0.12	2.04
1500	53.5	0.13	3.69
2000	52.1	0.13	5.49
2500	37.0	0.13	7.42

The effects of crack fillers for the other Rohr panels 31 through 137 are given in Figures 32 through 34. Similar trends as noted for panel 001 may be seen.

EVALUATION OF FIBER COATINGS

The multi phase composite cylinder assemblage module of NDP 9.2 was exercised to determine the influence of oxidation resistant fiber coatings on unidirectional T300 fiber bundle properties. Consideration was given to the evaluation of boron nitride, silicon nitride, and silicon carbide coatings. The properties for each of these materials are presented in Tables 11-13, respectively. In addition to the evaluation of coating type, the influence of coating thickness was also considered. The analysis assumed a constant volume fraction of "effective fibers", such that an increase in coating thickness resulted in a decrease of T300 volume.

The results obtained from the study are presented in Figures 35 - 37. Figure 35 presents the influence of silicon carbide coatings on composite axial Young's modulus and free thermal strain. Results for boron nitride and silicon nitride are presented in Figures 36 and 37, respectively.

As the results indicate, increase in coating thickness gives rise to a decrease in Young's modulus and an increase in thermal expansion. This may be explained by the constant volume faction of coated fibers assumption which leads to fiber material being replaced by coating

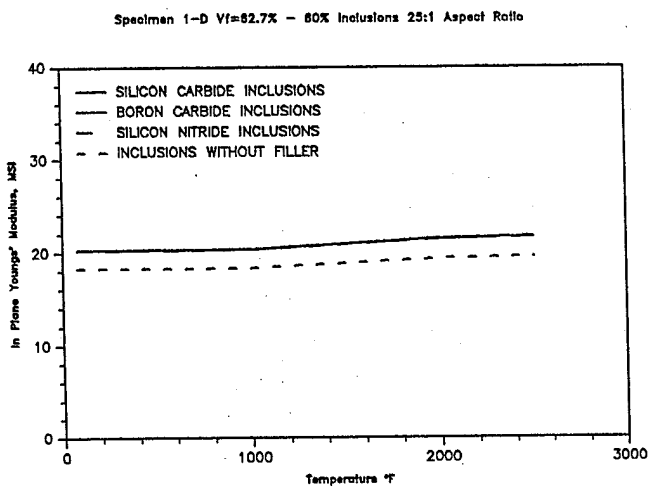

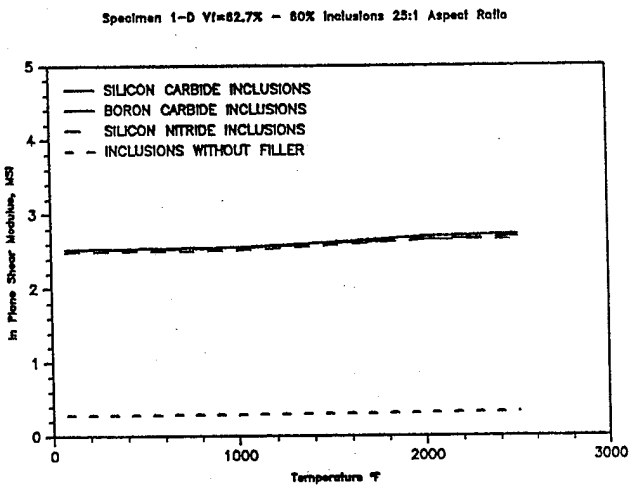

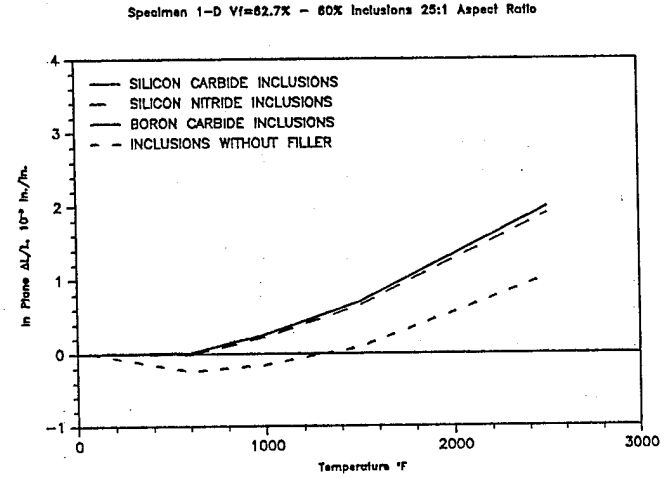

Panel 001

- **Small Increase In Youngs' Modulus**
- **Large Increase In Shear Modulus**
- **Elimination Of Negative Expansion Behavior**
- **Variation In Filler Type Has Negligible Effect**

Figure 31. The results of the analyses showing the impact on composite mechanical properties of filling the volume of open cracks in panel 1 with various oxidation inhibitors.

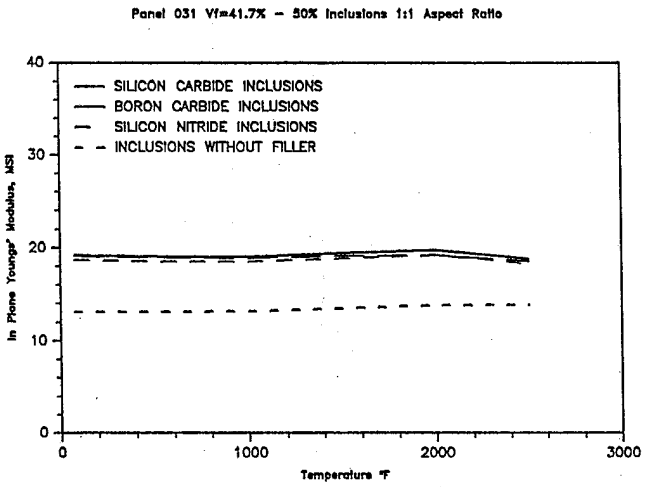

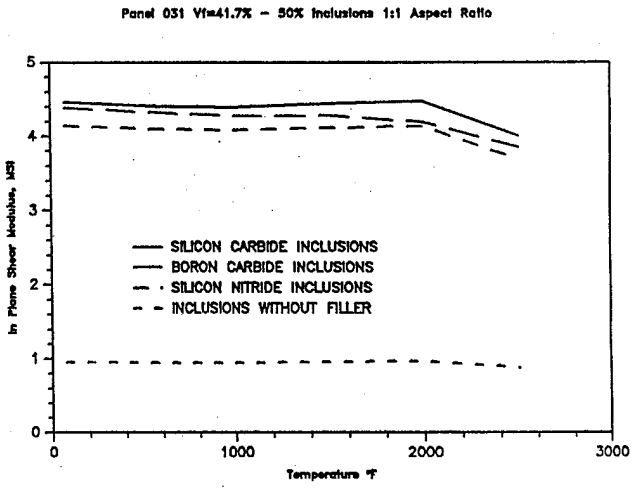

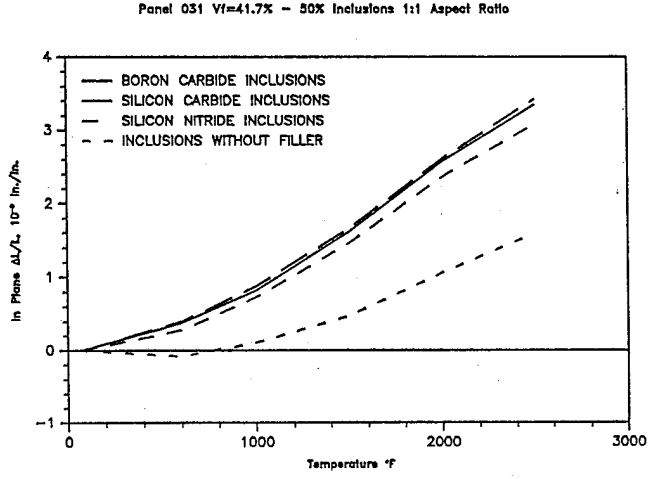

Panel 031

- **Moderate Increase In Youngs' Modulus**
- **Large Increase In Shear Modulus**
- **Elimination Of Negative Expansion Behavior**
- **Variation In Filler Type Has Small Effect**

Figure 32. The results of the analyses showing the impact on composite mechanical properties of filling the volume of open cracks in panel 31 with various oxidation inhibitors.

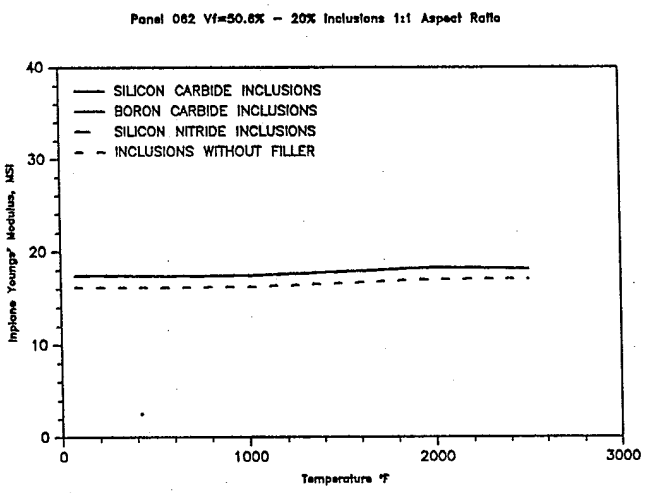

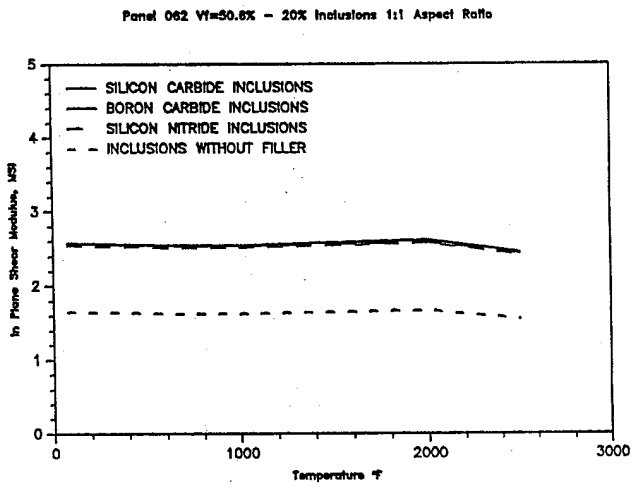

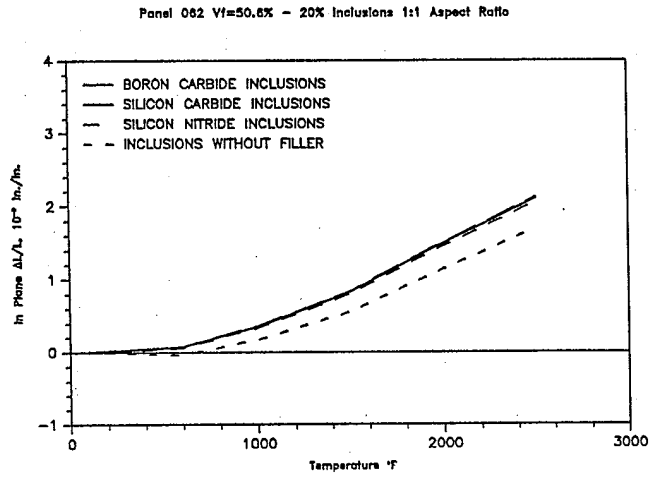

Panel 062

- **Small Increase In Youngs' Modulus**
- **Moderate Increase In Shear Modulus**
- **Elimination Of Negative Expansion Behavior**
- **Variation In Filler Type Has Negligible Effect**

Figure 33. The results of the analyses showing the impact on composite mechanical properties of filling the volume of open cracks in panel 62 with various oxidation inhibitors.

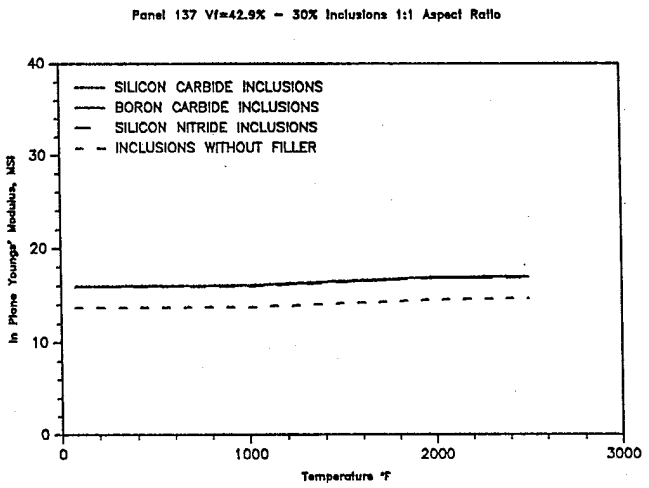

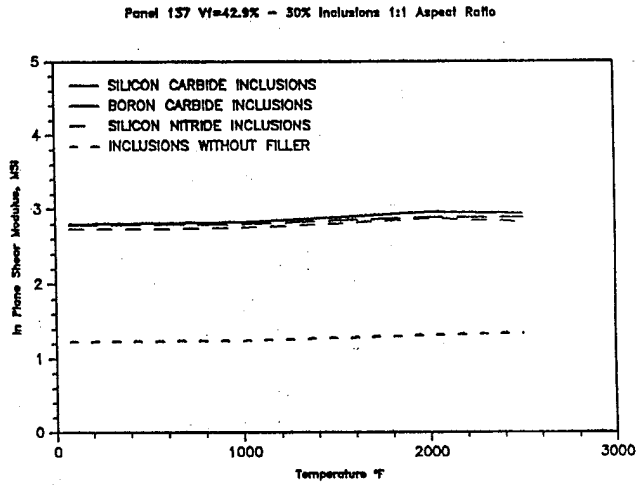

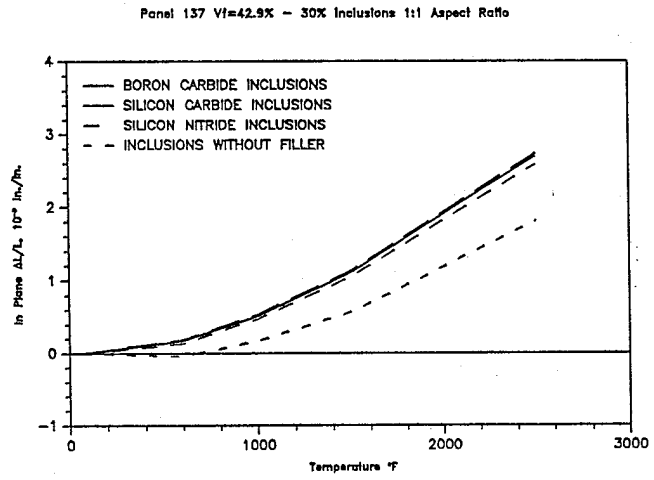

Panel 137

- **Small Increase In Youngs' Modulus**
- **Large Increase In Shear Modulus**
- **Elimination Of Negative Expansion Behavior**
- **Variation In Filler Type Has Negligible Effect**

Figure 34. The results of the analyses showing the impact on composite mechanical properties of filling the volume of open cracks in panel 137 with various oxidation inhibitors.

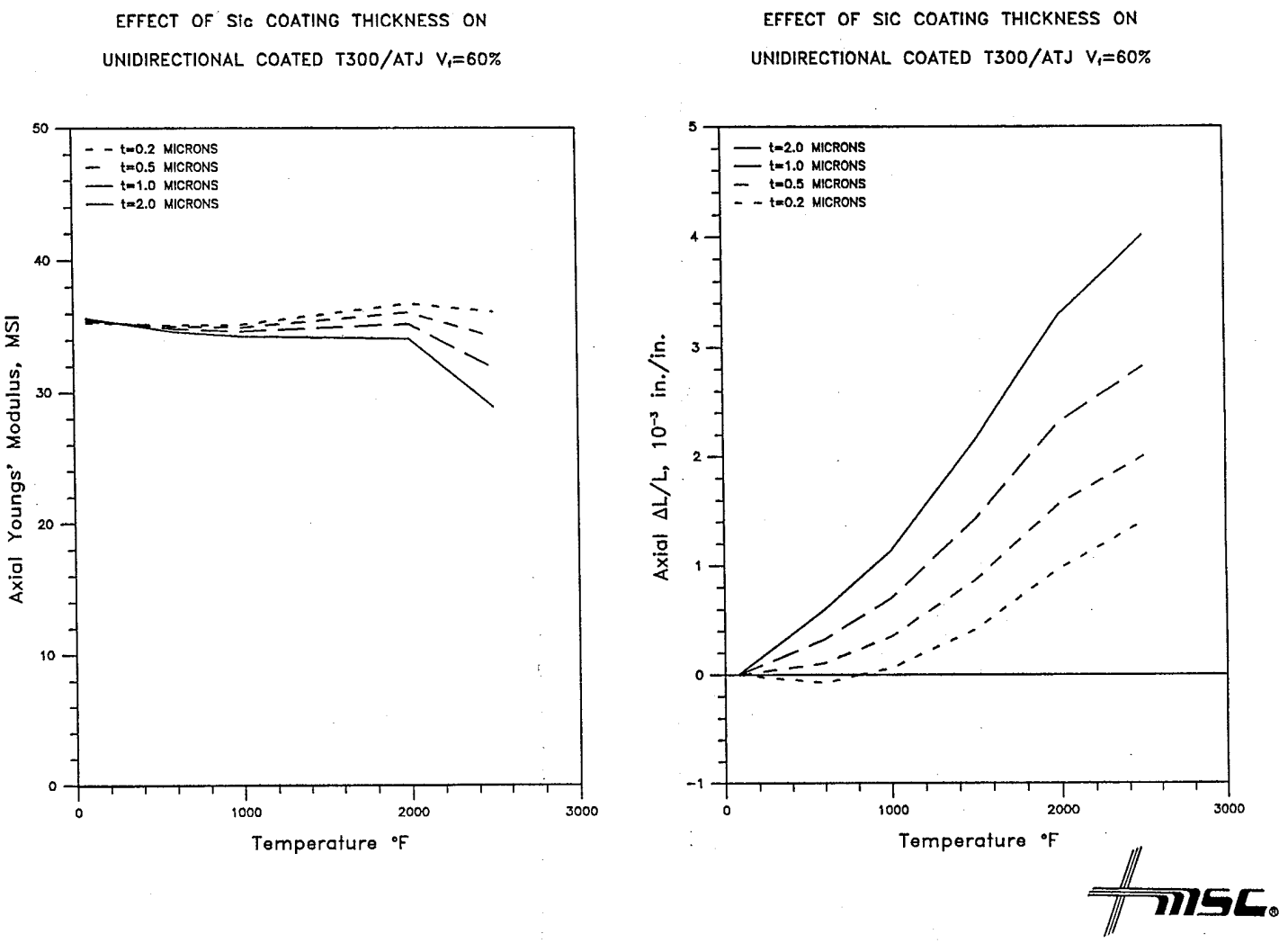

Figure 35. The effect of SiC fiber coatings on the modulus and expansion behavior of ORCC materials.

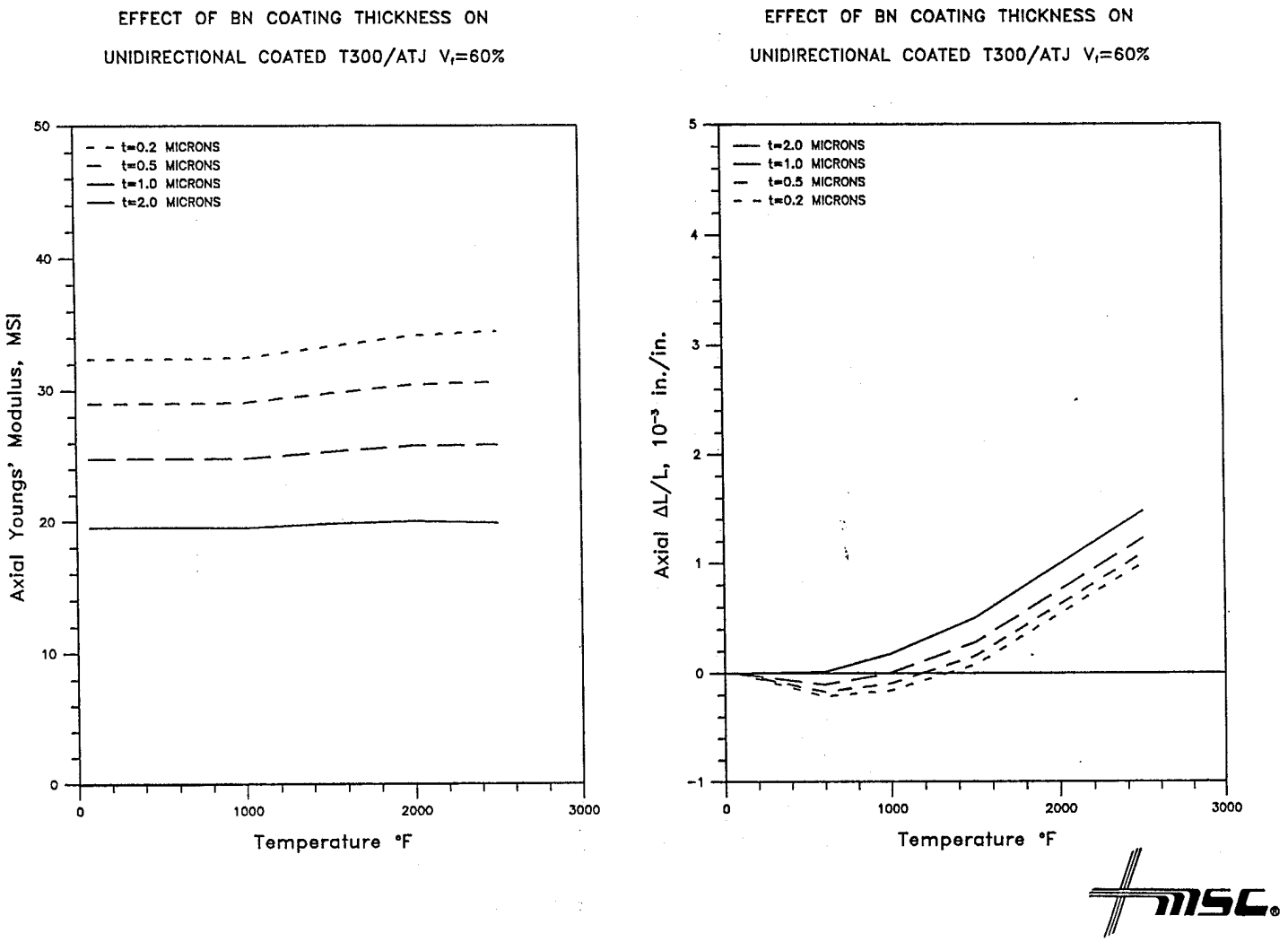

Figure 36. The effect of BN fiber coatings on the modulus and expansion behavior of ORCC materials.

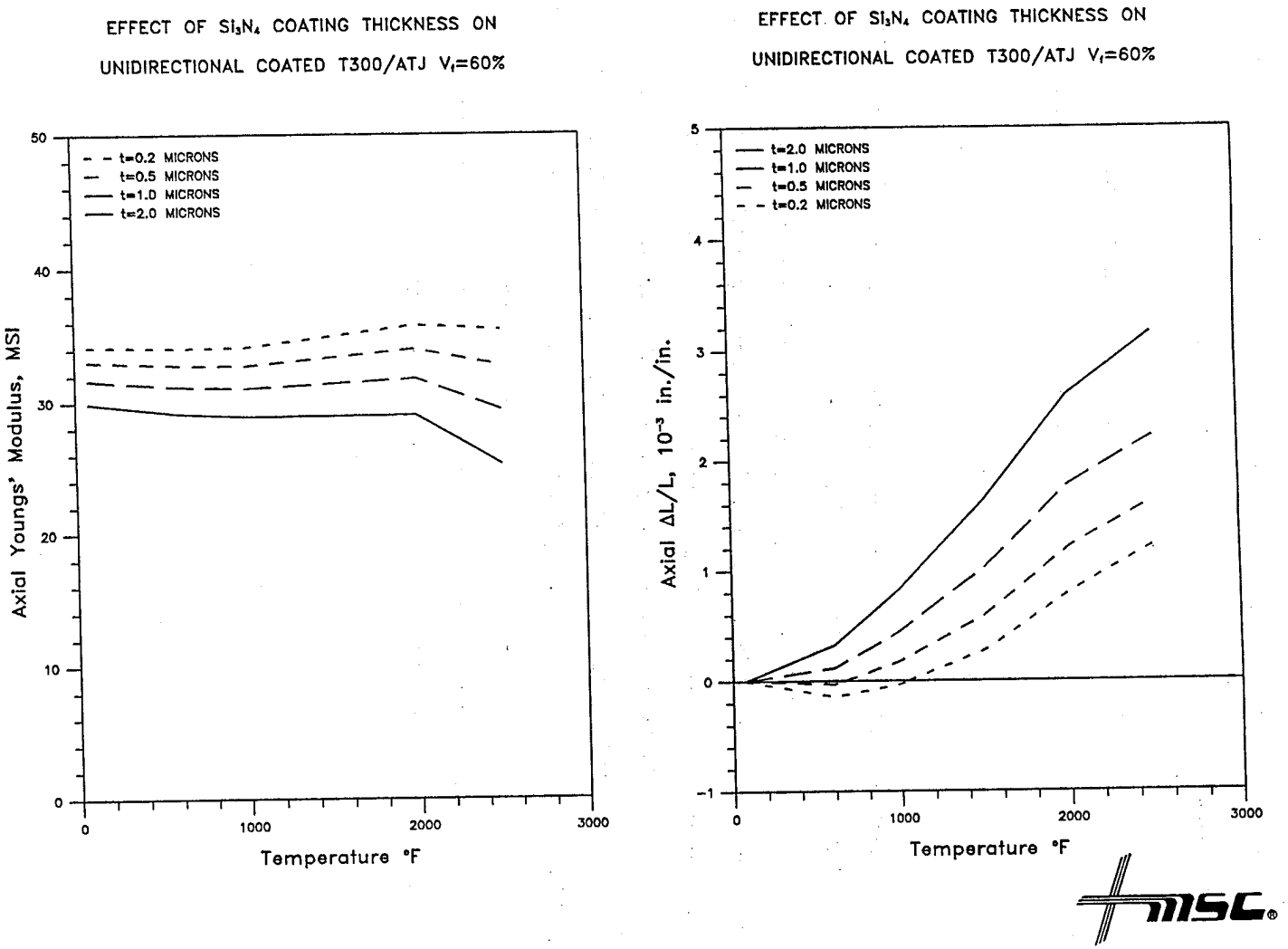

Figure 37. The effect of Si_3N_4 fiber coatings on the modulus and expansion behavior of ORCC materials.

material as the thickness increases. Thus, as the fiber coatings are generally lower modulus and higher expansion materials than the heat-treated T300 fibers increase in fiber coating thickness serves to lower the composite modulus and increase the expansion.

Thus in terms of a crack management strategy, fiber coatings are a good way to go. Of course the general trend will be that as more carbon is replaced by ceramic material as fillers or fiber coatings, the material will tend towards the behavior of a ceramic matrix composite rather than a carbon-carbon composite.

RESIDUAL STRAIN EFFECTS

In order to determine the effect of fiber coatings on a crack management strategy, a 0/90° laminate was constructed using coated T300 fiber bundle properties established under the MMOP effort and a residual thermal strain was calculated for the laminate on cooldown from an assumed coating deposition temperature of 2500°F. Two types of external coating material and two types of fiber coating material were investigated: SiC and Si_3N_4, and BN and SiC, respectively. The results are given in Figures 38 and 39. As may be seen greater thermal strains were developed for the SiC coated materials, and the SiC fiber coatings had the greatest effect in modifying the substrate thermal strain, while the BN coating had little effect even at a 2 micron thickness.

In terms of a crack management strategy, the preferred material combination would be SiC fiber coatings with a Si_3N_4 overcoat.

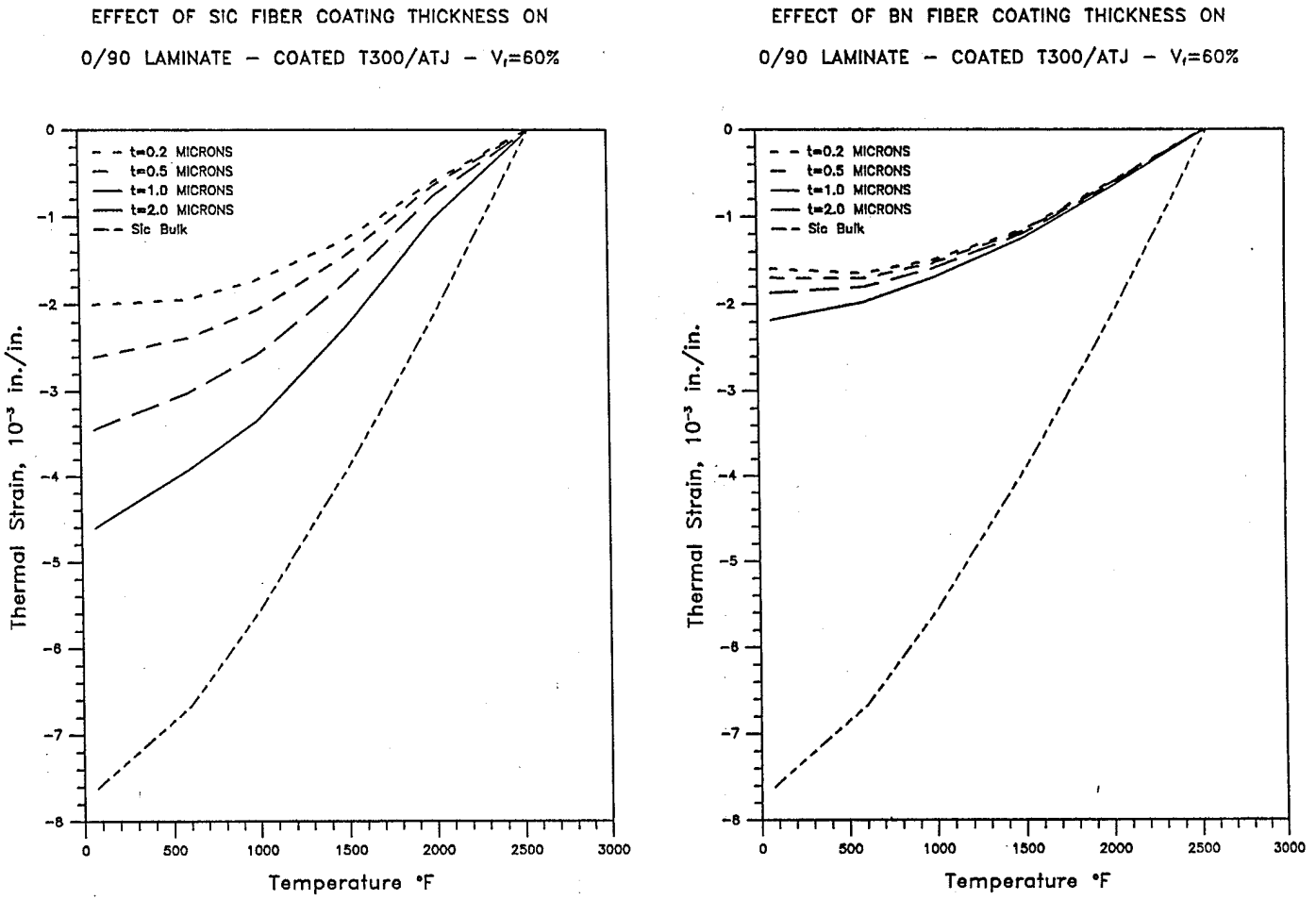

Figure 38. A thermal cooldown analysis shows the influence of SiC and BN fiber coatings on the reduction in thermal strain mismatch between the ORCC substrate and a SiC external coating.

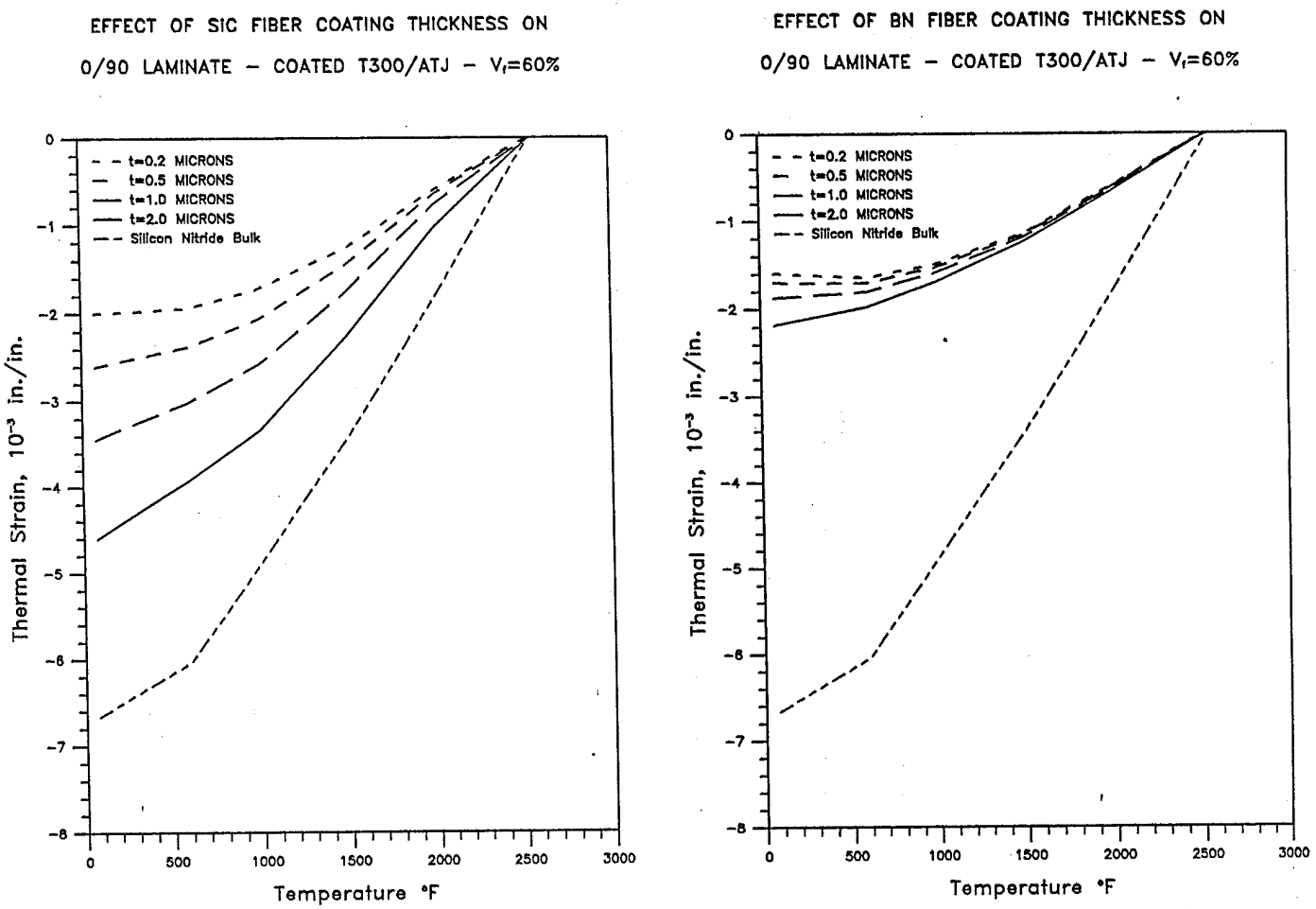

Figure 39. A thermal cooldown analysis shows the influence of SiC and BN fiber coatings on the reduction in thermal strain mismatch between the ORCC substrate and a Si_3N_4 external coating.

4.0 THE CRACK MANAGEMENT (CM) MODEL

The objective of this task was to develop an analytical capability for determining the influences of materials and process parameters (substrate and coating) on the development of the thermally-induced microcrack network in the ORCC external coatings. The experimental data obtained during the Clarkson studies, and described in Section 2, was used to validate the analytical model predictions. The analytical method was then used to investigate possible materials and/or processing strategies for "managing" the microcrack pattern to produce a more effective oxidation barrier.

During the course of these activities, several competing analytical techniques were utilized: a finite element (FE) based modeling approach, and fracture mechanics based approach.

During the finite element studies, the MMOP models (Section 3) were integrated into a commercial finite element code to monitor the effects of various bundle level oxidation protection schemes on the development of thermal stresses in the substrate and coating. Studies were also conducted to investigate the sensitivity of the coating stresses to stress risers in the substrate associated with the weave architecture. Finally, an attempt was made at using the finite element method to provide insight into the progressive nature of the coating cracking and possibly to correlate findings with the observed crack spacings in the Clarkson data.

The FE method was able to provide an estimation of the stress distribution in the coating prior to crack initiation. However, the explicit nature of the problem definition required in the finite element approach proved unsuitable for modeling the initiation or progression of the coating cracks.

Following the results of the FE approach, an alternative fracture mechanics-based approach was adopted, in which the focus was shifted from monitoring individual cracks to monitoring the onset and saturation of the cracks via a crack density, or crack spacing approach. This approach was successful in providing a generalized description of the crack spacing as a function of temperature for various material parameters, and showed good correlation with the data from the Clarkson studies. This approach was then used to investigate the sensitivity of the crack spacing to changes in coating/substrate material parameters and to identify possible crack-free coatings.

4.1 FINITE ELEMENT STUDIES

Preliminary finite element studies focused on integrating the MMOP bundle-level models (Section 3) into the FE codes for predicting changes in macro response based on changes in material constituents or microstructure. The general purpose FE code in use at MSC during the course of these analyses was ABAQUS [20].

The first step was to use the MMOP model to take a look at the general stress and strain distribution in the substrate fiber bundles as a result of a typical coating cooldown cycle (an assumed thermal differential of -1000°C). The results from the analyses are given in Figure 40 and indicate that the general stress state within the bundles is axial compression and transverse tension. The predicted transverse stress level is high relative to the very low transverse bundle strengths usually associated with this class of material, and is consistent with the observed damage distribution which shows multiple cracking in the transverse bundle direction (Figure 2).

Another observation from these analyses was the presence of localized strain gradients on the surface of the substrate associated with the weave pattern and the fiber bundle cross-over points. A typical surface stress contour of a SiC coated 3 harness satin weave substrate is shown in Figure 41. This figure shows the axial stress in a 10 mil SiC coating over a 200 mil carbon-carbon substrate after cooldown from 1800°F to 1180°F. Previous analyses had shown that the normal coating stress would have been approximately 65 ksi if the C-C substrate had been modeled as a homogeneous material. However, by incorporating the MMOP model, the substrate was modeled as an assemblage of interlaced bundles consistent with the 3 harness weave pattern and the weave-induced stress concentrations were able to be distinguished. This analysis showed a peak stress of 67 ksi at the cross-overs and represents a 3% rise over the "background" stress level. As expected, the effect of the weave cross-overs became more pronounced as the coating thickness decreased. For instance, at a 5 mil coating thickness, the stress concentration effect was approximately 6%.

This would suggest that the influence of the weave pattern on coating crack pattern will only be significant for the thinner coatings.

This is in agreement with experimental observations which indicate that weave pattern is not a dominant effect in defining the coating crack pattern. For a typical harness satin weave fabric, the cross-over pattern repeats every 60 mils. However, review of the specimen

MODEL INTEGRATION - RESULTS

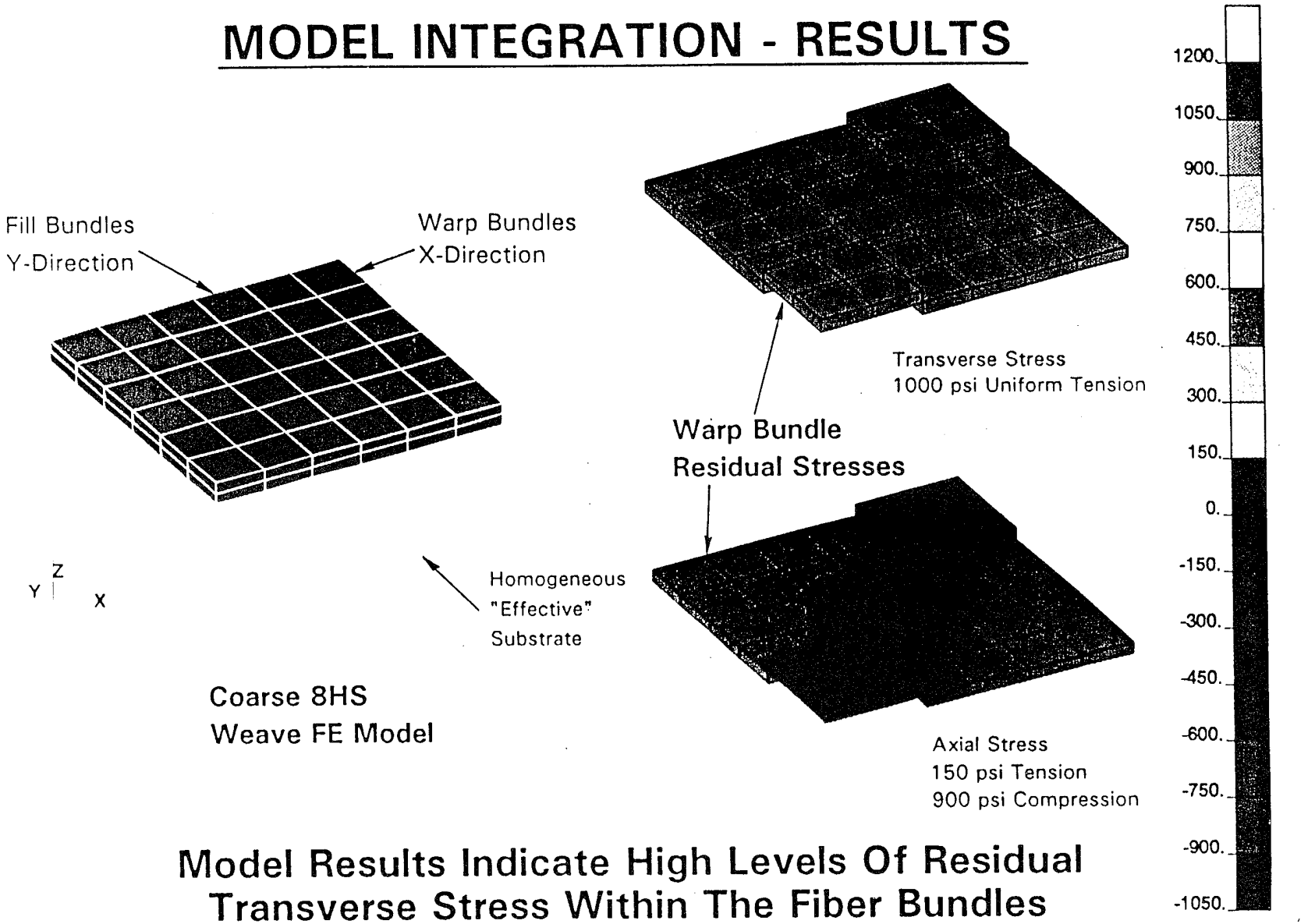

Model Results Indicate High Levels Of Residual Transverse Stress Within The Fiber Bundles

Figure 40. Integration of the MMOP model into the ABAQUS finite element code revealed a high transverse stress state in the bundles.

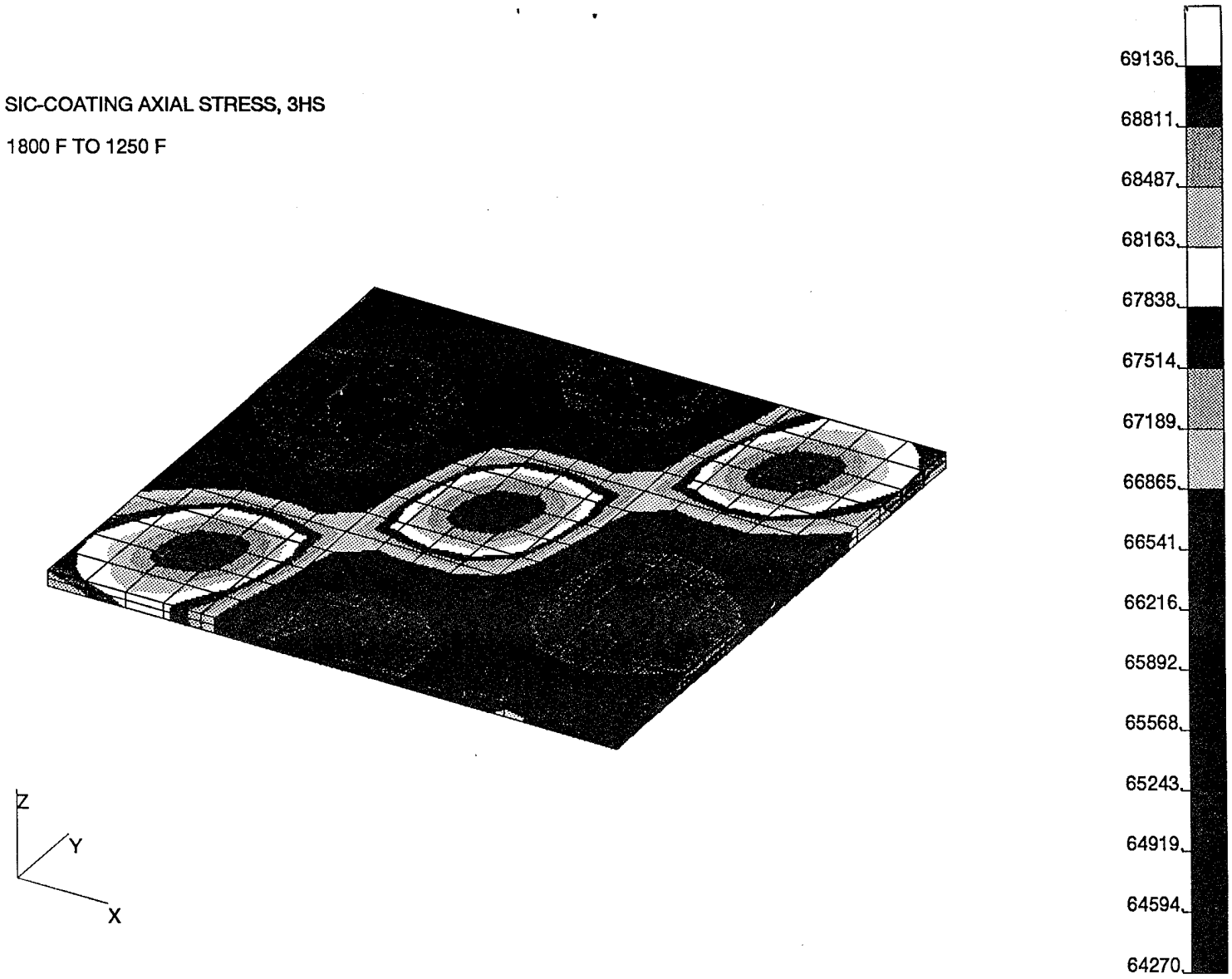

Figure 41. Further finite element analyses revealed a small stress riser effect in the external coatings associated with the weave pattern in the underlying substrate (axial stress in a 5 mil SiC coating on an ORCC substrate on cooldown).

data from Section 2 indicates that typical crack spacings are of the order of 5 mils. Thus, while these weave induced stress concentrations may have an effect in determining the sites for initiation of early cracks, the disparity in numbers between cracks and yarn bundles indicates that there are many other factors influencing crack initiation and saturation.

In addition to the weave effect study, there was some concern that specimen geometry may play a role in controlling crack spacing, particularly as it was observed that there were approximately twice as many cracks along the long specimen axis as there were along the short axis. The calculated thermal stress distribution in the substrate and coating as a function of distance from the free edge is given in Figures 42 and 43. It may be seen that there is an edge effected zone approximately 0.5 ins. wide at each edge. Therefore, a 3x1 in. specimen will have a highly edge effected crack pattern along the short axis, and a uniform distribution within the center 2 ins. of the long axis of the specimen. It would also indicate that the presence of holes will have a significant effect on the coating crack pattern.

A small amount of effort was also spent analyzing the effects of cracks on the redistribution of stresses in the coating and substrate, i.e., would it be possible to introduce a crack in the FE model and determine where and when the next crack would form, or whether the existing crack would propagate into the substrate. In this effort, ABAQUS crack elements were explicitly included in the model at a spacing much finer than experimentally observed. These cracks were set to open at a stress appropriate to SiC material strength. It was hoped that these crack elements would be activated individually as the local stress level reached the SiC material strength. However, this proved to be an unrealistic expectation, and it was found not possible to control the crack elements on an individual basis. They could have been controlled by varying the material strength at each element, but this would have required anticipation of an expected crack pattern, with the results of the analysis confirming information already held.

4.2 FRACTURE MECHANICS ANALYSES

The fracture mechanic approach used in this analysis is based on the work of Chatterjee and Yen [21]. In their analysis, composite stiffness reduction as a result of crack formation is accounted for by energy change due to the increased surface area associated with the cracks.

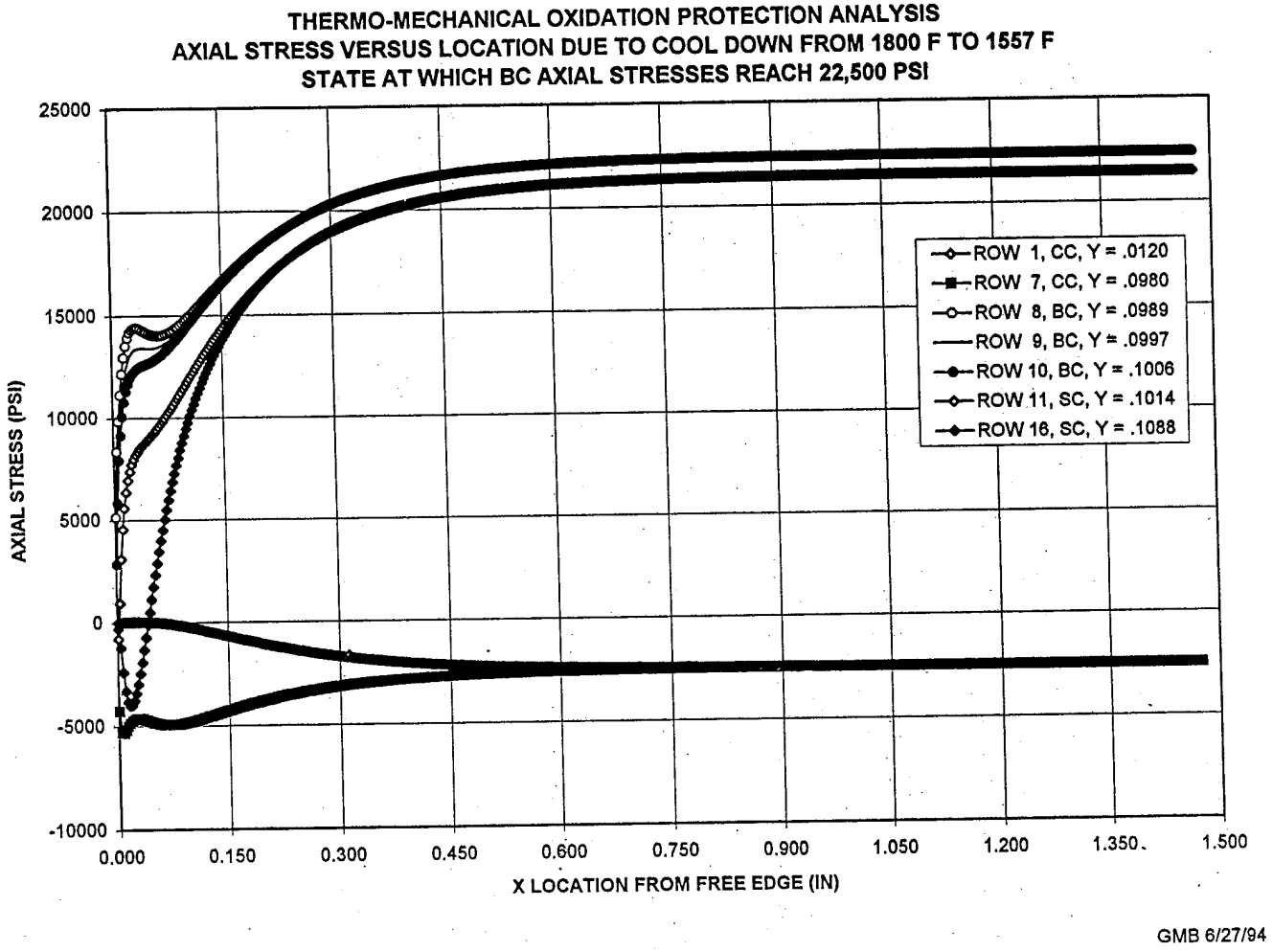

Figure 42. Finite element derived thermal stress (axial) distribution from the free edge of a coated ORCC coupon (CC - ORCC substrate, BC - coating sealant layer, SC - coating SiC layers).

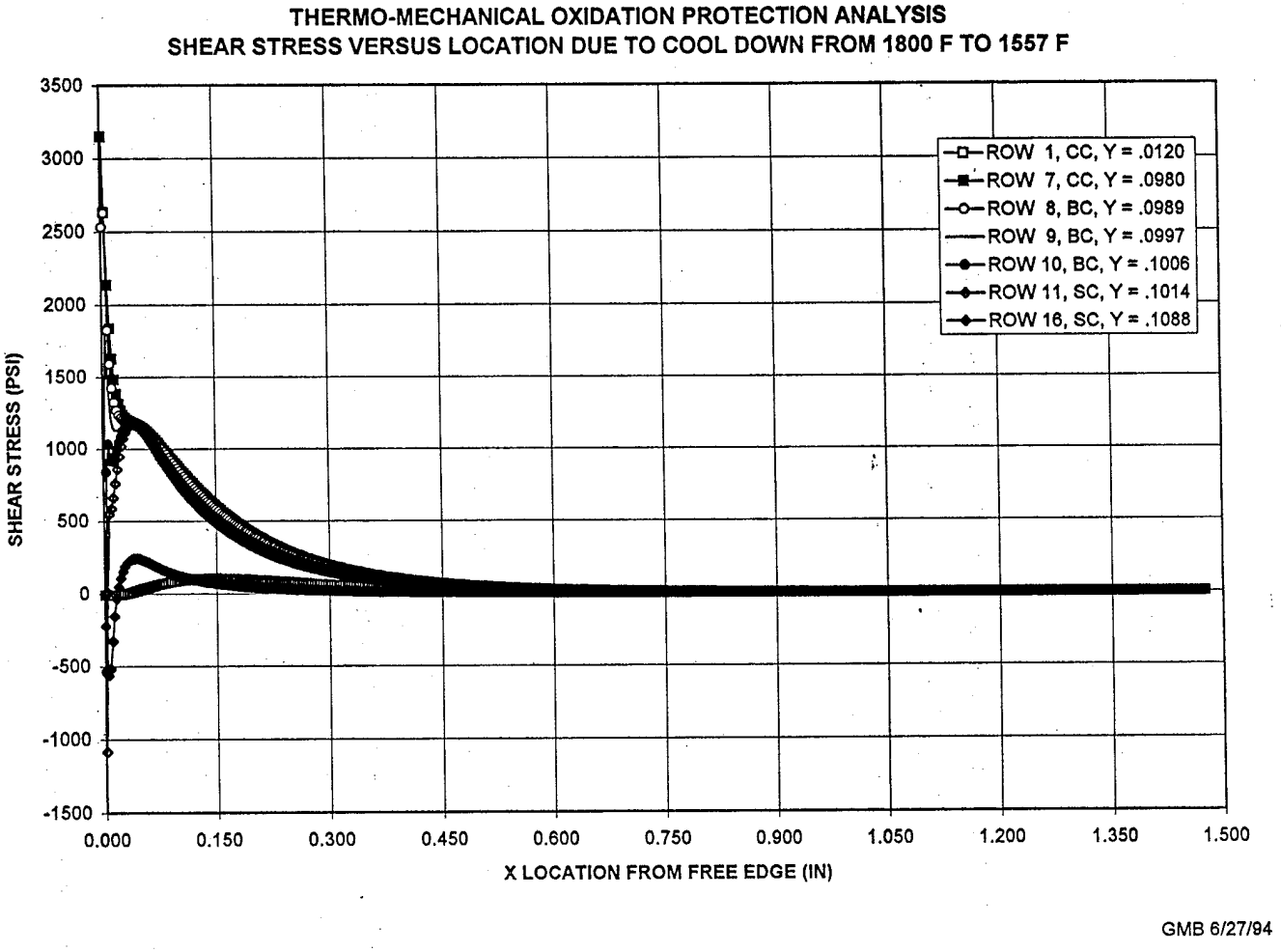

Figure 43. Finite element derived thermal stress (shear) distribution from the free edge of a coated ORCC coupon (CC - ORCC substrate, BC - coating sealant layer, SC - coating SiC layers).

This model makes the following assumptions:

1. The composite bundles are in transverse tension only.
2. There is no separation (delamination) between the coating and substrate.
3. Cracks occur in coating only.
4. Material properties used are the average properties predicted at fracture temperature.

The model inputs are composite construction, elastic constants of layers, the load history and coating strain energy release rate (G_{IC}). The elastic constants used in the analysis are listed below and are assumed to be "typical" for a 0/90 C-C and SiC coating.

$E_{C\text{-}C}$ = 20 Msi

$\alpha_{C\text{-}C}$ = $1.0 \times 10^{-6}/°F$

$E_{Coating}$ = 60 Msi

$\alpha_{Coating}$ = $3 \times 10^{-6}/°F$

The value of G_{IC} for the SiC was taken from reference [22] as being between 0.14 and 0.34 $\frac{\#}{in}$.

Figure 44 shows the predicted crack spacing for three values of G_{IC}. The analysis assumes a 5 mil SiC coating on a 84 mil thick $[0/90]_s$ C-C substrate. The applied temperature change was from 1800°F to room temperature. As may be seen, increasing G_{IC} of the coating resulted in a slightly increased crack spacing (for the given material construction) and a lower crack initiation temperature.

Figure 45 shows the crack spacing in the same substrate as described above, but for a constant G_{IC} of 0.24 $\frac{\#}{in}$ and a range of coating thicknesses between 2.5, 5 and 10 mils.

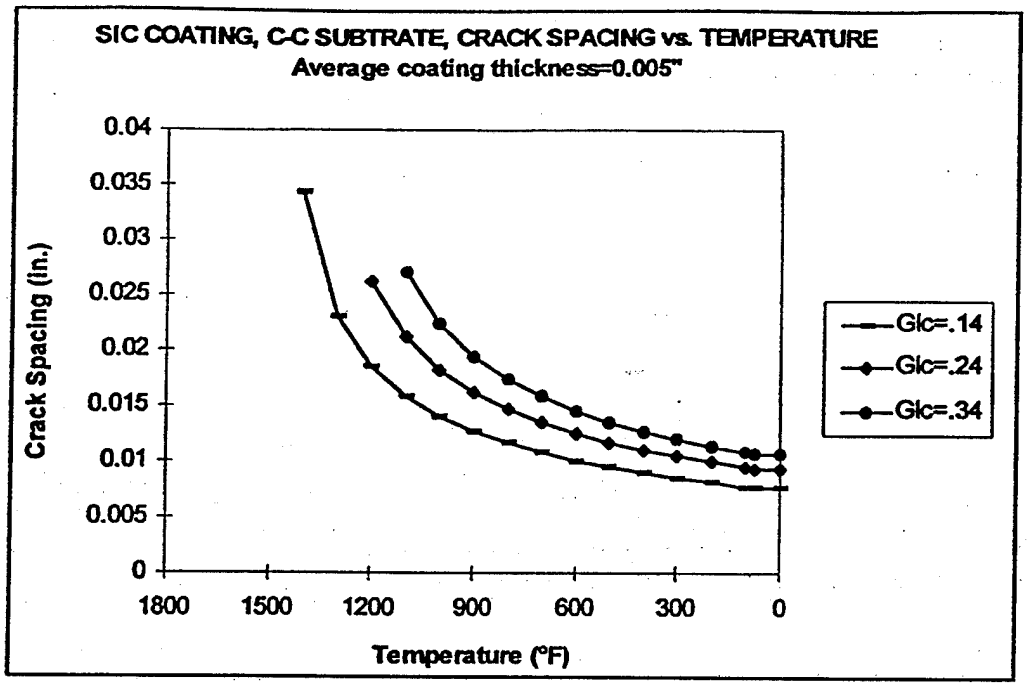

Figure 44. The fracture mechanics model showed a strong correlation between crack initiation temperature and coating fracture toughness.

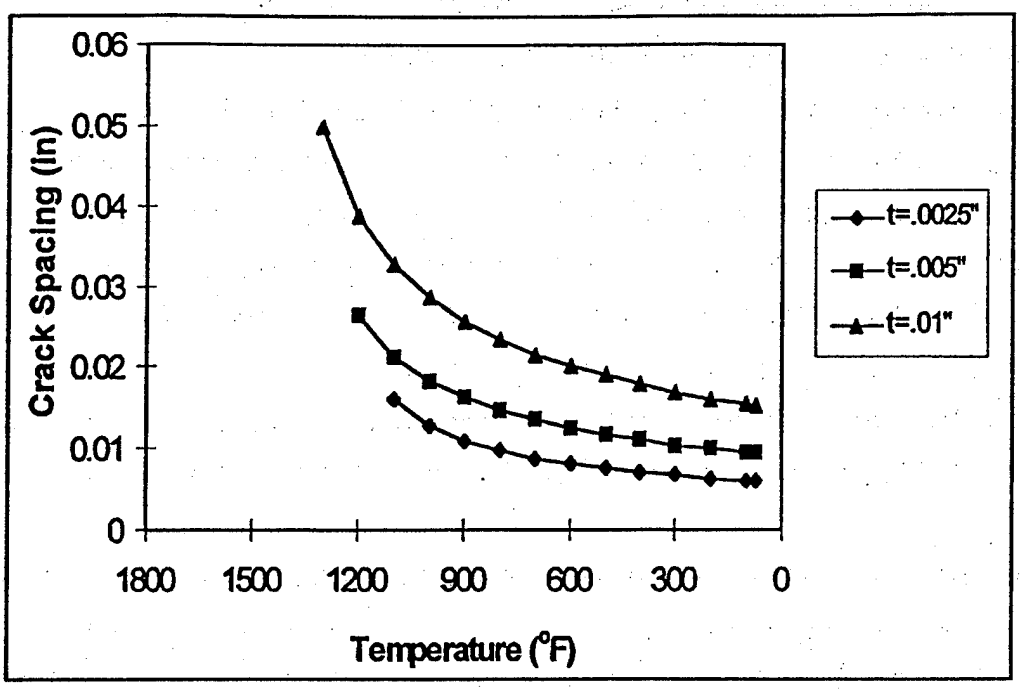

Figure 45. The fracture mechanics model showed coating thickness to have little effect on crack initiation temperature and strong effect on final crack spacing.

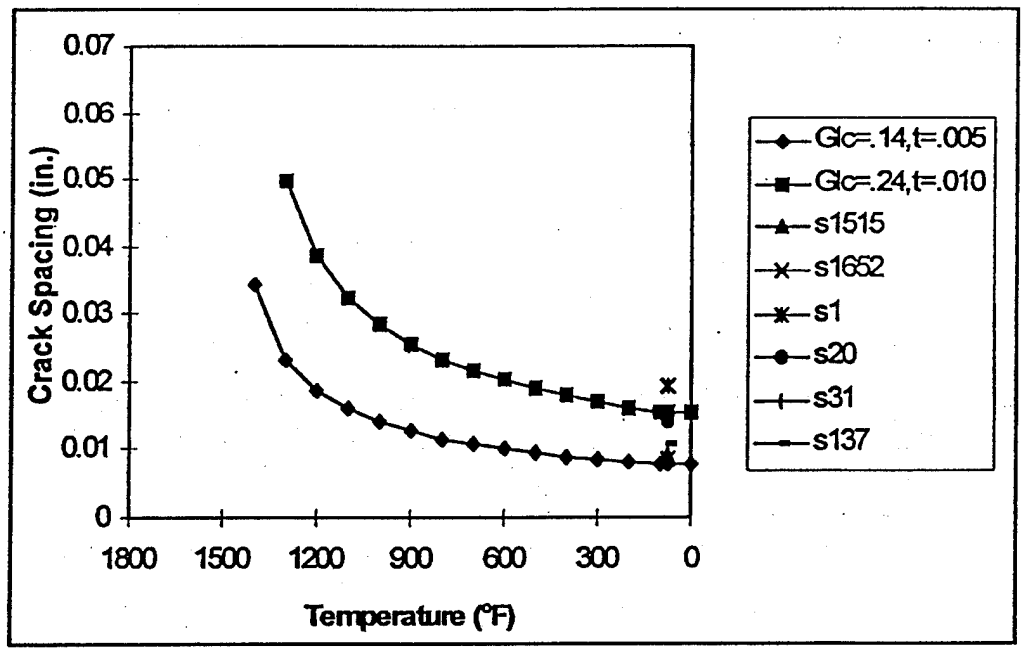

Figure 46. The fracture mechanics model predictions bracketed the measured range of room temperature crack spacings from the Clarkson study.

These thicknesses encompass the range of coating thicknesses in the Clarkson data. The plot shows that increasing the coating thickness from 2.5 mils to 10 mils increased the crack spacing from about 7.5 mils to 17 mils. Although this increase is substantial, it is clear that other parameters must be varied if coating cracking is to be eliminated.

Selected results from Figures 44 and 45 along with the Clarkson averaged crack spacing data are plotted in Figure 46. This figure shows that the MSC predicted crack spacings offer reasonable agreement with the predicted data. It also shows that process parameters such as heat treatments, material inhibitor, or defects, do not especially dominate the coating crack problem. Finally, Figure 46 verifies that the fracture mechanics approach will be a useful tool in developing material architectures and combinations which reduce or eliminate coating cracking.

Figures 47 and 48 show the results of a parametric study where the ratio of substrate Young's modulus to coating Young's modulus and substrate thermal expansion coefficient (CTE) to coating CTE were varied to determine the influence of each parameter on the coating crack problem. In each case, realistic ratio values are 0.33.

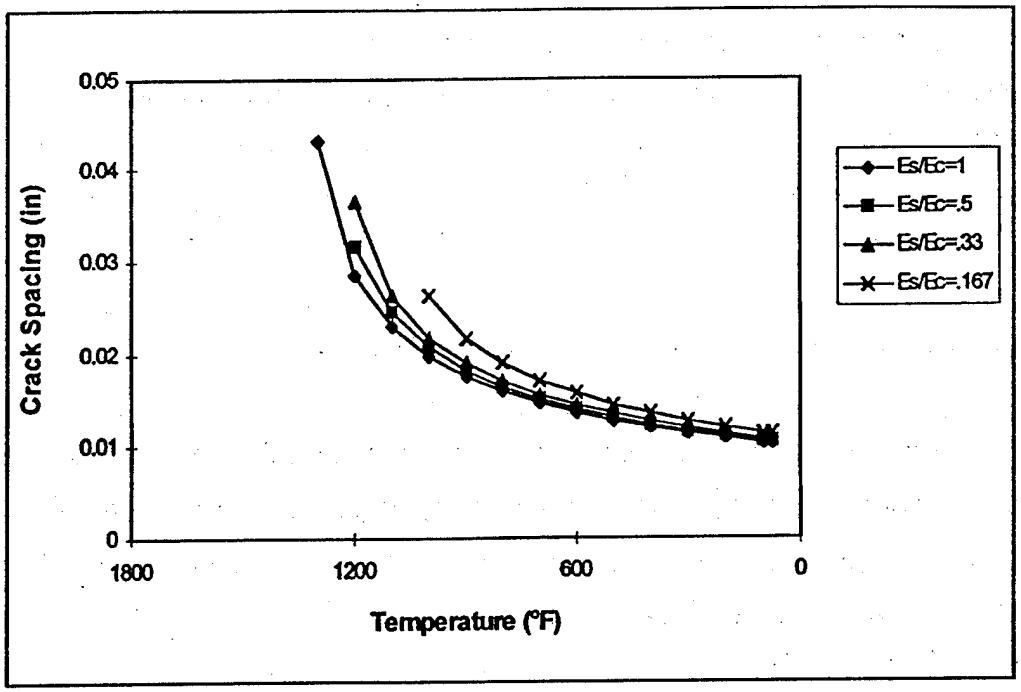

Figure 47. The fracture mechanics model showed the coating:substrate modulus ratio to have little effect in effect on crack initiation or saturation.

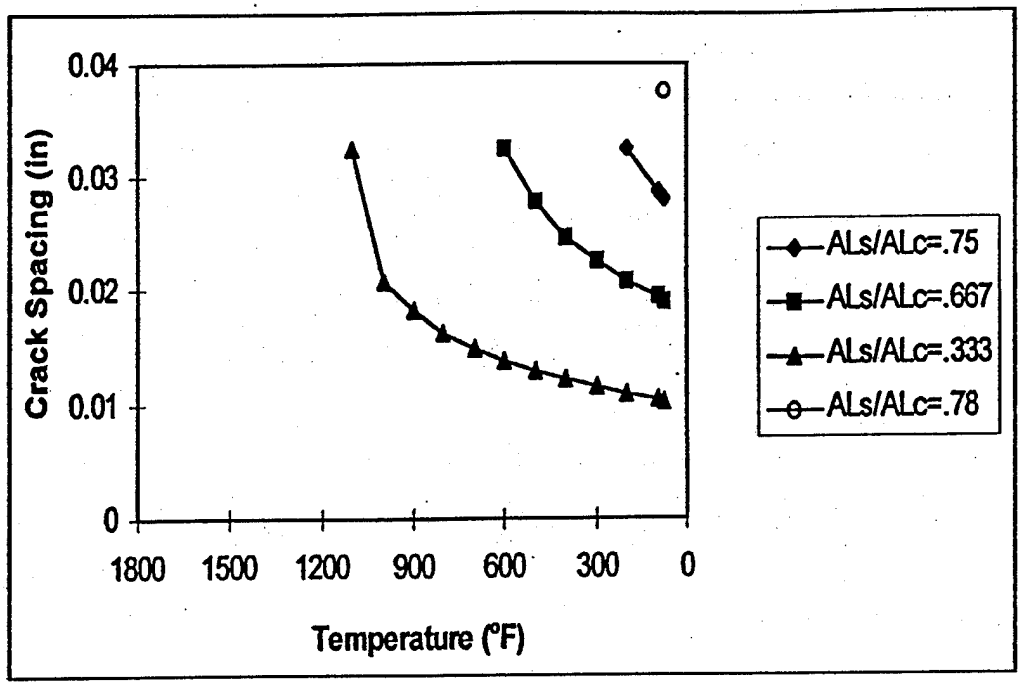

Figure 48. The substrate:coating thermal expansion ratio was found to be the major factor influencing crack initiation and saturation.

Figure 47 shows that Young's modulus primarily effects crack initiation and the temperature change required for crack initiation, but has little effect on final crack spacing as the final crack spacing for each modulus value was very similar. While this may not be as immediately expected, this result reinforces the fact that the driving force behind the coating crack is the thermal strain differential developed as the high CTE coating cools on the low CTE substrate.

This fact is further emphasized by the results shown in Figure 48, which gives the effect of coating:substrate CTE ratio on crack spacing, and shows that CTE mismatch is the dominant effect controlling final crack spacing in the fully cooled coating. This figure also gives an indication of the conditions under which cracking may be suppressed: if the substrate CTE is within 20% of the coating CTE, cracking in the coating will not occur.

However, typical candidate coating materials such as SiC, B_4C and Si_3N_4 will not provide a 20% CTE match with the C-C $[0/90]_s$ substrate when directly applied, and in and of themselves cannot provide crack-free coatings. This is illustrated in Figure 49 which shows the free thermal strain curve for each material.

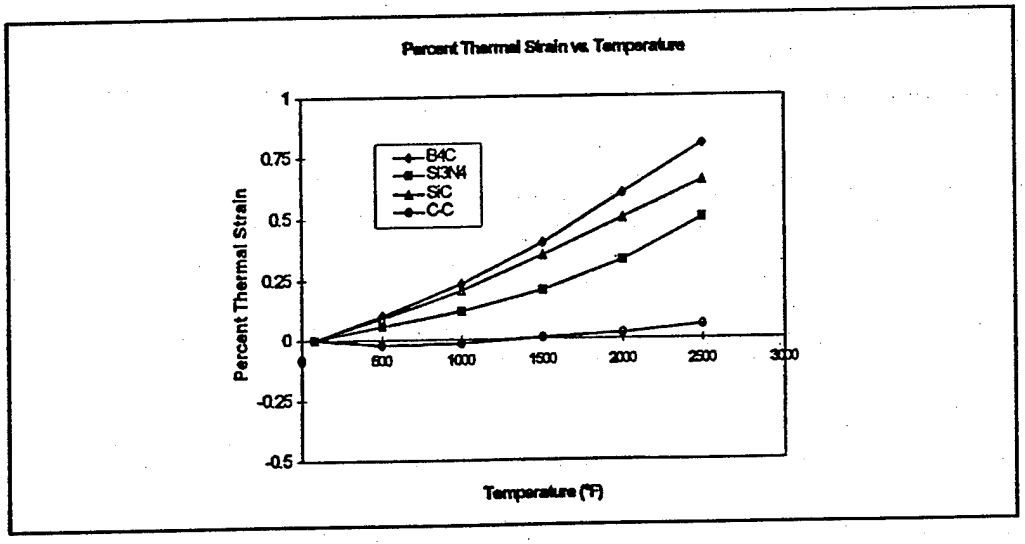

Figure 49. The difference in thermal expansion behavior between ORCC substrates and candidate materials is too great to prevent crack initiation on cooldown.

The main conclusion which may be drawn from these analyses is that functional material grading will be required in order to minimize the CTE mismatch between substrate and coating. One possible material grading approach would be to grade from a C-C substrate to a C-SiC substrate, and thence to a SiC coating by varying the volume fractions of SiC, carbon matrix and T300 fiber as a function of thickness.

4.3 FUTURE WORK

In addition to functional material grading studies using the fracture mechanics model described above, alternate methods of minimizing coating cracking will be considered. The methods may include coating process simulations which attempt to initiate coating cracks in known locations to reduce stress build-up between the coating and substrate. Subsequent processing steps would then be used to fill the known cracks with additional coating material with its own known crack pattern effectively staggering the coating cracks. These methods will only be effective if reasonable (approximate .25") crack spacings can be "built" into the material.

Other methods which may be considered are additions of "sacrificial" layers. Material which is added to the composite structures and allowed to oxidize over time, giving the material or structure a known life time.

5.0 CONCLUSIONS

During the course of this program, analytical tools were developed and utilized to study the thermo-mechanical interactions driving the oxidation resistance of carbon-carbon materials. The study was conducted at two levels: Level 1 - The Micro-Mechanics of Oxidation Protection (MMOP) Models. Given a basic fiber and matrix architecture, how do additives such as particulate inhibitors, crack fillers, and fiber coatings affect the thermo-mechanical response of the substrate? and Level 2 - The Crack Management (CM) Model. Given an applied external ceramic coating, what are the material characteristics of the coating and substrate which determine the development of cracks in the coating? and, How may this crack network be managed for maximum oxidation resistance?

The MMOP models were developed based on proven composite micromechanical analysis methods and were incorporated into MSC's existing composite analysis code NDP 9.2. A refinement was introduced which allowed the effects of a quantified substrate crack volume to be included in the analysis. Previous analytical methods had dealt with matrix cracking through an "efficiency factor".

Examination of the predicted transverse and axial bundle stresses in a typical ORCC after cool-down from elevated temperature confirmed the existence of high transverse tensile stresses within the fiber bundles and quantified their magnitude. The development of these high tensile stresses is entirely consistent with the predominance of the observed transverse bundle failure mechanism.

The crack volume analysis was correlated against experimental data from five current generation oxidation resistant carbon-carbon substrates. For each substrate, a crack volume was established and the MMOP model was then utilized to study the influence of various crack fillers on the substrate thermo-mechanical properties. Crack fillers were thought to be generally good for oxidation resistance as they tended to increase the substrate thermal expansion coefficient. The other major effect was an increase in matrix dominated shear modulus. Crack fillers had little effect on in-plane fiber dominated substrate properties. In terms of effectiveness, high modulus, high expansion crack fillers had the most effect. Thus, the three crack filler materials evaluated, ranked in order of effectiveness, were: SiC (most), Si3N4, and BN (least).

An analytical model of the interface stresses between these crack fillers and the substrate, showed a high tensile stress and a likely debonding of these fillers from the surrounding substrate. Thus, the benefits of crack fillers was determined to be more in terms of modifying the substrate mechanical properties rather than reducing the internal surface area of exposed carbon by a crack sealing mechanism.

In a similar fashion to the crack filler model, a model for evaluating the effects of fiber coatings on substrate thermo-mechanical properties was developed and encoded into NDP 9.2. High modulus, high expansion fiber coatings were found to have the most effect in terms of increasing substrate thermal expansion, with a corresponding increase in substrate matrix dominated properties. In-plane properties were little affected. Thus, the most effective fiber coatings were determined: SiC (most), Si3N4, and BN (least). These MMOP models were utilized in quantifying the benefits of these concepts in a 0/90 laminate carbon-carbon laminate with a Si3N4 external overcoat. The results indicated that the thermal strain differential between coating and substrate could be halved by the use of coated fibers.

The development of the microcrack network in the external ORCC ceramic coating on cool-down from process temperatures (CM Model) was investigated using finite element and fracture mechanics approaches. The finite element approach suggested a stress raiser effect of the weave pattern in the surface ply of the substrate, and it was thought that this may offer an approach for crack management via proper consideration of ply weave architectures. However, on further examination, these stress risers were found to be of insufficient magnitude and insufficient frequency to offer much in the way of crack management. One other result from the finite element analyses was that there was a significant edge effect zone around the perimeter of any coated carbon-carbon coupon before the full thermal strain distribution was built up, and the size and shape of the test coupon will have a strong influence on development of the crack pattern. The presence of these edge effect zones should be considered in the design of oxidation test coupons.

The fracture mechanics based CM model was more effective in allowing an investigation of the effects of various substrate and coating material parameters on the development of the coating microcrack network. These analyses quantified the effects of the major driving forces behind the initiation and development of these cracks as the difference in coefficient of thermal expansion (CTE) between coating and substrate (for crack initiation), and coating fracture toughness (for crack spacing).

Cracking may be eliminated if the substrate:coating CTE ratio is greater than 0.8, but with ORCC materials it is unlikely that this ratio will be achieved with the conventional range of coating materials.

Given that coating cracking is a fact of life, management of oxidation resistance requires a coating crack management strategy which minimizes the open crack area (which controls the amount of oxygen penetrating the coating), but maximizes the number of cracks formed to accommodate the thermal strain. This would be accomplished by maximizing the substrate:coating CTE ratio, and by minimizing the coating fracture toughness, i.e., high expansion substrates with weak, low expansion coatings. Unfortunately, the program ended before these recommendations could be evaluated in practice.

One final crack management note. The very fine spacing measured for the coating crack spacings, of the order of 0.01 to 0.02 in., would appear to indicate the impracticality of crack management via some extrinsic means such as the placement of crack initiation artifacts as a pre-coating surface preparation step, and that intrinsic material modifications (lowering of the coating G_{IC}) are the only practical options.

6.0 TECHNICAL INTERACTIONS AND TECHNOLOGY TRANSFER

6.1 TECHNICAL INTERACTIONS

During the course of this program, the following presentations were made in order to disseminate the objectives, approach, and findings of this program to the ORCC research community:

- "Some Observations on ORCC Oxidation", Presented at the 18th. Annual Conference on Composites, Materials and Structures, American Ceramic Society, January 1994.
- "Thermo-Mechanical Considerations in the ORCC Oxidation Process", Presented at Air Force Carbon-Carbon Conference, Pennsylvania State University, Sept. 1994.
- "Thermo-Mechanical Analysis of Oxidation Resistant Carbon-Carbon", Presented at the 19th. Annual Conference on Composites, Materials and Structures, American Ceramic Society, January 1995".

Following the Penn State presentation a visit was made to the ORCC group at WL/ML, WPAFB, Dayton, OH, with regard to acquiring some of their surplus materials for crack management studies. Unfortunately, these materials did not become available.

Material property prediction and bundle data generated under the MMOP model were supplied to Prof. Whitcomb of Texas A&M University for utilization in their weave architecture models.

6.2 TECHNOLOGY TRANSFER

While the objective of this program made specific reference to thermo-mechanical interactions in ORCC materials, there is nothing unique to these materials which precludes utilization of these models in other material systems where the effects of fiber coatings and matrix cracks are important. Similarly, the fracture mechanics Crack Management model is applicable to any brittle coating on an elastic substrate.

At the time of writing, the following activities are in-progress, or have been completed, with regard to utilization of the ORCC models in other programs:

- **"Continuous Fiber Ceramic Composites (CFCC) Program"** Under this DoE sponsored program, MSC, under contract to Martin Marietta Energy Systems, has integrated the MPCCA fiber coating module into the CFCC Macro-Mechanics design and analysis software utility - CLASS-CFCC. This utility program is currently being made available to those participants in the CFCC program.

- **"CFCC Material Modeling and Design Support"** Under this subcontract to Amercom Inc., Chatsworth, CA, MSC is using the MMOP model to develop properties for candidate CFCC materials for industrial and automotive applications.

- **"Rapid Densification of Carbon-Carbon Components"** Under this ARPA sponsored program, MSC, under contract to Textron Specialty Materials, has applied the fracture mechanics crack management model to assist in the design and fabrication of functionally-gradient crack resistant C-SiC materials.

REFERENCES

1. McKee, D., "Oxidation Behavior and Protection of Carbon-Carbon Composites", Carbon, Vol. 25, p. 551 (1987).
2. McCormick, E.S., "Extended-Life Oxidation Protection for Carbon-Carbon Composites", WL-TR-93-4053, October 1989.
3. Holloway, G., Meade, R., and Jones, M.L., "Advanced Carbon-Carbon 2D-CD Nozzle Structures Program", Final Report, Contract F33615-84-C-3225, August 1988.
4. Sheehan J.E., "High Temperature Coatings on Carbon Fibers and Carbon-Carbon Composites", p. 223 in Carbon-Carbon Materials and Composites, J.D. Buckley and D.D. Edie, eds., Noyes Publications, Park Ridge, New Jersey (1993).
5. Sheehan, J.E., McCormick, E.S., and Porter, J.T., "Advanced Inhibition/Protection Systems for Carbon-Carbon Composites", Final Report WL-TR-94-4069, Feb. 1994.
6. Strife, J.R., "Fundamentals of Protective Coating Strategies for Carbon-Carbon Composites", p. 121 in Damage and Oxidation Protection in High Temperature Composites, G.K. Haritos and O.O. Ochoa, eds., ASME (1991).
7. Starrett, S., Southern Research Inc., Private Communication, 1989.
8. Nixon, T., "Inhibitor Mechanisms in Carbon-Carbon Composites", M.S. Thesis, Dept. Ceramic Engrg, The Ohio State University (1987).
9. Sheehan, J.E., Porter, J.T., Price, R.J., and Bacon, R., "Coated Carbon Fiber Development for Oxidation Protection of Carbon-Carbon Composites", Final Report WL-TR-93-4003.
10. Yurgartis, S.W., Bush, M.D., and Mast, B.E., "Morphological Description of Coating Cracks in SiC Coated Carbon-Carbon Composites", Surface and Coatings Technology, Vol. 70, 1970, pp. 131-144.
11. Hemstad, S., BF Goodrich, Private Communication, Jan. 1994.
12. Rosen, B.W., Chatterjee, S.N., and Kibler, J.J., "An analysis Model for Spatially Oriented Fiber Composites", Composite Materials Testing and Design, ASTM STP617, American Society for Testing and Materials, 1977, pp. 243-254.
13. Hashin, Z., "Theory of Fiber Reinforced Materials", NASA CR-1974, March 1972.
14. Mura, T., "Micromechanics of Defects in Solids", M. Nighoff, 1987.

15. Hashin, Z., "Theory of Analysis of Composite Materials - A Survey", J. Appl. Mechs., Vol. 50, 1983, pp. 481-505.
16. Kibler, J.J., "Mechanics of Multi-Directional Carbon-Carbon Composite Materials" in Carbon-Carbon Materials and Composites, Edited by John Buckley, Noyes Publications, 1993, pp. 169-196.
17. Yen, C.F., and Buesking, K.W., "Advanced Composite Material Evaluations", MSC TFR 2019/1422, July 1989.
18. Sullivan, B.J., and Hashin, Z., "Determination of Mechanical Properties of Interfacial Region between Fiber and Matrix in Organic Matrix Composites", 3rd. Int. Conf. on Composite Interfaces, Case Western Reserve, Univ. of Cleveland, OH, May 1990.
19. "Thermal Expansion Measurements of Uncoated Carbon-Carbon Composites", Engineering Materials Testing Laboratory, Final Report No. 1568, August 1993.
20. Hibbitt, Karlsson, and Sorensen Inc., "ABAQUS User's Manual - Ver. 5.3", Pawtucket, Rhode Island, 1993.
21. Chatterjee, S.N. and Yen, C-F., "Ply Cracks and Load Redistribution in Laminated Composites", Proceedings of the 12th Army Symposium on Solid Mechanics, Plymouth, MA, November 1991.
22. Metals and Ceramics Information Center, "Engineering Property Data on Selected Ceramics, Vol. 2, Carbides, MCIC-HB-07, August, 1973.Quantification of Microcracks and Oxidation Damage in Carbon-Carbon Substrates and of the Microcrack NeYurg1G